THE OHIO STATE UNIVERSITY

RESEARCH FOUNDATION

1314 KINNEAR ROAD COLUMBUS, OHIO 43212

Report No. COO-2018-4 (Q-1)

STRESS CORROSION CRACKING AND GENERAL CORROSION OF IRON, NICKEL, CHROMIUM AND THEIR ALLOYS IN CAUSTIC SOLUTIONS

D. V. Subrahmanyam and R. W. Staehle
Department of Metallurgical Engineering

January 15, 1969 - April 15, 1969

U. S. Atomic Energy Commission
Chicago Operations Office
Argonne, Illinois

Contract No. AT(11-1)-2018

DISCLAIMER

LEGAL NOTICE

DISTRIBUTION LIST

	Copies
U. S. Atomic Energy Commission Division of Reactor Development & Technology, Headquarters Washington D.C. 20545	
Attn: Assistant Director, Engineering Standards	1
Assistant Director, Nuclear Safety	1
Assistant Director, Plant Engineering	1
Assistant Director, Program Analysis	1
Assistant Director, Project Management	1
Assistant Director, Reactor Engineering	2
Assistant Director, Reactor Technology	1
Chief, Fuels and Materials Branch	3
Chief, Fuel Engineering Branch	1
Chief, Reactor Vessel Branch	1
U. S. Atomic Energy Commission Division of Research, Headquarters Washington D.C. 20545	
Attn: Asst. Director for Metallurgy & Materials Program	1
U.S. Atomic Energy Commission Division of Space Nuclear Systems, Headquarters Washington D.C. 20545	
Attn: Asst. Director for Space Electric Power	1
Deputy Manager, SNPO	1
U. S. Atomic Energy Commission Division of Naval Reactors Washington D.C. 20545	
Attn: Chief, Nuclear Materials Branch	1
U. S. Atomic Energy Commission Div. of Technical Information Extension Washington, D.C. 20545	32
United States Atomic Energy Commission P. O. Box 62 Oak Ridge, Tenn. 37831	1
Manager, Research United Nuclear Corporation Research & Engineering Center Grasslands Road Elmsford, New York 10523	2

DISTRIBUTION LIST

	Copies
Manager Chicago Operations Office U. S. Atomic Energy Commission 9800 South Cass Avenue Argonne, Illinois 60439	1
Patent Group Chicago Operations Office U. S. Atomic Energy Commission 9800 South Cass Avenue Argonne, Illinois 60439	1
Director LMFBR Program Office 9800 South Cass Avenue Argonne, Illinois 60439	1
Director, Metallurgy Division Ames Laboratory Iowa State University Ames, Iowa 50012	2
Director, Metallurgy Division Argonne National Laboratory 9800 South Cass Avenue Argonne, Illinois 60439	2
Manager, FFTF Project Pacific Northwest Laboratory P. O. Box 999 Richland, Washington 99352	2
FFTF Fuels Department Pacific Northwest Laboratory P. O. Box 999 Richland, Washington 99352	2
Manager, Chemistry and Metallurgy Division Pacific Northwest Laboratory P. O. Box 999 Richland, Washington 99352	5
Division Leader, Chemistry and Metallurgy Division (CMB) Los Alamos Scientific Laboratory P. O. Box 1663 Los Alamos, New Mexico 87544	2

DISTRIBUTION LIST

	Copies
Director, Metallurgy and Material Science Division Brookhaven National Laboratory Upton, New York 11973	2
Director, Metals and Ceramics Division Oak Ridge National Laboratory P. O. Box X Oak Ridge, Tennessee 37830	5
Division Chief, M & S Division NASA - Lewis Research Center 2100 Brook Park Road Cleveland, Ohio 44135	2
Director Liquid Metal Engineering Center P. O. Box 309 Canoga Park, California 91305	1
Manager-Advance Development Activity General Electric Company Knolls Atomic Power Laboratory P. O. Box 1072 Schenectady, New York 12301	2
General Manager Westinghouse Electric Corporation Bettis Atomic Power Laboratory P. O. Box 79 West Mifflin, Pennsylvania	2
Director, LMFBR Technology Program Atomics International P. O. Box 309 Canoga Park, California 91304	1
Associate Manager, Materials Engineering Department Battelle Memorial Institute Columbus Laboratories 505 King Avenue Columbus, Ohio 43201	2
Director, Nuclear Development Center The Babcock & Wilcox Company Atomic Energy Division Lynchburg, Virginia 24501	2

DISTRIBUTION LIST

	Copies
Manager, Nuclear Laboratories Combustion Engineering Inc. Nuclear Division Prospect Hill Road Windsor, Connecticut 06095	2
Technical Director Westinghouse Electric Corporation Advanced Reactors Division Cheswick, Pennsylvania 15024	3
Assistant General Manager for Research Gulf General Atomic, Inc. P. O. Box 608 San Diego, California 92112	2
Manager, Sodium Reactor Technology General Electric Company Breeder Reactor Development Operation 310 DeGuigne Drive Sunnyvale, California 94086	3
Project Engineer Demonstration Plant Development General Electric Company Breeder Reactor Development Operation 310 DeGuigne Drive Sunnyvale, California 94086	2
Director, Nuclear & Chemical Technology Division Idaho Nuclear Corporation P. O. Box 1845 Idaho Falls, Idaho 83401	1
Director, Nuclear Engineering & Materials Section E. I. duPont de Nemours Company Savannah River Plant Aiken, South Carolina 29801	2
Director, Metallurgy & Reactor Materials U. S. Naval Research Laboratory Washington, D. C. 20390	3

INTERNAL DISTRIBUTION

The Ohio State University
Department of Metallurgical Engineering

Attn: M. G. Fontana	1
F. H. Beck	1
J. W. Spretnak	1
J. P. Hirth	1
R. W. Staehle	45

RF Project 2765

Report No. COO-2018-4

QUARTERLY

REPORT

By

THE OHIO STATE UNIVERSITY
RESEARCH FOUNDATION

1314 KINNEAR RD.
COLUMBUS, OHIO 43212

To. U. S. ATOMIC ENERGY COMMISSION
Chicago Operations Office
9800 South Cass Avenue
Argonne, Illinois 60439
Contract No. AT(11-1)-2018

On STRESS CORROSION CRACKING AND GENERAL CORROSION OF IRON, NICKEL, CHROMIUM AND THEIR ALLOYS IN CAUSTIC SOLUTIONS

For the period January 15, 1969 - April 15, 1969

Submitted by D. V. Subrahmanyam and R. W. Staehle
Department of Metallurgical Engineering

Date February 2, 1970

ABSTRACT

This review considers the problems of general corrosion and stress corrosion cracking for Fe-Cr-Ni alloys in caustic environments. Environments considered are primarily NaOH-H_2O over a broad range of temperatures. Information is presented in areas of thermodynamics, electrochemical kinetics, corrosion rates, SCC phenomena, structures of passive films, and inhibitors. Materials considered are iron, chromium, and nickel, as well as binary and ternary alloys.

SUMMARY AND CONCLUSIONS

This review considers the corrosion behavior of Fe-Cr-Ni alloys in caustic environments, which are mainly aqueous solutions containing alkaline metal hydroxides (Na,K,Li). There is no specific information herein on anhydrous fused salts nor on sodium-based solutions.

This review was prepared in support of the liquid metal cooled, fast breeder reactor program from the point of view that any accidentally spilled or leaked sodium would oxidize or hydrolyze to produce NaOH-HaO-H_2O solutions. These solutions, in a general way, are very aggressive toward this alloy system and particularly toward iron base alloys. A series of soluble species is formed at higher pH's which have identities like $HFeO_2^-$ and $FeO_2^{=}$.

The corrosion of these alloys in caustic environments takes the form of either (a) general corrosion or (b) stress corrosion cracking, depending subtly on specific features of the environment.

The review considers first the pure materials, iron, nickel, and chromium. This is followed by the binary and then the ternary alloys. Each section considers stress corrosion, general corrosion, and electrochemistry of the respective material system. Structures of protective oxide films are also discussed.

In addition to considering the general technological and mechanistic behavior, methods for prevention or diminution of both general corrosion and SCC are described.

With respect to stress corrosion cracking there is a paucity of data compared to chloride-induced SCC.

Important general observations from this review are summarized as follows:

1. Stress corrosion cracking becomes most severe for iron base alloys. This is contrary to the trend for chloride SCC where the very iron-rich alloys are immune.

2. In general the effects of temperature, alloy, stress, and caustic concentration are critically interrelated. In iron SCC will occur at temperatures as low as 70°C. The detailed nature of this interrelationship is not completely clear but these variables produce results in expected directions. Susceptibility to SCC is decreased as the total Ni and Cr content is raised, as temperature is reduced, as stress is lowered, and as the $[OH^-]$ is lowered.

3. The onset of caustic SCC is shown to be critically related to the electrochemical potential. The mean potential at which caustic

SCC occurs for iron is generally independent of the temperature and caustic concentration. This range of potentials is associated with the anodic peak of the potential-time curve. A secondary range of cracking occurs near the transpassive transition. These patterns are reasonable in terms of patterns observed for other alloys.

4. The caustic SCC, in general, appears to be dominated by electrochemical parameters. The initiation and propagation of stress corrosion cracks appear to be related critically to transient anodic processes; a reducible species (O_2, H_2O) is required for cracking to be sustained.

5. The information on general corrosion rates and electrochemical parameters will be useful in estimating rates of general corrosion of Fe-Cr-Ni alloys in caustic solutions.

TABLE OF CONTENTS

TABLE OF CONTENTS - (Continued)

LIST OF FIGURES

LIST OF FIGURES - (Continued)

LIST OF FIGURES - (Continued)

LIST OF FIGURES - (Continued)

LIST OF TABLES

LIST OF TABLES - (Continued)

STRESS CORROSION CRACKING AND GENERAL CORROSION OF IRON, NICKEL, CHROMIUM AND THEIR ALLOYS IN CUASTIC SOLUTIONS

I. INTRODUCTION

Stress corrosion cracking is the spontaneous failure of a metal caused by the combined effect of corrosion and stress. When the corrosive environment happens to be an alkali, the resulting phenomenon is known as either caustic cracking or caustic embrittlement. The effects of this type of failure can be very dramatic as in the explosion of a boiler[1] or the failure of a steel hook permitting a facing block from the side of a building to fall into a street below.[2] Of the three metals—iron, nickel, chromium and their alloys—discussed in this review, the caustic cracking of iron has been known for many years and has been a continuing problem in steam boilers. The American Association of Railroads was conducting extensive research[3] on this problem during the early 1930's. In addition, failures of stainless steel heat exchangers due to caustic stress corrosion cracking have been frequently reported. This often occurs when additives are used to raise the pH and thereby prevent general corrosion; if there is a leak or a process where the hydroxide is concentrated, then caustic cracking occurs.

This review has been prepared from the point of view that caustic stress corrosion cracking may be a major problem in materials used for fast breeder reactor systems. Since the overall reactor system contains both sodium and water in generally intimate juxtaposition, there is certainly the reasonable incentive that materials selection should consider resistance to caustic stress corrosion cracking.

While the usual precaution taken to prevent leakage of sodium and the availability of moisture-laden air would seem to be adequate, there is always the inevitable accident. An inadvertent spillage of sodium or a small leak at a minor component may perhaps be subsequently hydrolyzed by available moisture; and thereafter, when the system is operating at elevated temperatures, rapid SCC can ensue.

SCC is different from many failure modes which may occur during reactor operation; i.e., neutron damage, low cycle fatigue, liquid metal embrittlement, mass transfer, and radiation-induced bubble formations. SCC can occur at any time during construction, installation testing, operation, shutdown, and cleaning.

A matter of substantial concern with respect to materials for IMFBR is that caustic SCC becomes more virulent at lower alloy concentrations. Thus the incentives for economy and for avoiding chloride SCC lead directly to heightened sensitivity to caustic SCC.

During recent years several important symposia in the area of SCC have been conducted and numerous books and reviews have been prepared.[4-14]

This review covers the following aspects with respect to iron, chromium and nickel, and their alloys in alkaline media: a) thermodynamic basis for corrosion, b) stress and general corrosion, c) electrochemistry and d) preventive methods for both kinds of attack.

II. THERMODYNAMIC BASIS FOR DISSOLUTION IN CAUSTIC ENVIRONMENTS

The essential basis for corrosion behavior in the caustic region is related to the solubilizing effects of $(OH)^-$. Adjacent to this region, passive films can form. The regions of pH and potential, in which these two processes can operate, are delineated in Figs. 1-3,[15] which show potential-pH behavior for the iron, nickel and chromium components separately in water at 25°C. Little work has been conducted above 25°C to obtain the necessary thermodynamic data for extending these diagrams to higher temperatures; however, up to about 300°C the qualitative aspects of these diagrams can be assumed to apply. Initial work at Ohio State University has shown that the general aspects of these diagrams remain the same but the area of caustic solubility increases with increasing temperature.

A. IRON

The region of stability for various species of iron in water are shown in Fig. 1.[15] Detailed information leading to the construction of these diagrams is described by POURBAIX.[15] Essentially, they are constructed by calculating all possible equilibria between solid and soluble species and then determining the regions of potential at pH where certain species are the most stable. Thus, in Fig. 1 above line (17) and to the right of line (28) Fe_2O_3 is the most stable form of iron in aqueous environments at room temperature; below lines (23), (13), and (24) elemental iron is the most stable, and this is the basis for lowering the potentials in cathodic protection.

At high pH iron will dissolve as the dihypoferrite ion according to the half-cell equilibrium:

$$Fe + 2H_2O = HFeO_2^- + 3H^+ + 2e \qquad (1)$$

Further, the protective iron oxides will solubilize according to the equilibria:

$$3HFeO_2^- + H^+ = Fe_3O_4 + 2H_2O + 2e \qquad (2)$$

$$2HFeO_2^- = Fe_2O_3 + H_2O + 2e \qquad (3)$$

The triangular region in Fig. 1 in which the $HFeO_2^-$ ion is stable should be especially noted. Here a soluble species is surrounded at higher potentials by stable insoluble products. Thus, there is a

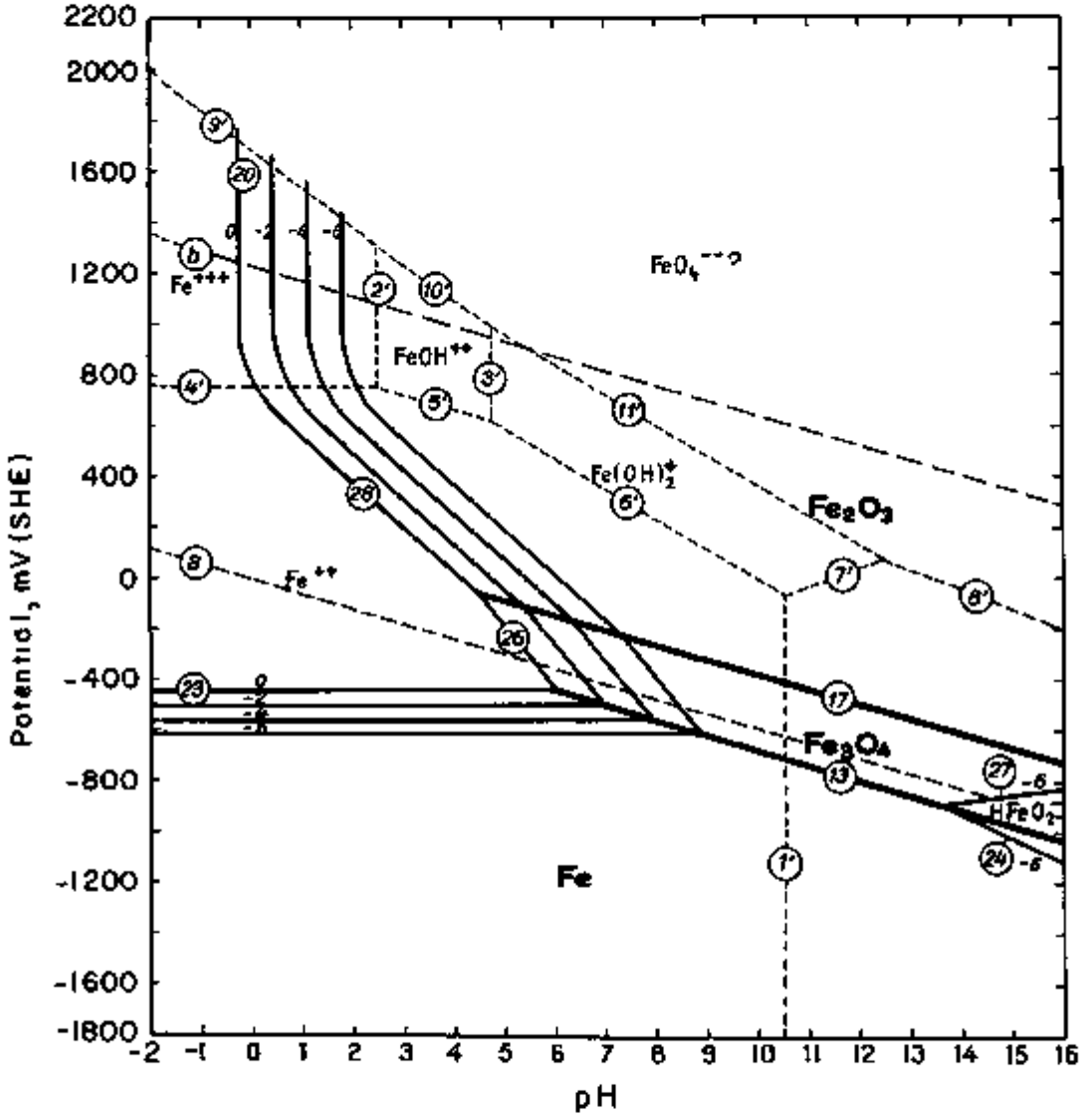

Fig. 1 - Potential-pH equilibrium diagram for the system iron-water at 25°C.[15]

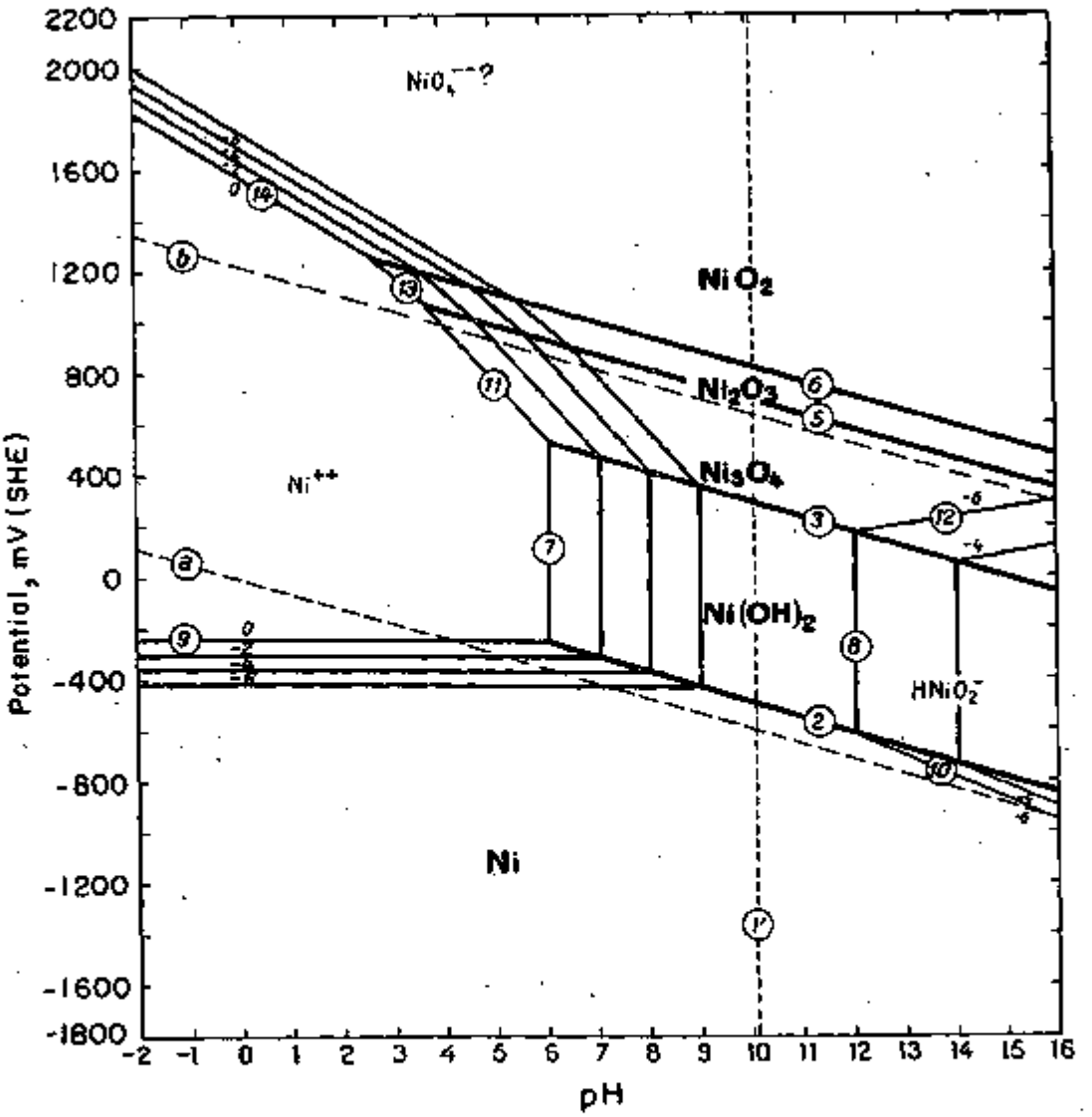

Fig. 2 - Potential-pH equilibrium diagram for the system nickel-water at 25°C.[15]

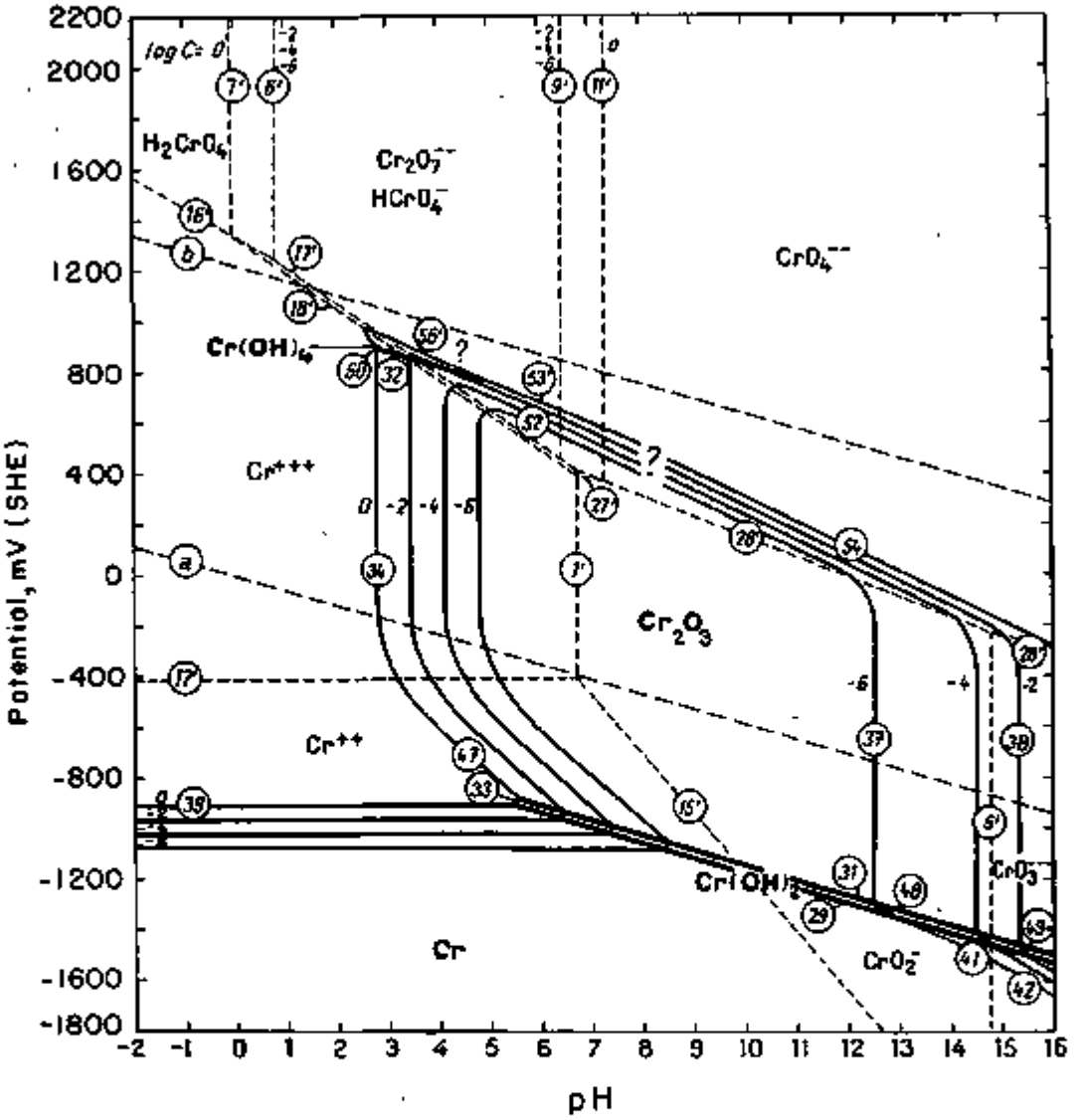

Fig. 3 - Potential-pH equilibrium diagram for the system chromium-water at 25°C.[15]

possibility for dissolving at a lower potential but immediately passivating. This possibility is probably an important condition for stress corrosion cracking. The application of these ideas will be discussed later.

B. NICKEL

The potential-pH relationship of Fig. 2 for nickel is generally the same as for iron. Similar equilibria apply. It is particularly noteworthy that the region of stability of the $HNiO_2^-$ ion is broader, thus implying that film formation will be more difficult if a transient dissolution event should occur. This pattern is in accord with the observation that nickel base alloys are much less susceptible to stress corrosion cracking in caustic environments.

C. CHROMIUM

The potential-pH stability diagram for chromium-water at 25°C is shown in Fig. 3.[15] The soluble species at high pH is $CrO_3^=$.

III. CORROSION OF IRON

A. STRESS CORROSION CRACKING

The general problem of caustic cracking of iron is of long standing and is well known. The initial concern originated from the experiences with steam boilers. Various reviews have appeared in the published literature.[16-18] These reviews considered the overall picture of caustic cracking in the United States, case histories of steel plant experiences under varying liquor stages of chemical processing, exploratory testing methods with reference to embrittlement detectors, and theories of stress corrosion and prevention. These reviews include little useful mechanistic information.

1. Crack Morphology

The SCC of iron in caustic is generally intergranular with some few observations of transgranular behavior. CHAMPION[18] suggests the following significant morphological characteristics of caustic SCC:

1. The cracking is intercrystalline and isolated with branching at the tip. Small portions of the crack, and especially the path of final fracture, were found to be transcrystalline, owing to the imposition of purely mechanical forces in addition to stress corrosion.

2. The width of the crack, as observed metallographically generally decreases with increasing penetration and ends in a fine point, as distinct from the blunted cracks often seen with fatigue or corrosion fatigue.

3. The cracks are transverse to the main tensile stress.

4. The surface of the metal is known to have been exposed to a high concentration of caustic alkali, but relatively little corrosion is observed especially within the crack.

CHAMPION,[18] SCHROEDER and BERK[19] and WEIR[20] have reported intercrystalline type of failure. Similar failure has been reported by SHVARTS et al.[21] in their experiments with cylindrical specimens exposed in sodium hydroxide concentration between 25-30% in the temperature range 250-300°C. On the other hand, at higher concentrations between 35-70% in the same temperature range, EVANS[22] observed transcrystalline type of failure. Caustic SCC of mixed type has been reported by HAMER and COLEBECK,[23] RATH[24] and AZHOGIN.[25] BOHNENKAMP[26] has observed transgranular cracking of steel in sodium hydroxide solution as shown in Fig. 4. The basis for the change in the mode of cracking from intercrystalline is not clear but many metal-environment systems exhibit such behavior.

2. Early Theories for Origin of Cracks

Early theories of caustic SCC suggested that the important feature of a mechanism involved in the potential differences between grain boundaries (anodic) and the bulk grains (cathodic).

As early as 1928 PARR and STRAUB[27] suggested that a coherent coating of Fe_3O_4 is formed on the steel in contact with the hot caustic. This coating was believed to be resistant to attack unless it was ruptured by strain in restricted areas. In 1937 SCHROEDER and co-workers[28] suggested that oxide forms over the grain surfaces but not over the boundaries. This presumably produces an electrolytic attack at the grain boundaries.

EVANS[29] suggested that crack propagation may be produced by a concentration cell where the advancing crack has high alkali and the surface a lower alkali. Such a cell would be as follows:

iron (cathode)	dilute alkali	concentrated alkali	iron (anode)
surface		inside crack	

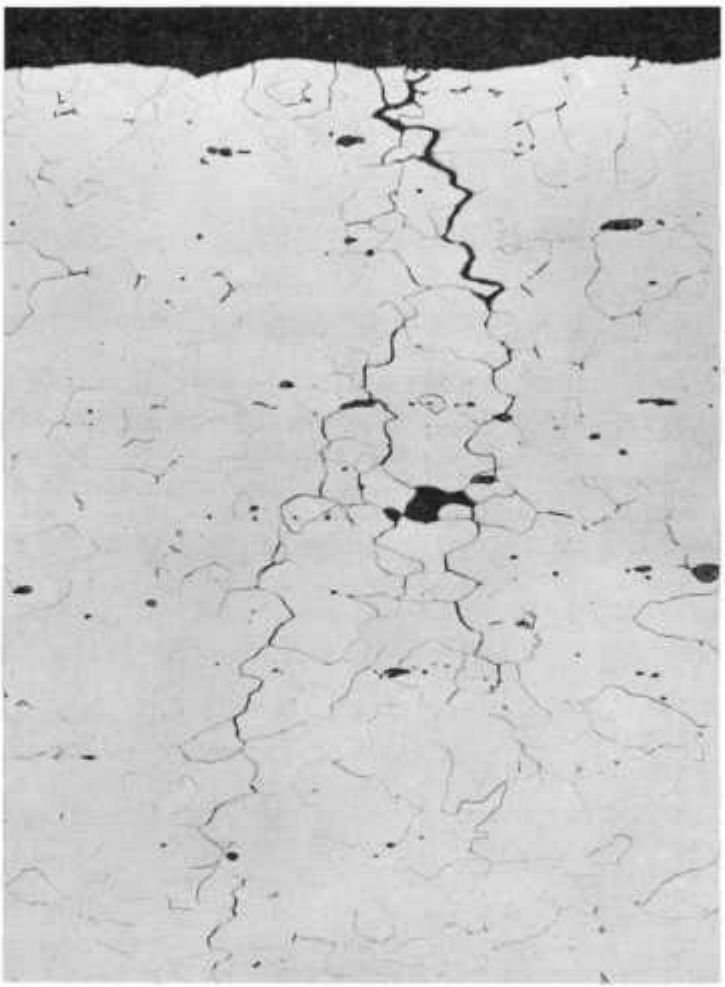

Fig. 4 - Photomicrograph of a cross section of stressed steel in boiling 33% NaOH at E_h = -700 mV (failure time = 4.8 hr).[26] 200X

EVANS[29] further pointed out that at the more anodic regions iron dissolves as a ferroate (Na_2FeO_2 or $Na_2O{\cdot}FeO$) i.e., Fe^{++} or as Fe^{+++} at high potentials (cathodic/anodic area very large). If the ferroate diffuses into a region where the alkali concentration is lower, Fe_3O_4 will precipitate according to the effect of pH on this equilibrium. Under tensile stress, iron (or steel) may be attacked at the grain boundaries where the passive film is coated with the remainder of the surface being protected.

An outline of a reasonable mechanistic hypothesis based on modern ideas is given in Section C.

3. Effects of Controlled Potential or Controlled Current

Electrochemical control of corrosion experiments provides a highly reproducible and fundamentally reliable basis for interpreting stress corrosion cracking experiments. Using these tools, together with controlled environmental chemistry, it is possible to specify uniquely the occurrence of desired reactions on the metal surface. For example, by comparison with Fig. 1, the application of potential at pH 15 can cause the metal surface to exist in the region where Fe_2O_3 (higher potentials) or $HFeO_2^-$ (lower potentials) is stable. Lowering the potential below line @ can also reduce water to hydrogen so that the entry of hydrogen into the metal can be uniquely controlled and investigated.

Significant electrochemically controlled experiments on the SCC of iron in caustic solutions have been conducted by VENCZEL and WRANGLEN,[30] GRAFEN and KURON,[31,32] HUMPHRIES and PARKINS,[33,34] BOHNENKAMP,[26] ROBINSON and NEL[35] and PODGORNY.[36]

These electrochemically controlled experiments involved primarily the following:

1. Effects of applied potential on SCC as influenced by variables of stress, temperature, and hydroxide concentration.

2. The effect of applied potential on the current (i.e., polarization behavior).

3. Effects of applied potential on percent reduction in area of tensile tests.

4. The variation of potential with time or current with time.

5. Effects of potential on crack morphology crack growth rates, and structure of oxide films.

The most reasonable conclusion from these studies is that the nature of the oxide film is crucial in determining the onset of caustic SCC. Attempts to show that hydrogen uptake is critical have been shown to be futile. The important results from these studies are discussed in subsequent sections.

4. Range of Potentials for Caustic SCC

It has been clearly established that cracking occurs in restricted ranges of potential. One area of cracking occurs in the region of the anodic peak which, up to boiling temperatures, is in the range of -1000 to -600 mV_H. There is usually a second region which occurs just negative to the transpassive transition. Figure 5 relates the regions of potential in which cracking occurs to the polarization curves which define the nature of corrosion on the stressed surface. This includes the data determined by VENCZEL and WRANGLEN[30] (in 20% sodium hydroxide at 100°C, at load = 70% Y.S.), GRAFEN[31] (in 35% air-saturated sodium hydroxide at 80°C, at load = 70% of Y.S.) and HUMPHRIES and PARKINS[34] (in 35% boiling sodium hydroxide at a strain rate = 10^{-3}/sec).

It has been found that the mean potential at which cracking occurs is more or less independent of hydroxide concentration, strain rate (Fig. 6)[33] and temperature (Fig. 9).[28]

5. Effects of Sodium Hydroxide Concentration

Simple studies examining time-to-failure as a function of hydroxide concentration appear not to have been conducted for iron in caustic environments. However, a number of studies have been conducted which provide a qualitative basis for assessing such trends.

The reduction in area of straining specimens has been studied as a function of potential and concentration of hydroxide; the data are summarized in Fig. 6a. The most significant feature of this work is that raising the sodium hydroxide concentration expands significantly the range about the mean of potentials where caustic cracking occurs. Further, there is a trend for the reduction in area to be decreased as NaOH concentration is raised. The effect could be partially explained by temperature effects as the boiling point will be raised by 25°C as the concentration is increased from 25 to 50%.

Figure 7 shows the effect of hydroxide concentration on the current density at a constant applied potential of 158 mV_H and a temperature of 100°C. At 20% NaOH the current density drops to negligible values indicating the formation of a protective film of good quality. The corresponding plot of strength shows that this film is both resistant to ion transport and to mechanical breaking. These data are not immediately interpretable in terms of caustic SCC, but show that the protective films may vary substantially in their quality.

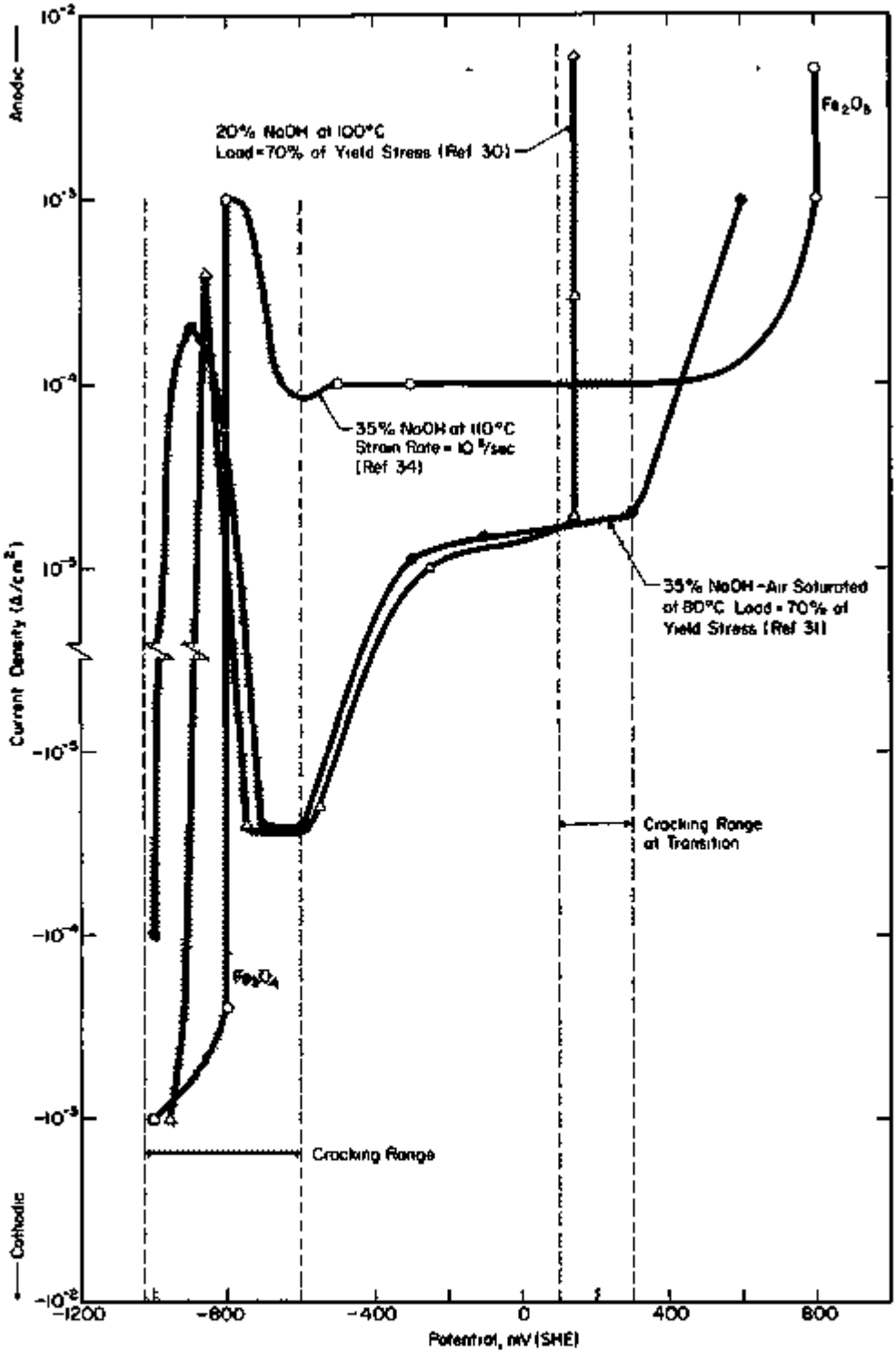

Fig. 5 - Potentiostatic polarization curves for steel in NaOH solutions.

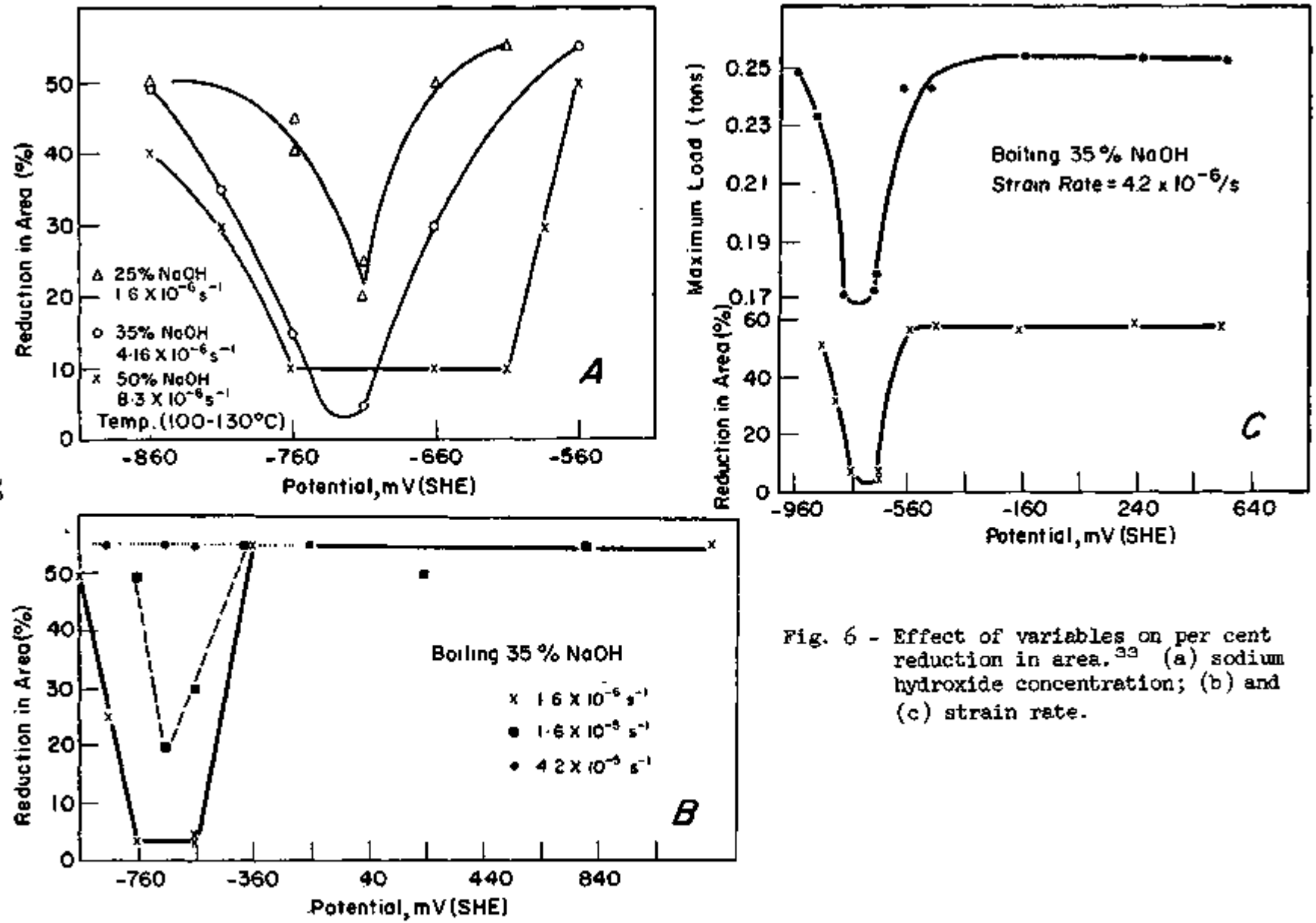

Fig. 6 - Effect of variables on per cent reduction in area.[33] (a) sodium hydroxide concentration; (b) and (c) strain rate.

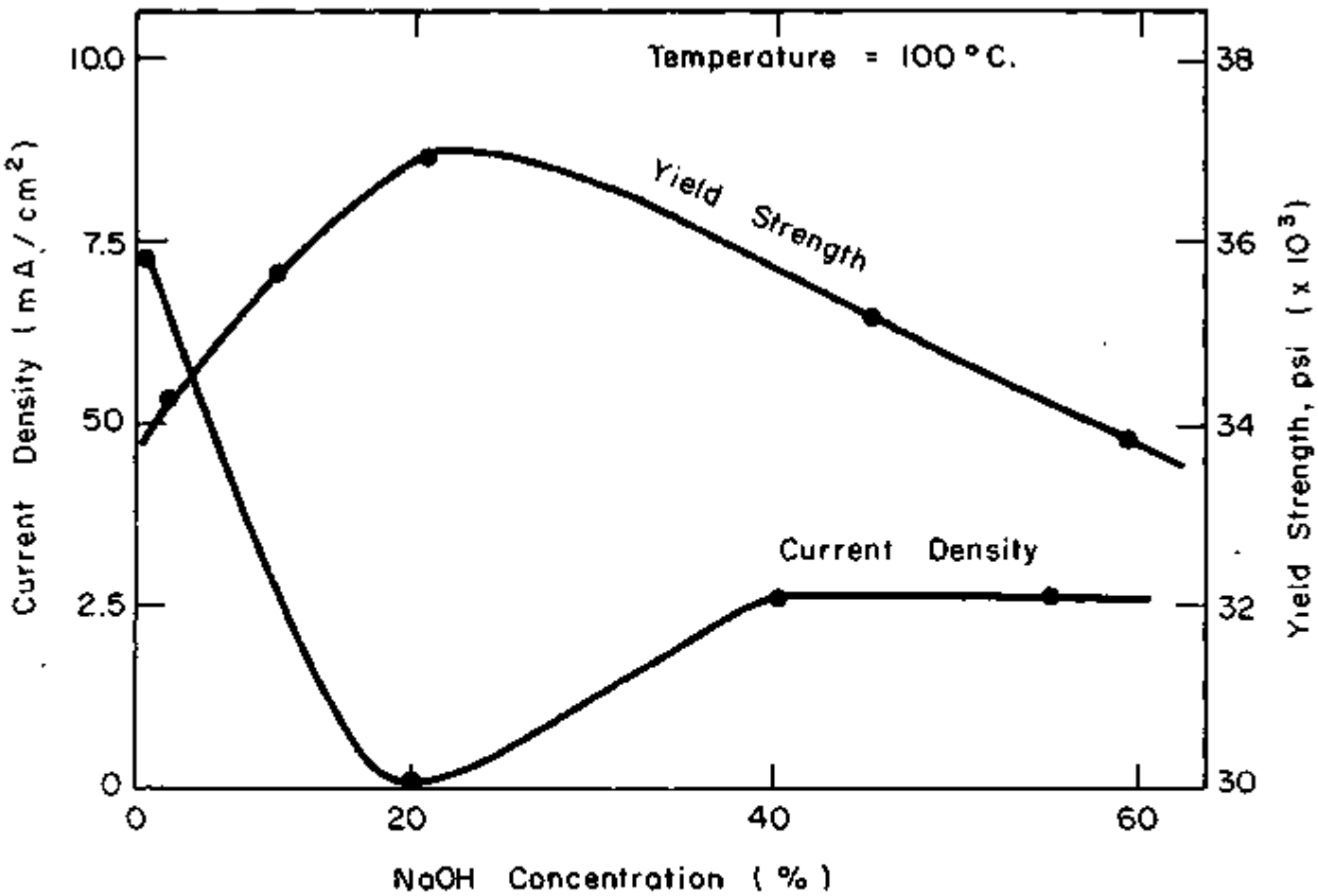

Fig. 7 - Influence of NaOH concentration on the current density and yield stress at passive potential, E = -158 mV_H.[30]

The interaction between applied potential and NaOH concentration has been determined also by VENCZEL and WRANGLEN[30] at 100°C. Figure 8 summarizes their data. Accelerated failure is observed in the ranges of potential at -1.0 to -0.8 V and at +0.4 to +0.6 V. Increasing NaOH concentration from 20% to 40% does not increase cracking susceptibility significantly. VENCZIL and WRANGLEN[30] do not report on morphological details of the cracking.

Early work at 250°C in autoclaves was conducted by SCHROEDER and BERK[19] and is summarized in Table I. The results do not exhibit clear trends and the effects of NaOH seem to depend greatly on the presence of sodium silicate. The probable action of the latter is to lower the over-all current so that the corrosion can be localized at advancing cracks.

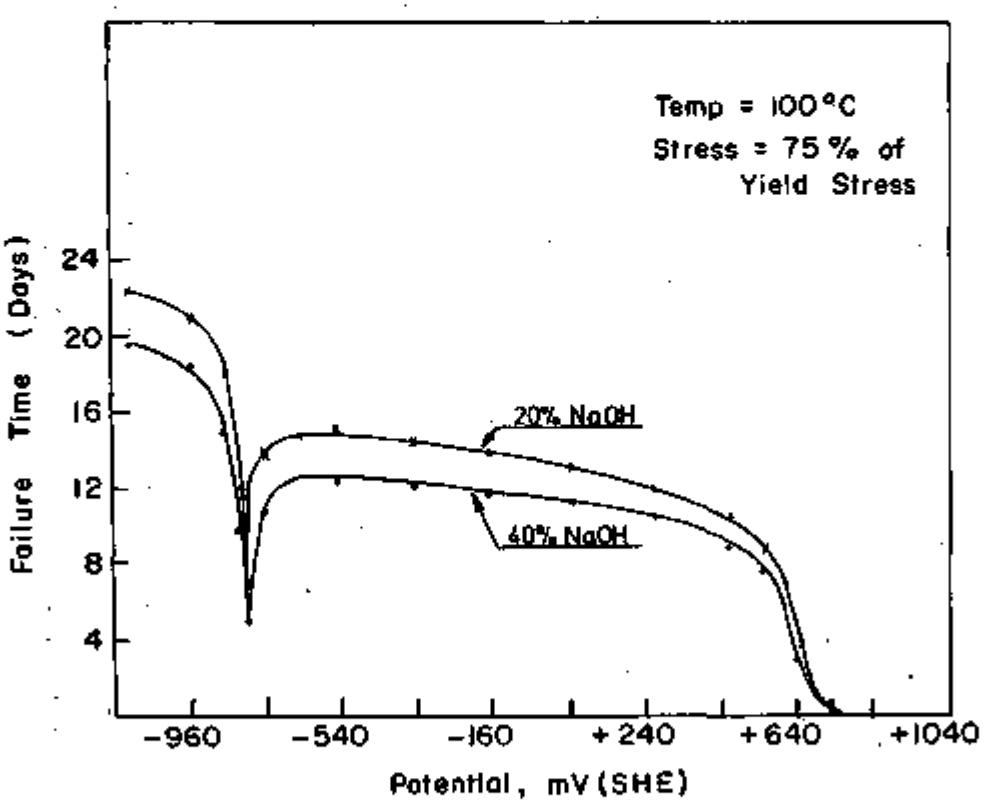

Fig. 8 - Specimen life as a function of applied potential in NaOH.[30]

Table I - Effect of Sodium Hydroxide Concentration on Failure of Steel Specimens at 250°C (after SCHROEDER and BERK)[19]

Average Applied Stress (psi)	Concentration (g/100 g) H_2O		Failure Time (hr)
	NaOH	Na_2SiO_3	
65,000	10		288 NF[b]
65,000	10		288 NF
60,000	10	0.75	54
60,000	10	0.30	50
60,000	7.5	0.75	336 NF
60,000	7.5	0.30	166
60,000	7.5	0.15	120
60,000	5.0	1.9[a]	240 NF
60,000	5.0	0.75[a]	240 NF
60,000	5.0	0.30	240 NF

[a]When removed from the bomb, specimens were found to be covered with a very tightly adhering scale.

[b]NF = no failure

6. Temperature

The effects of temperature in 33% sodium hydroxide solutions at 70, 90, and 120°C, at potentials from -800 to -600 mV_H, and at a load of 4.27×10^4 psi are summarized in Fig. 9. An increase of temperature from 70 to 120°C lowers the cracking time of steels in hydroxides[26] by almost two orders of magnitude at a potential of -700 mV_H.

7. Strain Rate and Stress

BOHNENKAMP[26] determined the effect of applied stress on failure time in 33% boiling NaOH at -700 mV_H. These data are shown in Fig. 10. He used the unusual procedure of determining stress by measuring the specimen diameter after tests but the error involved is not significant.

At a constant NaOH concentration of 35% PARKINS and HUMPHRIES[33] have studied the effect of strain rate. Figure 6b shows that the strain rate must be lower than 4.2×10^{-5} for an effect of the caustic to be discerned. As the strain rate is further lowered the range of potential where cracking occurs is widened. At a constant strain rate of 4.2×10^{-6} the maximum load at failure and the reduction in area are compared in Fig. 6c. These figures imply that the effects of caustic would not be observed at high strain rates; but as the strain rate becomes less, the sensitivity to environmental effects increases substantially.

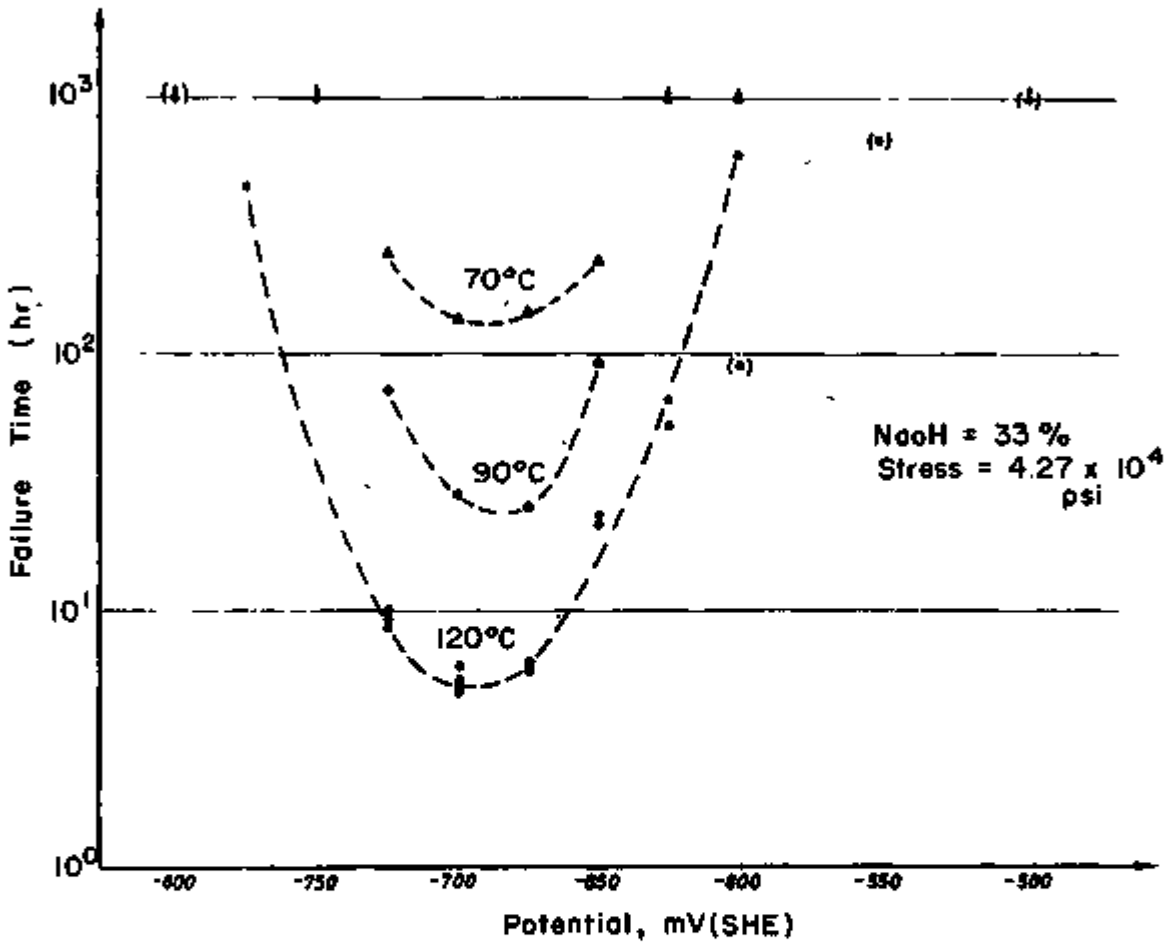

Fig. 9 - Effect of temperature on the failure time of mild steel in NaOH solution.[26]

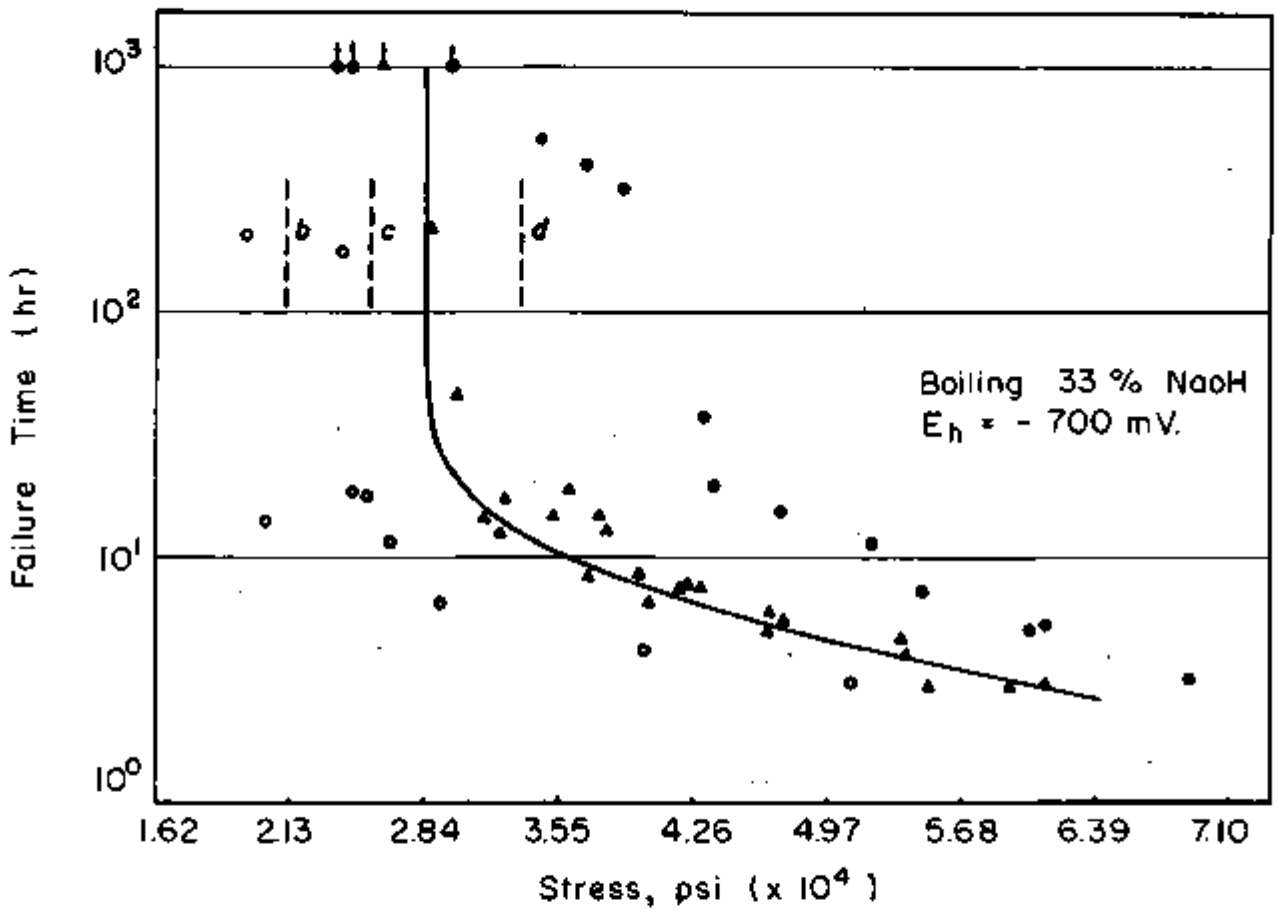

Fig. 10 - Effect of stress on failure times of mild steels in NaOH solution.[26]

Points	C	N	Al	Si	Mn	P	S	Cu	O
○—○ B	0.04	0.014	0.001	< 0.001	< 0.001	0.003	0.002	--	0.002
△—△ C	0.02	0.006	< 0.003	0.003	0.018	0.011	0.009	< 0.003	--
●—● D	0.11	0.009	0.004	0.01	0.31	0.022	0.039	0.03	--

Figure 11 from work by GRAFEN[31] compares the ease of passivation as affected by prior deformation in 35% sodium hydroxide at 80°C. The nondeformed specimen increases its open circuit potential from -800 to -400 mV_H in about one hour. This implies a decrease of anodic kinetics to the extent of about four orders of magnitude. On the other hand the previously deformed specimens remained at the same potential for over two hours indicating that prior deformation prevents the easy re-formation of stable passivity. This observation suggests a possible basis for propagation of stress corrosion cracks; a propagating crack would always have a highly deformed state at the crack tip while the crack sides had dissolved away the deformed metal.

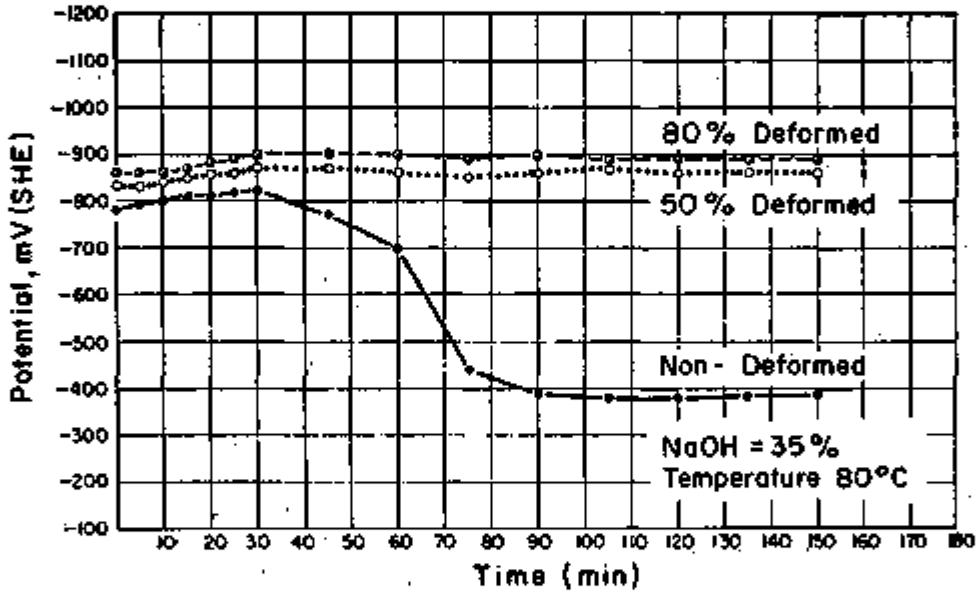

Fig. 11 - Effect of cold deformation of steels on open circuit potential-time curves in NaOH solution.[31]

The effect of increasing the applied load on the reaction current at constant potential has been studied by VENCZEL and WRANGLEN[30] their data are summarized in Fig. 12a and b. Figure 12a, at -58 mV_H, corresponds to potentials near the transpassive transition. At this potential the reaction current without load decreases continuously with time. As load is applied the breaking of the film produces positive bursts of current. Also as the load is increased, the specimen deforms discontinuously indicating fairly rapid SCC. At -1058 mV_H in Fig. 12b the transient behavior shows negative peaks. This can only be rationalized in terms of accelerated reduction of the oxide ($Fe_3O_4 + 8H^+ + 8e \rightarrow 3Fe + 4H_2O$) since an anodic transient due to, say $Fe \rightarrow Fe^{++}$, would produce a positive, or less negative transient.

8. Dilute Alloy Additions

GRAFEN and KURON[32] have studied the mechanism of intercrystalline cracking and the effects of carbon content using voltage-current measurements and potentiostatic creep-rupture tests. Two sets of iron-carbon alloys were compared. One was vacuum melted with carbon contents between 0.004 and 0.52% and the other was a series of commercial carbon steels with carbon contents between 0.06 and 0.37%. When the effect of carbon content on cracking was studied, there was no difference between the behavior of the two sets at a given carbon concentration. With respect to the effect of carbon, increases up to 0.12% increased specimen life; and thereafter, up to 0.52%, the life times exhibited erratic trends.

BOHNENKAMP[26] studied the effect of potential on cracking time for various dilute alloys where the data are plotted as from Fig. 9 already described. The potential at which the minimum in cracking time occurs is affected by the alloy composition. The potential for these minima are summarized as follows:

Alloy	Potential at Lowest Cracking Time, mV_H
Pure Fe	-660
Pure Fe + N, technical steel, alloy with Ti additions	-700
Alloy with aluminum	-750 to -725

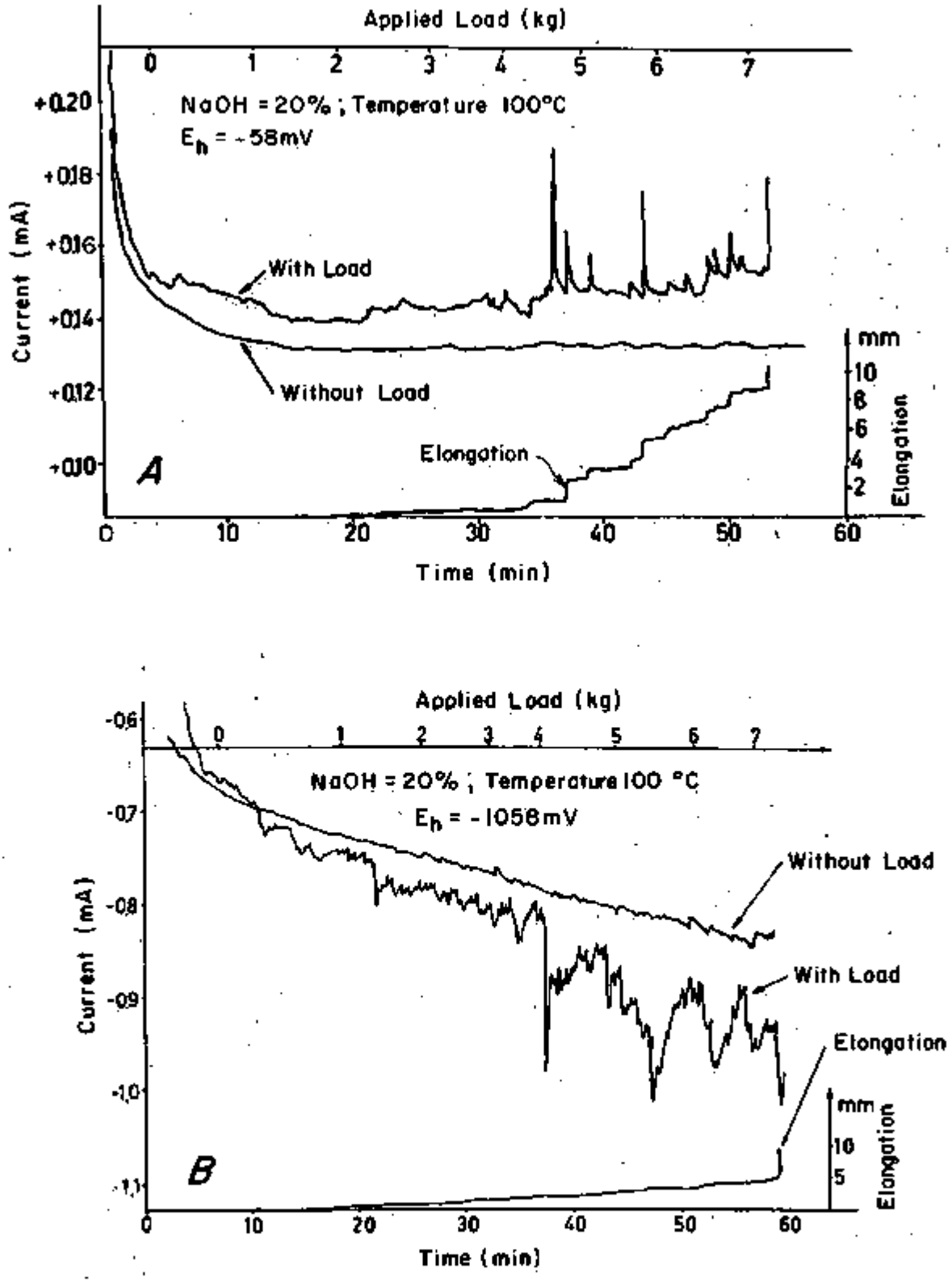

Fig. 12 - Current-time response curves for steel in boiling NaOH solution.[30]

9. Crack Growth Rates

The crack-growth rates for steel in boiling sodium hydroxide were measured using the following technique :[26] Specimens were loaded with 4.27×10^4 psi at a potential of -700 mV_H. The specimens were removed prior to fracture, maximum crack depth determined, and plotted as function of time as shown in Fig. 13. These results show that the cracks grow continuously. The acceleration of crack-growth with increasing stress obeys the following relationship:

$$\frac{dr}{dt} = -k\left[(\sigma(t) - \sigma_o\right] = -k\left(\frac{L}{\pi r^2 t} - \sigma_o\right) \qquad (4)$$

where r is the radius of the remaining cross section, k the rate constant, σ_o the lower limiting stress, and L the load.

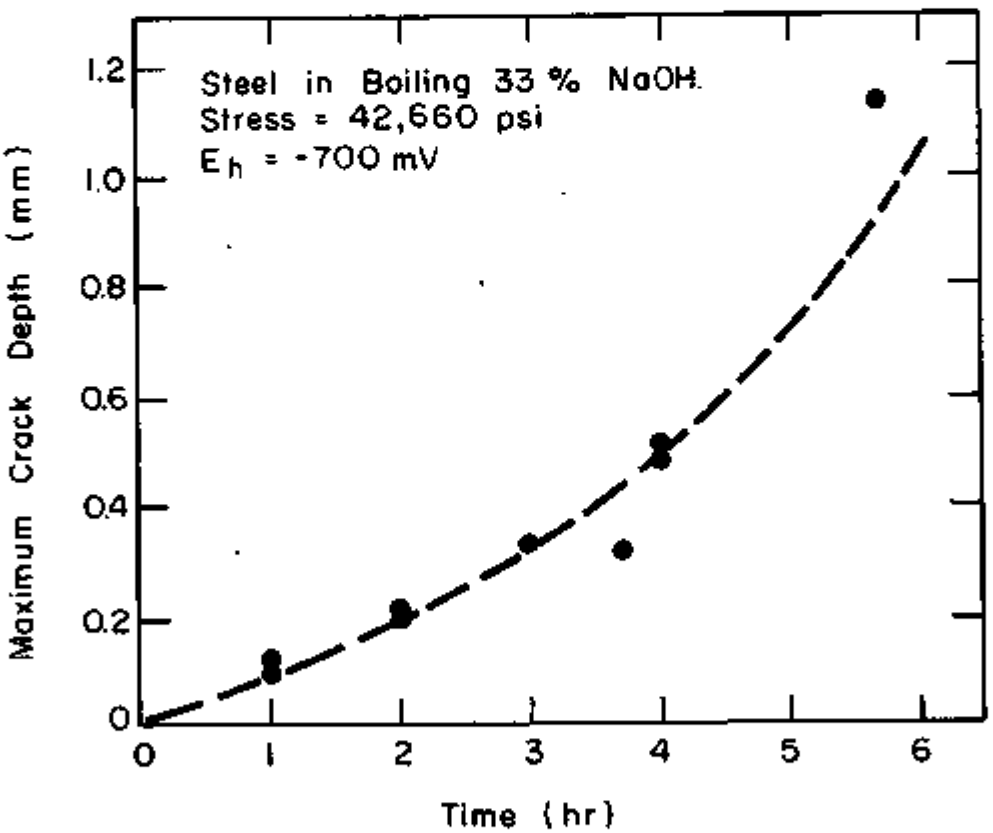

Fig. 13 - Maximum crack depth as a function of time.[26]

10. Properties of Oxide Films

The behavior and properties of the oxide films appear to be crucial to the onset of SCC for steels in caustic environments. The potential-pH diagram of Fig. 1 for iron shows that two oxides may exist depending on pH and potential. Fe_3O_4 can form at lower potentials and Fe_2O_3 at higher potentials.

The most extensive study of oxide films relative to their role in SCC has been conducted by HUMPHRIES and PARKINS.[34] They obtained x-ray powder photographs of oxide films formed over a range of potentials. At -710 mV_H, they obtained a Fe_3O_4 structure as predicted by Fig. 1 (a = 8.934Å); and at -50 mV_H they found a Fe_2O_3 structure (a = 8.355 Å). In the intermediate range the structure of oxides did not correspond to any of the above compositions. It is probable that between Fe_2O_3 and Fe_3O_4 iron oxides of steadily increasing ferric iron content might form.

Thin films formed on exposure to boiling 35% sodium hydroxide were examined by transmission electron microscopy.[34] Films obtained in the critical potential range where cracking occurred were comprised of square platelets. Selected area diffraction showed a high degree of preferred orientation among the platelets. The Fe_3O_4 film that was comprised of these platelets contained large number of holes or pores between some of the platelets, the pores frequently joining to form a continuous fault within the film. Films formed at -360 mV_H contained very small crystallites (0.2-0.4μ) having angular characteristics but without any obvious specific shape. The crystallites were more randomly oriented than were the platelets in the Fe_3O_4 film, but there were fewer pores apparent in the Fe_2O_3 film. At times stripped Fe_3O_4 films showed a network of holes corresponding to grain boundaries in the underlying metal; but it was difficult to discern whether these holes were produced in stripping the film or were indicative of the grain boundary regions. On straining these films, a network of cracks formed in positions corresponding to these grain boundaries of the metal surface, while additional cracks, roughly parallel to one another and normal to the principal tensile stress, developed over the grain surfaces.

Based on the above observations it can be concluded that: (a) Oxide films function in blocking the initiated cracks, and cracking in hydroxides occurs in the presence of Fe_3O_4 but not Fe_2O_3. (b) The straining of specimens coated with oxides at various potentials results in increased anodic current within the range of potentials wherein cracking occurs for hydroxide solutions. The magnitude of this increase is considerably greater than could be accounted for on the basis of the area of the unfilmed metal produced by the film rupture, and this difference could possibly be due to the fact that metal dissolution is enhanced by plastic strain. (c) The fact that cracking occurs only within the restricted range of potentials is most readily accounted for by the suggestion that cracking is associated with the formation of readily soluble iron, the range of potentials for cracking agreeing reasonably with that for the formation of $HFeO_2^-$.

11. Effect of Hydrogen on Caustic SCC

The negative potentials at which caustic SCC is most virulent suggest the possible alternative that hydrogen uptake may be the causative factor.

ROBINSON and NEL[35], based on mechanical tests with hydrogen charged steel specimens and PODGORNY[36] by his voltage-time behavior of the iron electrode in sodium hydroxide with and without sodium nitrate, tried to show that hydrogen uptake and subsequent embrittlement is a responsible factor for failure of steel in alkalis.

ROBINSON and NEL[35] studied the effects of hydrogen cathodically charged into alloys from caustic environments. They presumed that a key factor in the mechanism of caustic cracking was the hydrogen uptake and subsequent embrittlement. They performed various mechanical tests on the charged materials considering such variables as steel composition, applied stress, test temperature, caustic concentration, and deliberately added impurities. The hydrogen charging did not affect the upper yield strength, lower yield strength, and ultimate strength. Both the reduction in area at elongation were considerably reduced.

Notched bar bend tests revealed a diminution of the maximum load and amount of energy absorbed during bending as the charging time is increased. Susceptibility to caustic cracking decreases with temperature in the range 210-240°C. Cracking appears to be sensitive to even small changes in the chemical composition of the steel. Zone refined iron specimens remained unaffected after exposure to the most severe cracking conditions.

The effect of sodium nitrate addition to a caustic environment with respect to determining the open circuit potential of steel was investigated by PODGORNY.[36] His hypothesis was that conditions favoring lower potentials also favored cracking and that this indicated that hydrogen entering into the alloy was the causative agent in caustic cracking. The base solution used was 20% sodium hydroxide with 0.56 g/l sodium silicate and 0.2 g/l sodium chloride. When the 8% nitrate was added, the potentials rose significantly into the region where cracking did not occur; without this addition the potential remained active and was in the range where caustic SCC occurred. The conclusion that hydrogen was, therefore, a caustive agent based on the experiments is totally unfounded. There are too many other possible explanations of such observations.

12. Additives to the Caustic Environments

Anodic inhibitors have been extensively investigated for preventing stress corrosion. Among the most extensively investigated inhibitors are silicates, phosphates, sulphates, nitrates, carbonates, etc. The preventive methods has been studied by SCHROEDER and BERK,[18] RATH,[24]

PARTRIDGE et al.,[37] RADEKAR and GRAFEN,[38] WEIR,[39,40] and POCHEPTSOVA and TIMCHENKO.[41] Very recently HUMPHRIES and PARKINS[33] investigated the effects of adding various inhibiting and noninhibiting compounds.

The detailed investigations of SCHROEDER and BERK[19] considered particularly the effects of silicate at different stress and hydroxide concentrations. For instance, Table I shows that silicate exerted beneficial effect at low hydroxide concentrations. On the other hand, Table II shows synergistic effects of mixtures of hydroxide with carbonate, chloride, silicate, and alumina. It is clearly demonstrated that only introduction of silicate to mixtures of $CO_3^=$, Cl^-, and Al_2O_3, or singly, to hydroxide alone causes failure.

Table II - Failure of Steel Specimens in Solutions Containing Sodium Silicate and Sodium Hydroxide (SCHROEDER and BERK)[19]

Temperature, 250°C. Average Applied Stress, 70,000 psi. NaOH Concentration, 25 g/100 g H_2O.

Added Salts	g/100 g H_2O	Failure Time, hr
Na_2CO_3	0.5	96, 144 NF[d]
NaCl	0.13	
Na_2CO_3	0.5	168 NF[d]
NaCl	0.13	
Al_2O_3[a]	0.05	
Na_2CO_3	0.5	34[c]
NaCl	0.13	
Al_2O_3[a]	0.05	
Na_2SiO_3[b]	0.2	
Na_2CO_3	0.5	21
NaCl	0.13	
Na_2SiO_3[b]	0.2	
Na_2SiO_3[b]	1.5	77

[a]Added as aluminum chloride

[b]Baker's water glass 40% solution, used to introduce silica into bombs

[c]Failure at shoulder

[d]NF = no failure

Table III shows that adding a small amount of silicate accelerates SCC in caustic but as the amount added increases cracking is retarded.

Table III - Effect of Stress and Sodium Silicate Concentration on the Failure of Concentrically Ground Specimens (SCHROEDER and BERK)[19]

25 g/100 g H_2O; Temp., 250°C

Average Applied Stress (psi)	Na_2SiO_3, g/100 H_2O	Failure Time (hr)
70,000	0.077	240 NF[c]
70,000[a]	0.15	32
70,000	0.40	44
70,000	1.7	10
70,000	5.0	8
70,000	10.0	135
70,000	10.0	80
60,000[a]	3.0	135
60,000	3.0	120
55,000	0.16	240 NF
55,000[a]	0.16[b]	152

[a]Failure at shoulder

[b]Solution also contained 0.5 g Na_2CO_3 and 0.11 g NaCl/100 g H_2O Baker's c.p. sodium silicate ($Na_2SiO_3 \cdot 9H_2O$) used to introduce silica into bombs

[c]NF = no failure

PARTRIDGE et al.,[37] by using the embrittlement detectors and by counting the number of specimens not failed, could establish that silicate had inhibitive effects.

RADEKAR and GRAFEN[38] showed that bubbling oxygen through the solution also prevents cracking. The maintenance of sulphate-to-hydroxide ratio > 2.5 is still practiced as a means of preventing caustic cracking; presumably there is much experience of boilers not failing under these conditions. However, the statistical evidence of WEIR[39] shows no benefit to be derived from maintaining a high sulphate-to-hydroxide ratio and there is ample practical experience of cracking in boilers where the water conditions have met the specified minimum ratio. The evidence in support of the sodium nitrate and coordinated phosphate[40,24] treatments for the prevention of caustic cracking in boilers

is more convincing, although it is by no means universally accepted that nitrate treatment is completely effective or that the use of tannins for the same purpose may be regarded as established without doubt. During their tests on a carbon steel in autoclaves at 140°C, POCHEPTSOVA and TIMCHENKO[41] could obtain an effective reduction in corrosion rates under stress by manipulating the ratio of chloride plus carbonate to hydroxide < 0.5. They observed a corrosion rate of 48 mils/year without inhibitors. On addition of chloride and carbonate maintaining the above ratio, they found that the corrosion rates were 2 mils/year with polished specimens (without oxide) and 4 mils/year with unpolished specimens (with oxide).

HUMPHRIES and PARKINS[33] have studied the effects of additives on the percent reduction in area as a function of potential. A strain rate of 4.2×10^{-6}/sec was used. The compounds having inhibitive effects were added to maintain a concentration of 15% ($NaNO_3$, Na_2SO_4, NaH_2PO_4, valonea and quebracho), or saturated solutions. Those having accelerative effects were added in 0.2% by weight. The results are summarized in Fig. 14. The PbO, Pb_3O_4 and ZnO are without effect, as is the deaeration of the solution by the continuous bubbling of nitrogen gas. Quebracho and valonea tannins and NaH_2PO_4 completely inhibit cracking. The results with 5% silicate indicate that oxygen does have a partial inhibitive effect in agreement with RADEKAR and GRAFEN S[38] findings. From Fig. 14, it can be noted that $SO_4^=$, $NO_3^=$, and $KMnO_4$ have no marked inhibitive effect upon cracking, and are capable of producing intergranular or brittle fractures depending on the potential region, although they shift the potential of minimum for cracking.

Potential-time curves were obtained with the above additives at a constant strain rate and these results are summarized in Fig. 15. With $NO_3^=$, Pb_3O_4 and $KMnO_4$ the potentials were shifted to more noble values and intergranular cracking was observed. With 0.25% PbO the potential was still noble, in which case they observed long, very fine, and branched cracks. Specimens tested in solutions to which Na_2SO_4 or ZnO were added showed short intergranular cracks but fracture was accompanied by an appreciable reduction in the area. The specimens tested in silicates had neither visible cracks nor oxide film due to their potentials being in the critical potential range. With quebracho added, the specimens showed transgranular cracks to a depth of about 10μ and at intervals of 20μ.

GRAFEN and KURON[31,32] have shown evidence for the possibility of anodic protection of steels in caustic environments.

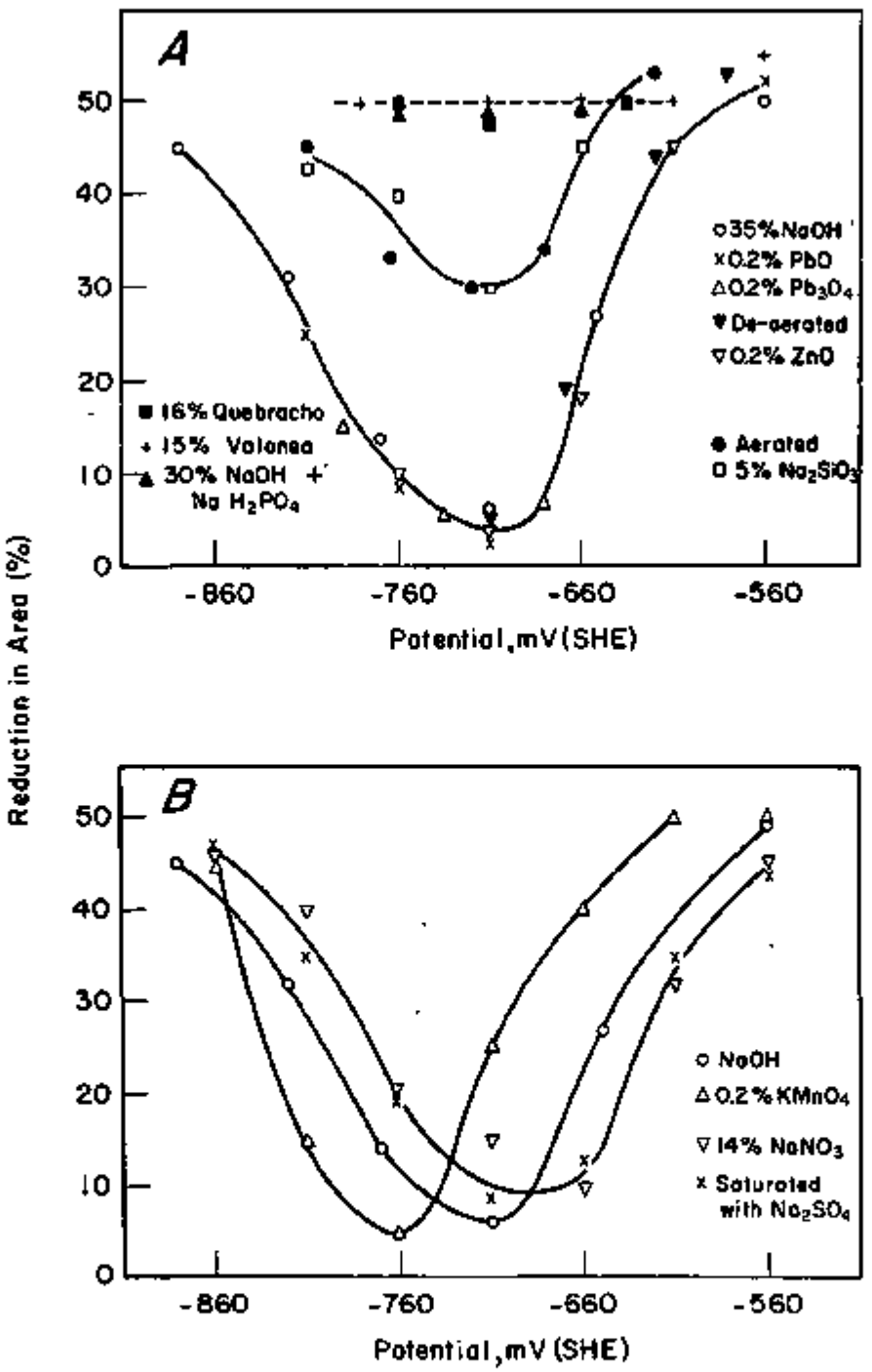

Fig. 14 - Effects of additives on per cent reduction in area (strain rate = 4.2×10^{-6}/s).[33]

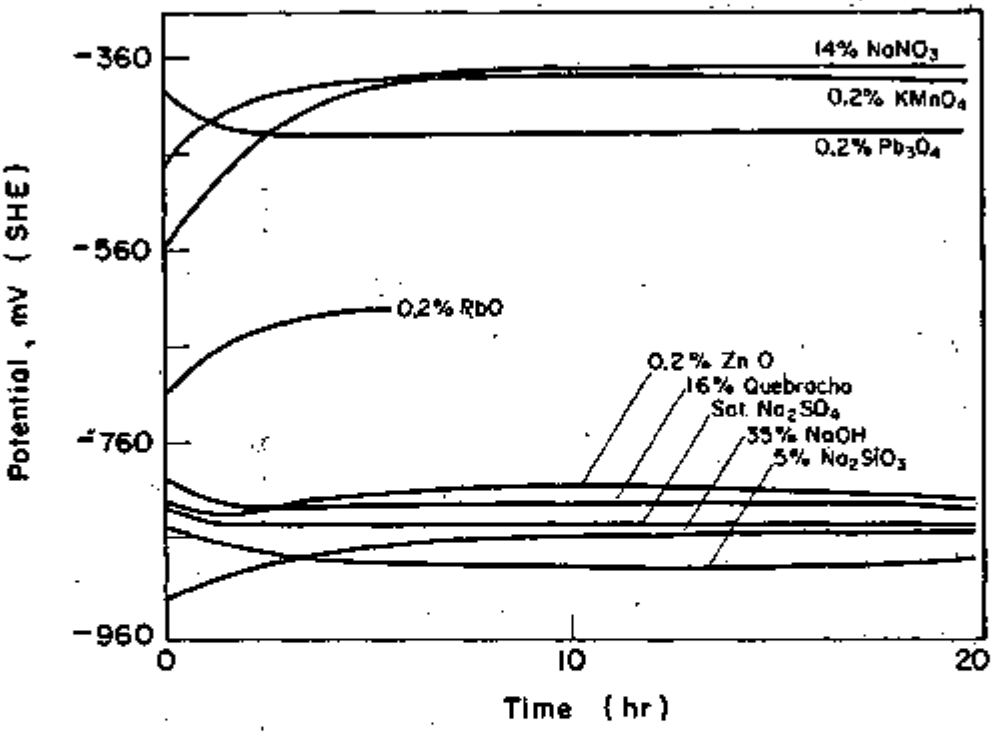

Fig. 15 - Potential-time curves for mild steel at a constant strain rate (4.2×10^{-6}/s) in boiling 35% NaOH containing various substances.[33]

B. GENERAL CORROSION OF IRON IN CAUSTIC ENVIRONMENTS

When compared to the stress corrosion cracking of iron, the general corrosion of the iron system has been more extensively studied. The published literature contains information on corrosion rates in various hydroxide media, properties of corrosion products, inhibition and electrochemistry. Consideration of general corrosion provides an important basis for understanding the conditions for the onset of stress corrosion cracking. This section will describe both the over-all corrosion rate phenomena as well as current knowledge of the structure and properties of protective films, and electrochemical aspects of uninhibited and inhibited systems.

1. Corrosion Below 100° in Sodium Hydroxide

The corrosion rates below 100°C has been studied by MASLOV and GERMAN,[42] and SAKWA and MARCINKOWSKA.[43] There has not been as much work on corrosion below 100°C as above 100°C.

The corrosion rate of the base metal of the st.3Kp steel (C 0.18, Si 0.02, Mn 0.38, Cr 0.06 and Ni 0.04%) in sodium hydroxide solutions of concentrations below 20% was measured[42] and it was observed that the rate is independent of temperature between 26-60°C. The maximum corrosion rate under these conditions was 0.17 mils/year. The maximum corrosion rate of a welded seam (C 0.10, Si 0.11, Mn 0.52, traces of Cr and Ni 0.06 per cent) under similar conditions was 0.3 mils/year. The corrosion rate increased sharply at > 30% sodium hydroxide; and at 100°C the maximum corrosion rate was 22 mils/year.

SAKWA and MARCINKOWSKA[43] studied the mechanical properties of gray cast iron, containing C 2.41, Si 1.33, Mn 0.66, P 0.11 and S 0.081% after immersing in 4.6-85% aqueous solutions of sodium hydroxides at room temperatures to 70°C and reported the incidence of pitting corrosion.

2. Corrosion Rates Above 100°C in Sodium Hydroxide

MUKAIBO and MASUKAWA,[44] MASAMICHI and SABURO,[45] THORNHILL[46] (0.001% to saturated NaOH) and ASAI and KAWASHIMA[47] have studied the corrosion behavior of iron in autoclaves.

In the range of 300-350°C, the corrosion rates increase with increasing sodium hydroxide concentration and temperature.[44,45] At low temperatures the corrosion rates are independent of concentration in the concentration range of 0.1-4%.[46] This value of 4% is in agreement with the concentration required to produce stress-corrosion cracking, which is above 5%. THORNHILL[46] further reports that the greatest rate of attack occurred in the concentration range of 50-70% NaOH. Using hydrogen effusion methods to measure corrosion rates ASAI and KAWASHIMA[47] reported complex effects of NaOH. They found that the corrosion rates remained almost constant up to 15% sodium hydroxide but

rapidly increased with further increase in the concentration at 300°C. When the concentration was as high as 40%, the corrosion rate decreased at first until a minimum was reached and then again started increasing rapidly with increasing concentration.

The corrosion rate decreased when oxygen was added to 0.4 to 4.0% NaOH solutions at 310-350°C.[44] This behavior could be probably explained by the effect of oxygen in raising the potential in the range where films are more stable.

3. Structure and Properties of Oxide Films Formed in Sodium Hydroxide Solutions

From Section C-1 it is clear that the incidence of stress corrosion cracking in caustic environments depends on the properties of the protective film of reaction products covering the metal. The structure and properties of such films in sodium hydroxide has been studied by POTTER and MANN,[48] CASTLE and MANN,[49] FRASER et al.,[50,51] KATO and ARAI,[59] and KRUGER et al.[53] The highlights of their investigations were as follows: (i) films on the iron surface are multilayered; (ii) growth kinetics are controlled by the inner layer (Fe_3O_4); (iii) there is an epitaxial relationship of the film to the iron substrate; and (iv) films include γ-FeO·OH, α-Fe_2O_3, and Fe_3O_4 mixtures having orthorhombic, hexagonal and cubic structures, respectively, in weak solutions of sodium hydroxide containing other anions.

In the experiments with mild steel in 5-20% hydroxide at 250-355°C the existence of multilayered oxide film over the corroded surface is convincingly demonstrated by POTTER and MANN,[48] and their results are summarized in Fig. 16. In Fig. 16 the corrosion rates were plotted against square root of time. From Fig. 16a and b it can be noticed that corrosion rates increase lineraly with time. The oxide formed under these conditions has three layers, one which adheres to the metal surface, an inner layer, and an outer layer. The growth rates of these layers are summarized in Fig. 16c. Their thicknesses are in the ratio outer:inner:adherent = 1:4:5. This structure and ratio remained constant at all temperatures and solution compositions studied.

CASTLE and MANN[49] conducted experiments to elucidate the mechanism for the formation of the multilayered oxide. It appears that the adherent layer is sufficiently unstable that iron ions dissolve therefrom but, at the same time can precipitate on oxide nuclei generated outside the surface of the adherent oxide. The solubilization and reprecipitation depend on local changes in pH and solubility of iron ions. Essential features of this process are epitomized in Fig. 17. CASTLE and MANN showed that the formation of the films is greatly dependent on flow of the solution. This verifies that the dissolution and precipitation process is related to subtle compositional gradients in the solution near the corroding surface.

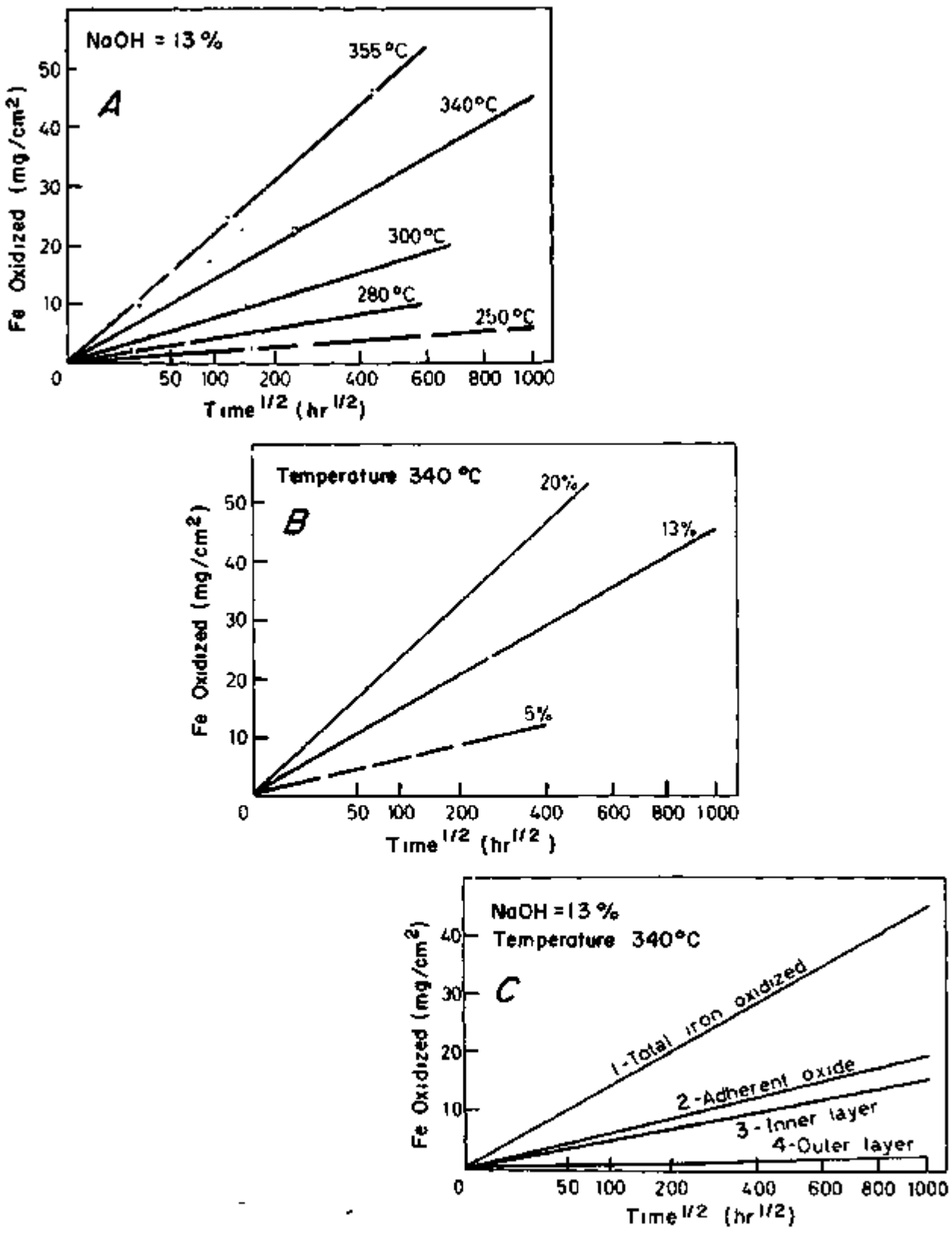

Fig. 16 - (a) Effect of temperature on corrosion rates, (b) effect of NaOH concentration on corrosion rates, (c) distribution of oxidized iron after oxidation of mild steel with time.[48]

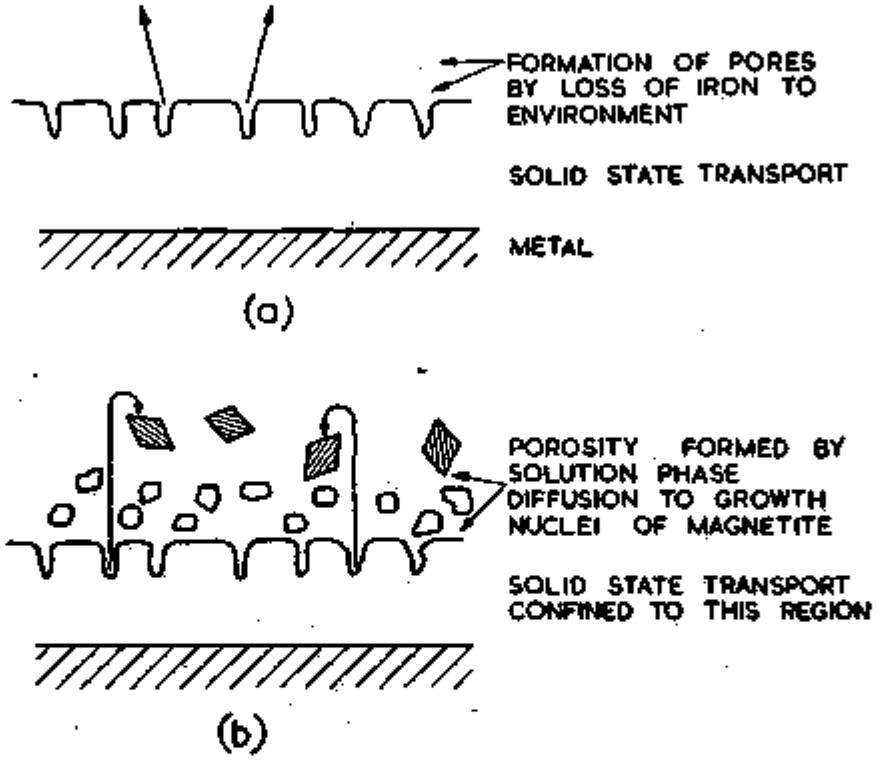

Fig. 17 - Illustration of successive stages in the production of the two-layered magnetite film on steel.[45]

The corrosion of mild steel in 40% NaOH at 316°C was investigated by FRASER et al.,[50,51] using the hydrogen effusion method. They also examined the morphology of the resulting oxide films and found that a compact oxide film would grow but severe pitting often occurred below this film.

With further experiments in 15% sodium hydroxide at 316°C FRASER et al.,[50,51] could show that two different rate-governing mechanisms are involved prior to the onset of pitting; (a) a large decrease of the initial rate controlled by the buildup of a protective film on the metal surface and (b) a subsequent small decrease in corrosion rate possibly controlled by penetration of the magnetite film by the corrosive solution. Figure 18 shows that their results could be fitted by an equation of the form:

$$y = y_o + k_1 \log [1 + k_2 (t-t_o)] \qquad (5)$$

where y = total penetration, t = time, and k_1 and k_2 are constants. It can be noted that there is an agreement between POTTER and MANN,[48,49] and FRASER'S thoughts concerning the growth kinetics of oxides of iron. However, Fraser's experiments are insufficient to show the existence of multilayered oxides.

KATO and ARAI[52] examined the morphology of oxide films using transmission electron microscopy and the crystal structure by reflection and diffraction patterns. When 10^{-3} N sodium and ammonium hydroxide containing 10^{-2} N ammonium chloride were saturated with oxygen, the oxides formed at 150 and 200°C were composed of mixtures of α-Fe_2O_3, Fe_3O_4 and γ-FeO·OH, having hexagonal, cubic and orthorhombic structures, respectively. When 0.01-0.1N sodium hydroxide and ammonium hydroxide were saturated with oxygen, then only mixtures of Fe_3O_4 and Fe_2O_3 were produced. This conforms to the findings of MANN and CO-WORKERS.[48,49] When the above solutions contained 10% each of KCl and KI saturated with hydrogen, the oxide films after three hours at 200°C were always composed of pure Fe_3O_4. The hydrogen undoubtedly operated to keep the Fe_2O_3 reduced.

KRUGER et al.,[53] examined orientation relationships between the oxide on {100}, {110}, {111}, {210} and {211} orientations of single crystals and metal substrate for specimens exposed in 0.1N NaOH at 25°C. They found that the Fe_3O_4 films formed in the prepassive on transpassive regions of the polarization curve on these single crystals showed an epitaxial relationship to substrate in all orientations except the {110} plane.

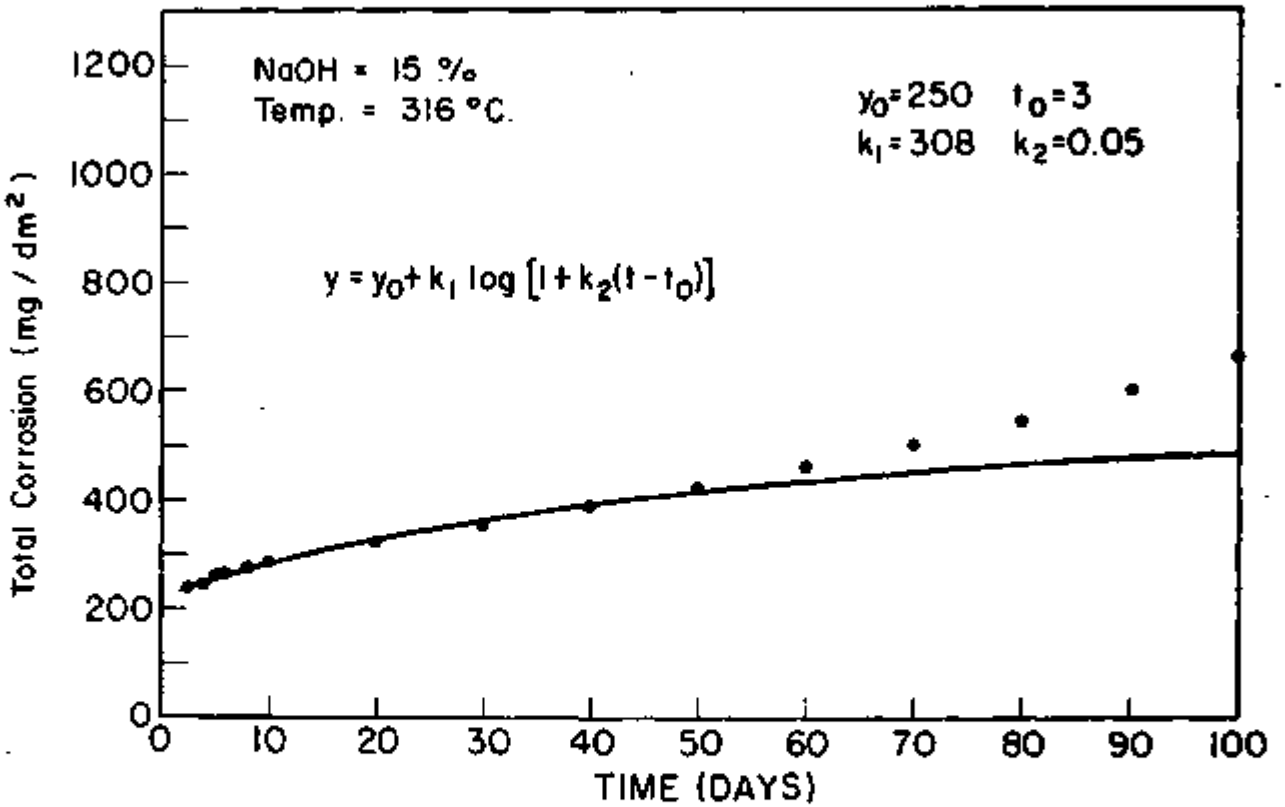

Fig. 18 - Corrosion of mild steel capsules containing 15% NaOH at 316°C.[51]

4. Corrosion of Iron and Properties of Oxide Films on Iron in Alkali Metal Hydroxides of Potassium, Lithium, Rubidium and Cesium

In the previous section the corrosion behavior of iron in sodium hydroxide solutions has been considered. Now, attention will be given to the corrosion behavior of iron or steel in hydroxide solutions of potassium, calcium, lithium, rubidium and cesium and studies on corrosion products. Corrosion in potassium hydroxide solution has been studied by LIEPINA et al.,[54] in calcium hydroxide by SHALON and RAPHAEL,[55] in lithium hydroxide by KRATZER,[56] BLOOM et al.,[57,58] ASAI and KAWASHIMA.[59] Relative aggressiveness of this metal in alkali metal hydroxides and corrosion products in these and mixtures of hydroxides has been studied by ASAI and KAWASHIMA,[60-63] and KOWAKA et al.[64] Noteworthy features in these studies are: (i) corrosion rates increase with increasing atomic weight of the cation, (ii) morphology of corrosion products are identical to those obtained in sodium hydroxide, and (iii) spiral steps were observed on {111} planes on the outer crystal surface of the oxide.

LIEPINA et al.,[54] have studied the corrosion products in 0.1N potassium hydroxide and 0.1 potassium hydroxide plus 1N potassium chloride. Below pH 11, γ-FeO(OH) and γ-lepidocrocite (modification of geothite) and above pH 11 α-FeO(OH) (goethite) having orthorhombic structures have been identified. The transition between γ- and α-FeO(OH) is accompanied by changes in the absorptive power of the hydroxide and a reversal in the particle charge.

SHALON and RAPHAEL[55] studied the behavior of mild steel in calcium hydroxide solutions and found that the corrosion decreases gradually with increasing pH until inhibition starts.

KRATZER[56] has described the potential problem when lithium hydroxide is used for controlling the reactor coolant pH. They predict the increased damage to corroded steam generator tubes resulting from lithium hydroxide concentration in the defects.

BLOOM et al.,[57,58] have studied the corrosion of mild steel in in lithium hydroxide solutions at 316°C. Figure 19 shows the corrosion rate-time curves of mild steel in a capsule containing 28.5% lithium hydroxide. The corrosion rate decreased in the early stages as the protective film developed and then rose sharply after passing a minimum value and once again passivated after nine days. The acceleration of attack was accompanied by a partial destruction of the protective magnetite film and the occurrence of a nonadherent brown powder. Four different oxide phases are generated depending on the lithium hydroxide concentration. At concentrations below 0.5%, only an adherent protective spinel-structured film is generated. At a concentration range of 1-4.5%, an adherent tight film is formed. It consists of a spinel next to the steel and a low temperature form of $LiFeO_2$ over the spinel.

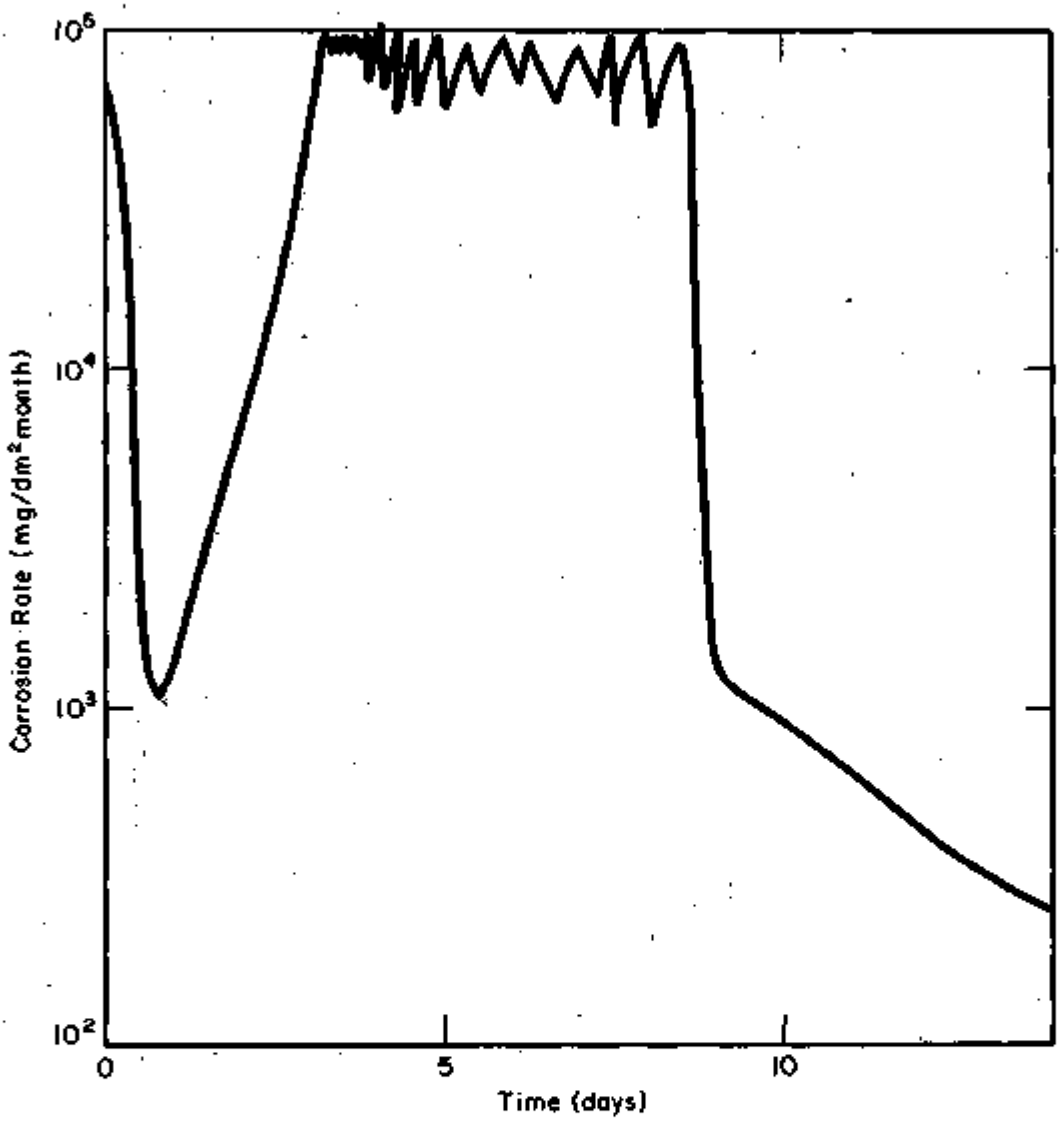

Fig. 19 - Corrosion rates of mild steel in 28.5% LiOH at 316°C.[57]

The spinel structure contains lithium and in a solution of 4.5% lithium hydroxide, gives the x-ray pattern of lithium saturated spinel $LiFe_5O_8$. Above 5%, a corrosion product film of high temperature $LiFeO_2$ is identified. Lithium hydroxide is consumed by the following scheme of reactions:

$$Fe + LiOH + H_2O = LiFeO_2 + 3/2\ H_2 \qquad (6)$$

$$Fe_3O_4 + 3\ LiOH = 3\ LiFeO_2 + H_2O + 1/2\ H_2 \qquad (7)$$

$$5\ Fe_3O_4 + 3\ LiOH + H_2O = 3\ LiFe_5O_8 + 5/2\ H_2 \qquad 8)$$

ASAI and KAWASHIMA[59] reported that the rate of corrosion at 300°C decreases generally with increasing time when the lithium hydroxide concentration is below 0.7N. When the concentration is greater than 1N, a minimum and maximum of corrosion rate appear within 100 hours after beginning of the corrosion experiment. When the concentration is greater than 0.5N, $LiFeO_2$ and Fe_3O_4 are formed. The rate of corrosion follows a parabolic law for less than 0.3N lithium hydroxide. Their results are summarized in Fig. 20.

In a comparative study with the hydroxides of Na, K, Rb, and Cs at 300°C and above 1N solutions ASAI and KAWASHIMA[61] established that the aggressiveness was in the order: Na < K < Rb < Cs. Increase of corrosion rate is observed with increasing atomic weight. Also, the corrosion rates in dilute solutions (less than 0.1N) obeyed the cubic law and in solutions between 0.1N and 1N, a linear law.

KOWAKA et al.,[64] contrary to ASAI and KAWASHIMA[61] observed that NaOH solutions are more aggressive than KOH solutions.

ASAI'S[60] investigations of steel corrosion in various alkali metal hydroxides support the existence of multilayered oxides at low concentrations. Alkali metals are present in the outer layer crystals as a solid solution. The concentration of these alkali metal atoms in solid solution in the outer layer increases with the increase in the ionic radius of the alkali metal. The lattice constant of the outer layer crystals is related directly to the ionic radius of the alkali metal as shown in Fig. 21. The effect is larger with the increase in the ionic radius of the alkali metals. He also observed spiral steps on the 111 plane on the outer surface of the oxide indicating that these crystals grow by the deposition from the solution. The iron necessary for the growth was supplied by the dissolution of the inner oxide layer. Their findings are similar to observations of MANN and CO-WORKERS[48,49] in sodium hydroxide solutions.

Addition of small amounts of lithium hydroxide to the sodium hydroxide solutions (greater than 5N) at 300°C, reduced the corrosion rates. This effect observed by ASAI and KAWASHIMA[62] has been attributed

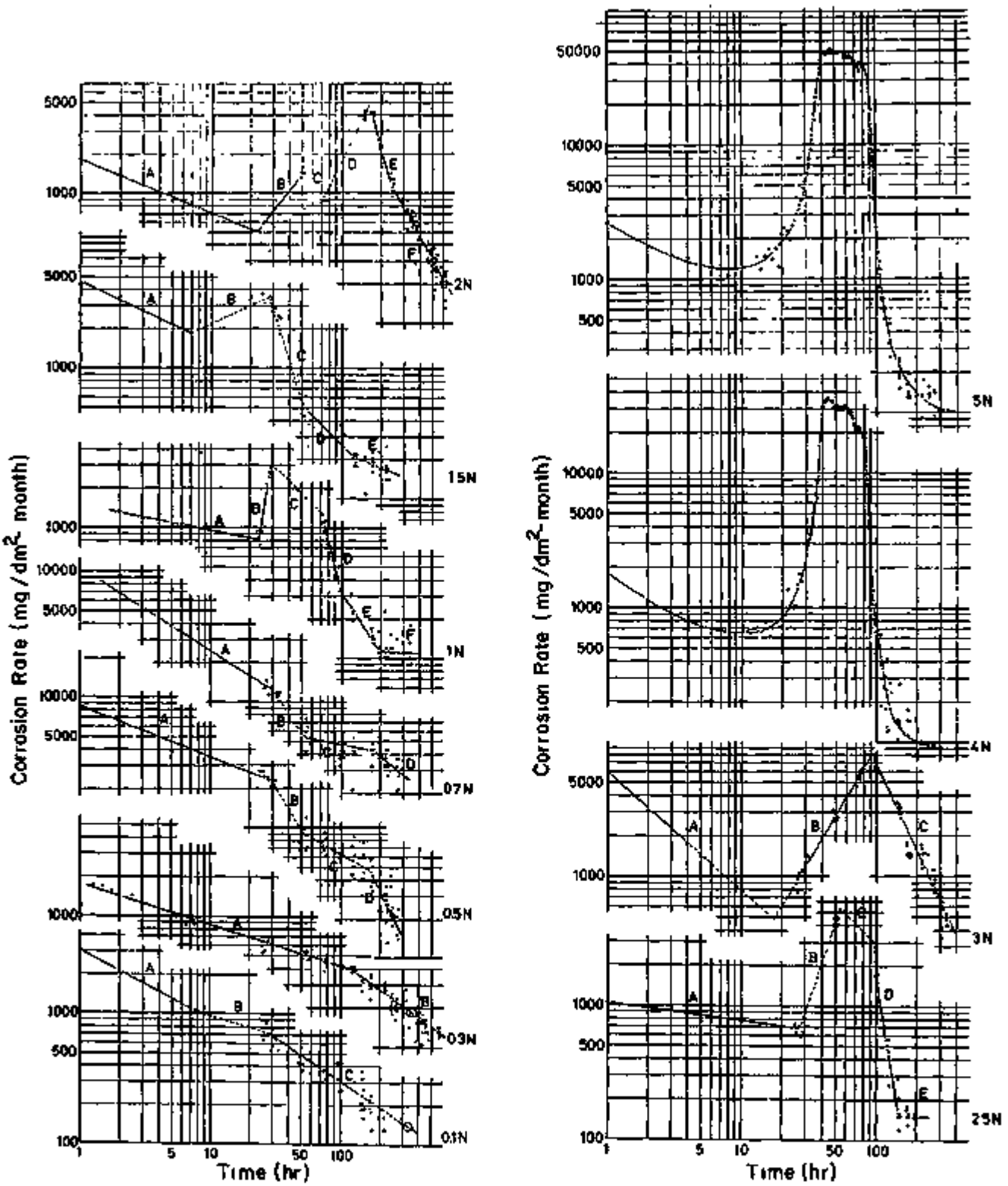

Fig. 20 - Corrosion rates in LiOH solutions at 300°C.[59]

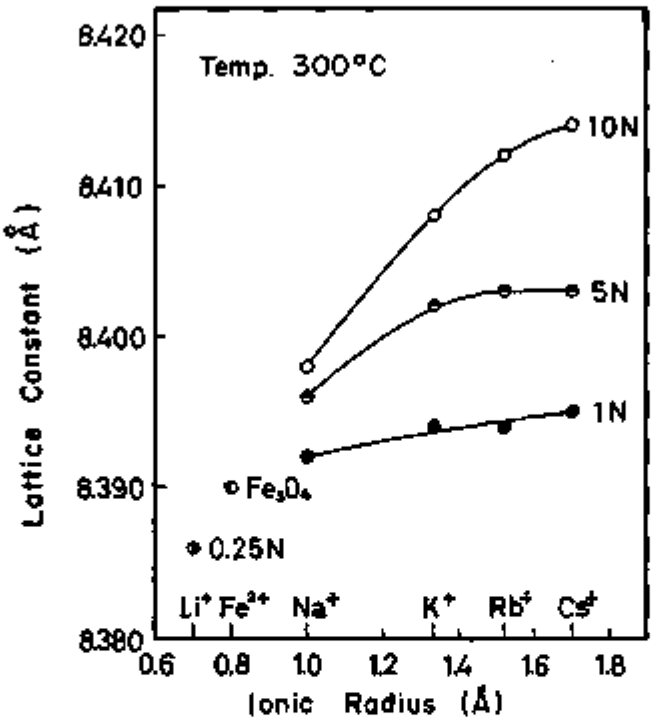

Fig. 21a - Plot of lattice constant (Å) of oxide containing alkali metal in outer layer against ionic radius of alkali metal.[60]

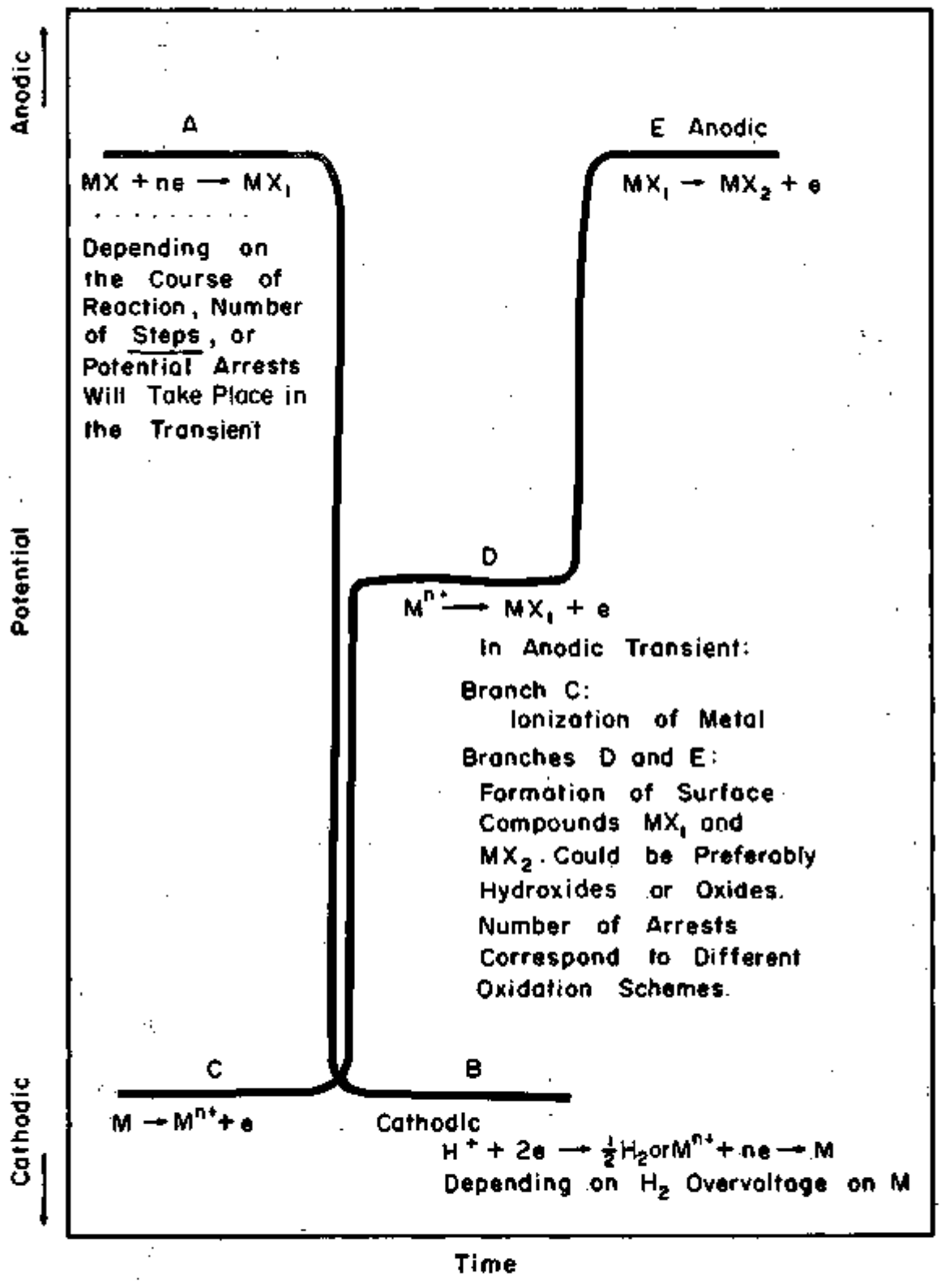

Fig. 21b - Schematic potential-time curves indicating the possible processes in transients.

to the lattice defect reduction in the dense inner layer caused by the dissolution of lithium into the layer forming a solid solution. In the above mixed solution, they observed a parabolic law. Similar effects of lithium hydroxide on corrosion in potassium, rubidium and cesium hydroxides were observed by these authors.[69] Corrosion rates obeyed the following laws for the above solutions:

(i) Corrosion rates $\propto t$ at low concentrations of caustic

(ii) Corrosion rates $\propto t^3$ at high concentrations

where t is the time. These rate laws are similar to those observed by ASAI and KAWASHIMA[61] in the respective solutions of hydroxides.

5. Polarization Behavior without Inhibitors

Polarization measurements have been used on iron base alloys in caustic solutions to study the cathodic and anodic behavior. In studies of cathodic behavior investigations have been carried out to study (i) the kinetics of reduction of reducibles such as H_2O and O_2 and (ii) the diffusivity of hydrogen in membrane electrodes. The anodic behavior has been studied under three different categories; namely, (i) active iron electrode, ($Fe \rightarrow Fe^{++} \rightarrow 2e$ or $Fe + 2H_2O \rightarrow HFeO_2^- + 3H^+ + 2e$ reactions), (ii) passive state kinetics, and (iii) destruction of the passive state by aggressive anions.

a. Studies in sodium hydroxide media - The kinetics of water reduction have been studied by AMMAR and AWAD,[65] Hurlen,[66] and BAGOTSKAYA.[67] The interesting features in these studies were that pH-independent cathodic reaction slopes resulted in the pH range 11-14 and polarization values depended on diffusion velocity.

The essential reduction reaction involved is

$$2e + 2H_2O \rightarrow 2OH^- + H_2 \qquad (9)$$

and the thermodynamic description of this equilibrium is line (a) in Figs. 1-3. The rate of this reaction in the cathodic direction obeys the general expression for activated kinetics

$$i_c = K_c \left[a_{H_2O}\right] e^{-\frac{\Delta G^*}{RT}} e^{-\frac{2F}{RT}(1-\alpha)E} \qquad (10)$$

where i_c = cathodic current density, K_c = rate constant for cathodic reaction, a_{H_2O} = activity of water molecules at the cathode surface, ΔG^* = energy of activation for the cathodic reaction, R = gas constant, T = temperature in °K, z = charge on the activated species, F = Faraday,

α = energy transfer coefficient and E = potential against the standard hydrogen electrode.

As the forthcoming sections will consider voltage-time behavior, it is worthwhile to describe briefly the utility and interpretation of these curves. The potential-time curves can be either on open-circuit or by passing currents. Potential transients can provide a direct insight into the mass transfer processes. A change in the electrochemical process can produce potential arrents. A potential-time curve can be a useful tool in cathodic region to analyze the reduction of passive layers, and hydrogen or metal deposition if the hydrogen overvoltage is quite large when compared to metal reduction potential. In the anodic region a potential transient can be used to detect the onset of passivity, formation of passive layers and oxygen evolution potentials.

Taking the concrete example of the Fe-H_2O system, the potential-pH equilibrium diagram for which is given in Fig. 1, the possible cathodic reactions are the reduction of higher oxide (namely, Fe_2O_3 to Fe_3O_4) and then to metallic iron. At this stage, if the solution contains Fe^{++} or Fe^{+++} ions in the solution, Fe deposition takes place on the surface. On the other hand, if oxygen is present, the reduction of molecular oxygen will take place at the interface. In the absence of Fe or O_2 in the system, the hydrogen reduction will take place. Reverse processes operate on the anodic branch in the following sequence: ionization of Fe to Fe^{++}, formation of $Fe(OH)^{++}$ or $HFeO_2^-$ ion, and oxidation to Fe_2O_3 via Fe_3O_4. O_2 and H_2 ionization also will take place if these are present in the solution phase. All these processes are potential- and pH-dependent and are discussed at relevant stages. A potential transient is supposed to show potential arrests in the above-mentioned sequence. Figure 21a depicts the schematic sequence of potential arrests in the cathodic and anodic regions, respectively.

AMMAR and AWAD[65] have studied the reduction of water ($H_2O \rightarrow OH^- + \frac{1}{2} H_2$) in 0.2, 0.5, and 1N sodium hydroxide at 25°C. The cathodic tafel plots are given in Fig. 22. They found values for $2.3\ RT/zF(1-\alpha)$ of 120-130 mV per decade which is in accord with $z = 1$ and $\alpha = 1/2$. From this figure, it can be noted that the slopes do not depend significantly on pH. HURLEN[66] has observed similar pH independent cathodic reaction slopes. Using membrane electrodes, BAGOTSKAYA[67] studied the effects of diffusing hydrogen through a membrane, the surface of which is exposed in 5N sodium hydroxide solution, and found that diffusion velocity had some effect on the polarization values.

The active iron electrode has been studied by HURLEN[66] and SCHULDINER and SHEPHERD.[68] HURLEN[66] has reported the polarization data for active iron electrodes in 0.1 to 3M sodium hydroxide. Figure 23

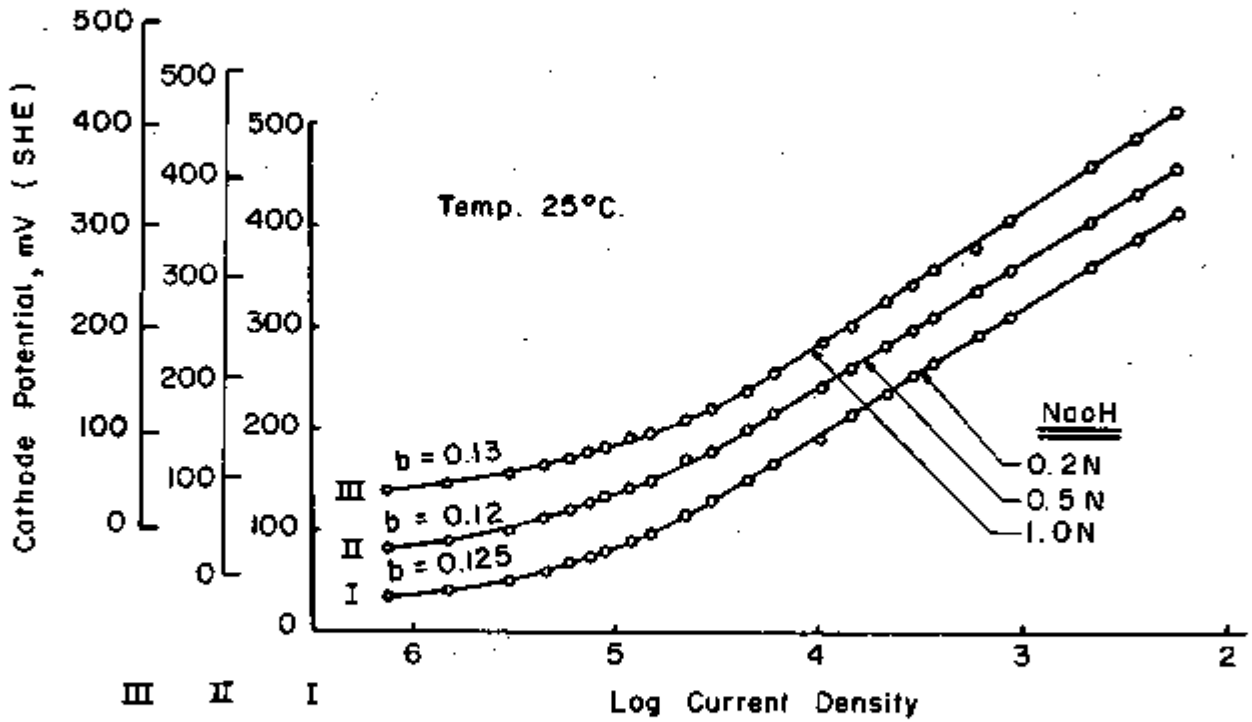

Fig. 22 - Cathodic tafel plots for iron at different NaOH concentrations.[65]

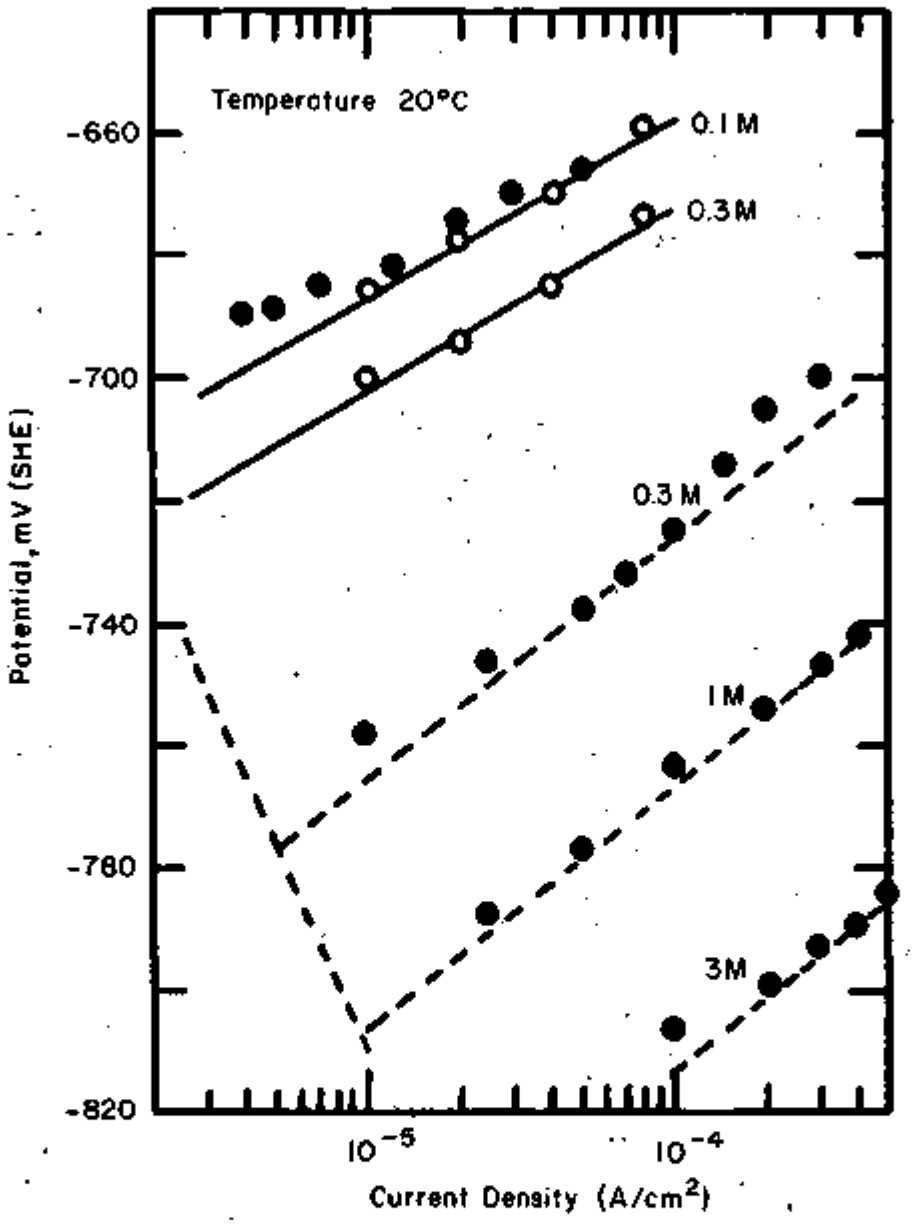

Fig. 23 - Tafel plots for active iron in solutions of various NaOH molalities (0.1-0.3M) from open cell (open points) and closed cell (closed points) experiments at 20°C.[66]

shows the anodic tafel lines for open cell* and closed cell** (open and closed circles, respectively) experiments. Though HURLEN claims differences between open cell and closed cell data, they are inconsistent at the 0.1 and 0.3M concentrations studied. The lines have a slope of 2.303 RT/2F and have a first order with respect to hydroxyl concentrations. These stipulated anodic tafel lines are believed to represent the hydrogen oxidation at active iron electrodes. The anodic hydrogen lines (oxidation of hydrogen to H^+) have a slope of 2.303 RT/3F and have a second order with respect to hydroxyl ions. The kinetic equations representing the above data must be:

$$2Fe + OH^- = 2Fe^{++} + OH^- + 4e$$

or

$$2Fe + OH^- = Fe(OH)^+ + Fe^{++} + 4e \qquad (11)$$

SCHULDINER and SHEPHERD[68] have compared the anodic oxide behavior of iron with platinum in 2N sodium hydroxide solutions at 25°C. Figure 24, shows potentiostatic anodic polarization curves for Fe, Pt and Fe-Pt couple. This couple was formed by spot welding 1 cm of 3-mil platinum wire to an iron wire of 0.65 cm^2. The intention of this technique was to check the Pt deposition on the working electrode, but the investigators were unsuccessful in this determination. They found that the small amounts of platinum on iron strongly retarded the hydrogen oxidation.

Passivation kinetics have been studied by TOUSEK,[69] HEUSLER et al.,[70] HANCOCK and MAYNE,[71] HURLEN,[66] RONZHIN and GOLUBEV,[72] and FRANCKE et al.[73] The general polarization behavior has been studied by HUMPHRIES and PARKINS.[33] The most interesting outcome in these studies were:

(i) the potential arrests corresponded to the sequential oxidation of Fe to Fe_2O_3 via $Fe(OH)_2$ and Fe_3O_4; and

(ii) the differential capacitance values show that the capacitance values decrease as the oxidation proceeds because of an increase in the ohmic component originating from the increased resistance of the oxide. Besides, the regions of active-passive transitions could also be identified by following changes in capacitance with applied potential.

*In open cell experiments, polarization was carried out in beakers, where there is a chance for the solution to become aerated.

**In closed cell experiments, there is no access to air. The solution could be aerated or deaerated or hydrogen-saturated at will.

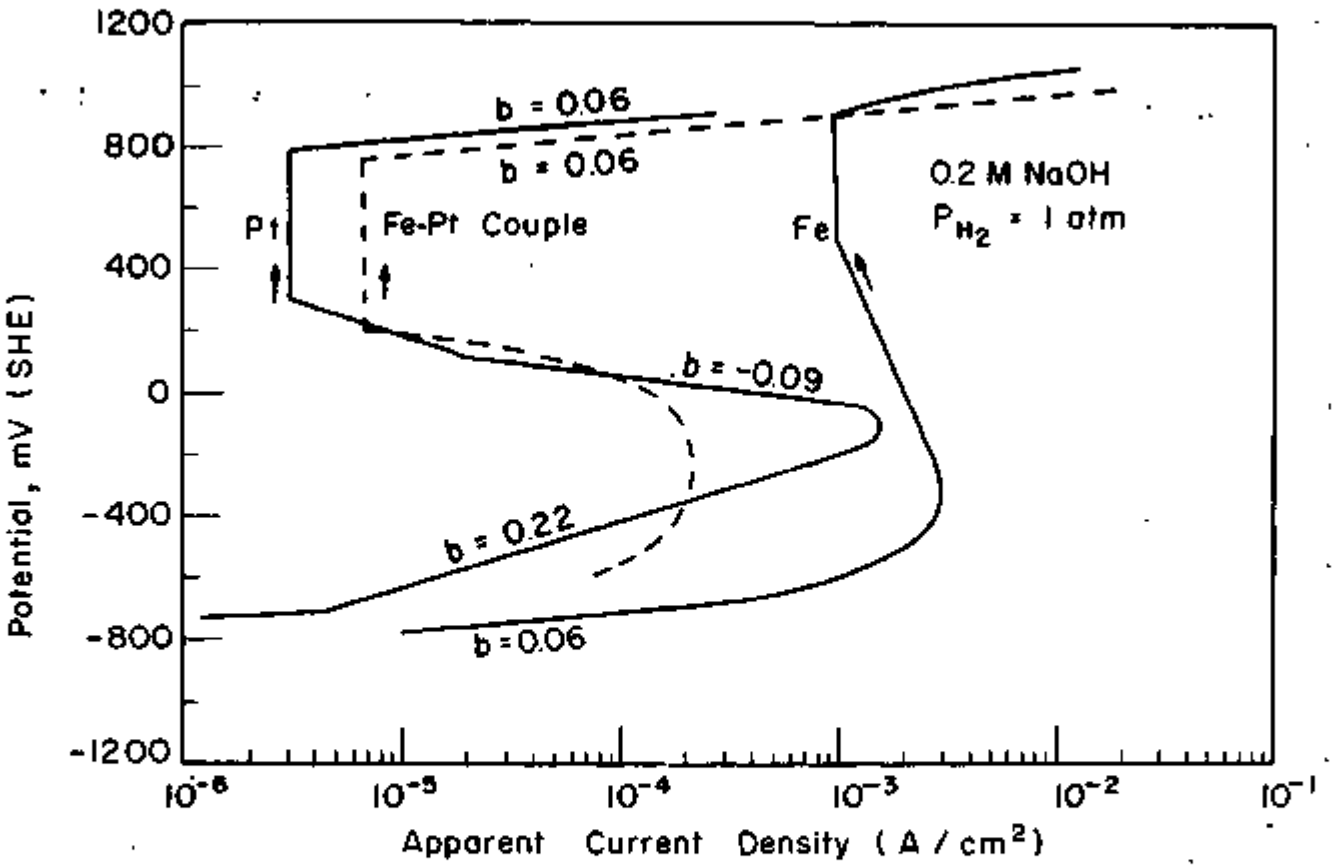

Fig. 24 - Comparison of Pt, Fe, and Fe - Pt electrodes for increasing potential sequence (anodic polarization curves).[68]

TOUSEK[69] determined the relationship between the open-circuit current density and time for iron electrodes in 1-18N NaOH solutions at 25°C. The relationship between time and current density is hyperbolic, as given by the expression

$$(i-i_o)\tau = K \qquad (12)$$

where

i is current density at a given time,
τ is time,
i_o is passivation current,

and

K is constant.

This is a phenomenological relationship and does not provide a direct insight into the mechanism of oxide growth.

In the pH range 9.3-14.0 at 50°C, HEUSLER et al.,[70] report a Flade potential of 615-920 mV on hydrogen scale. Flade potentials are determined by noting the potential arrest values in the current density-potential curves. Note that these arrests correspond to $MO \rightarrow M + e$. This phenomenon is applicable to oxide-covered metals. Flade potential relates to the value of potential where the oxide is reduced to metal as shown in Fig. 21a. This potential makes the potential of transition between activated and passive regions.

HANCOCK and MAYNE,[71] and HURLEN[66] studied the time-dependent anodic potential changes of iron and mild steel in sodium hydroxide solutions (0.1N NaOH at 25°C for HANCOCK and MAYNE[71] and 0.3N NaOH at 20°C for HURLEN).[66] Specimens were cleaned cathodically before passing the anodic currents. HANCOCK and MAYNE[71] and HURLEN[66] employed cathodic current densities of 20 and 100 $\mu A/cm^2$, respectively, for cathodic cleaning. In the range 10-80 $\mu A/cm^2$ of anodic current densities, potential arrests independent of applied cathodic current were reported. These potential arrests took place at -625 mV_H and -460 to -480 mV_H. The potential-time curves of HURLEN are given in Fig. 25. The observed arrests at -625 mV_H and -460 to -480 mV_H corresponded to the estimated reversible potential of $Fe(OH)_2/Fe(OH)_3$ and FeO/Fe_2O_3 couples, respectively. Hence, HURLEN[66] correlates these arrests to the formation of $Fe(OH)_2$ or $Fe(OH)_3$ at lower potentials and Fe_2O_3 at nobler potentials. This assumption lacks support by surface examination, which is rather vital.

RONZHIN and GOLUBEV[72] used the rotating iron electrode at 3000 rpm in 0.1N and 1N sodium hydroxide solutions at 25°C to follow the changes in galvanostatic potential-time curves in the anodic region. The potential-time curves showed two inflexions: (i) from -785 to -700 mV_H and (ii) from -550 to -560 mV_H in 1N sodium hydroxide.

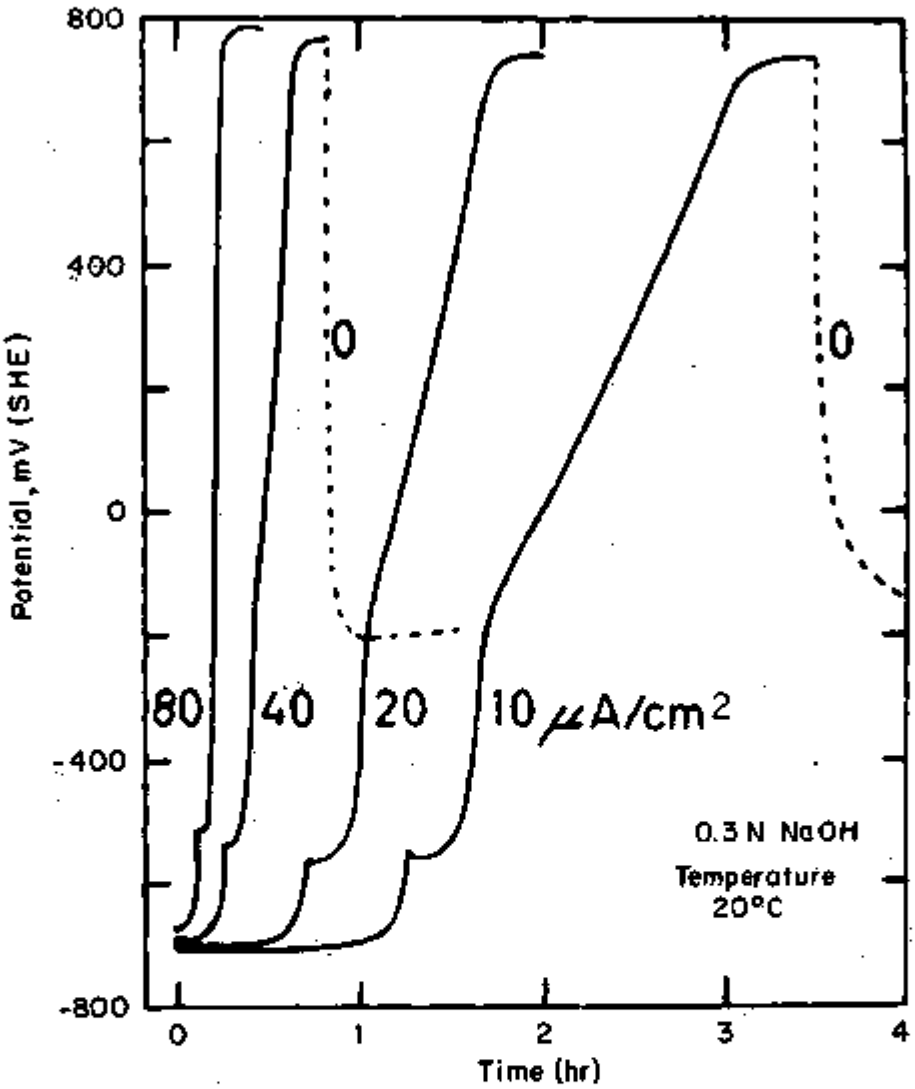

Fig. 25 - Anodic potential-time curves for iron in 0.3M NaOH at various applied current densities (10-80 $\mu A/cm^2$) put on half an hour after a cathodic activation for one hour at 100 $\mu A/cm^2$ (open cell, 20°C).[66]

Comparison of these values with those observed by HANCOCK and MAYNE[71] and HURLEN[68] who used stationary iron electrodes, shows that the potentials of inflection were shifted to negative values. Such results are not unreasonable in view of the differences in the experiments.

FRANCKE et al.[73] have measured phase boundary impendance of iron electrodes in 0.1N sodium hydroxide (in hydrogen atmosphere). Figure 26 shows the capacitance against applied potential curves in the anodic region (0-2000 mV against SHE) at frequencies 5, 20, and 105 Hz. In these curves a limiting value for capacitance can be observed which is due to adsorbed oxygen. The total capacitance C_p can be given by the following equation:

$$C_p = C_D + C_2 + \frac{2F^2}{RT} \cdot c_x \sqrt{\frac{2D}{\omega}} \qquad (13)$$

where C_D is double layer capacitance, C_2 is adsorptional capacitance, c_x is the concentration in mole/cm^3, D is diffusion coefficient (cm^2/sec), F is faraday, R is gas constant, T is temperature in °K and ω is frequency in Hz. In Eq. (13) the third term constitutes the ohmic component $1/R_p$, which is given by the following equation,

$$R_p = \frac{RT}{2F^2 c_x} \cdot \sqrt{\frac{1}{2_D/\omega}} \qquad (14)$$

all the terms having the same significance. Figure 27 shows the plot of the ohmic component against potential at different frequencies. From these results they observe an ohmic component caused by the resistance of the oxide film and they find clear changes in these components on going from active to passive state.

HUMPHRIES and PARKINS[33] have studied the effects of sodium hydroxide concentration on the potentiostatic polarization behavior. The potentiostatic polarization curves of iron electrode in boiling 5, 10, 20, 35, 50, and 75% sodium hydroxide solutions are given in Fig. 28. They find that at a concentration of 75%, the potential limits of the active region extended from -840 mV_H and -360 mV_H. On the other hand, at 5% sodium hydroxide the range of active dissolution is reduced to -780 to -660 mV_H. These changes in the magnitude of the currents flowing within the active dissolution range and the range of potentials limiting the active range, reflect the influence of concentration of sodium hydroxide upon cracking propensity.

b. Additions of aggressive anions - Destruction of passivity by aggressive anions in sodium hydroxide has been studied by PURINS and LIEPINA,[74] POPOVA and KABANOV,[75] RAJAGOPALAN et al.,[76] and ROZENTSVEIG et al.[77] The observations by these authors are: (i) passivity is degraded by chloride, suphate or radioactive sulphur (S^{35}) by competitive

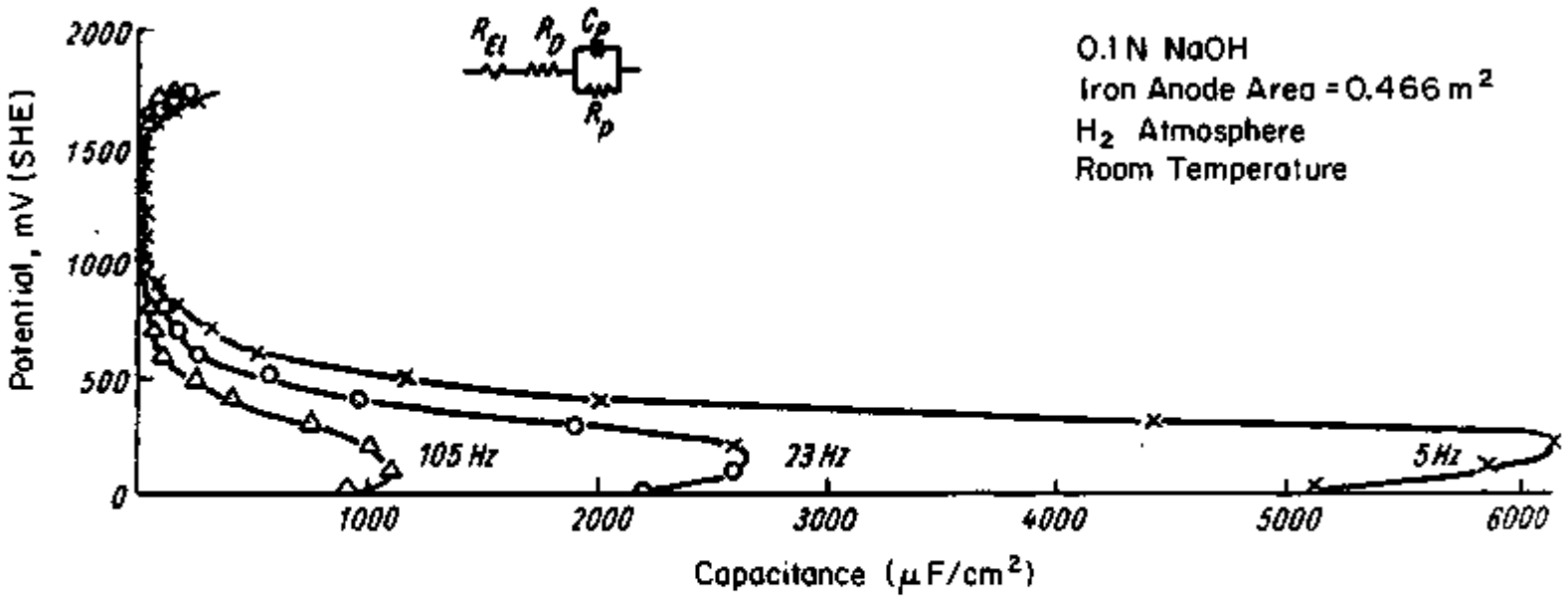

Fig. 26 - Plot of capacitance against applied anodic potential.[73]

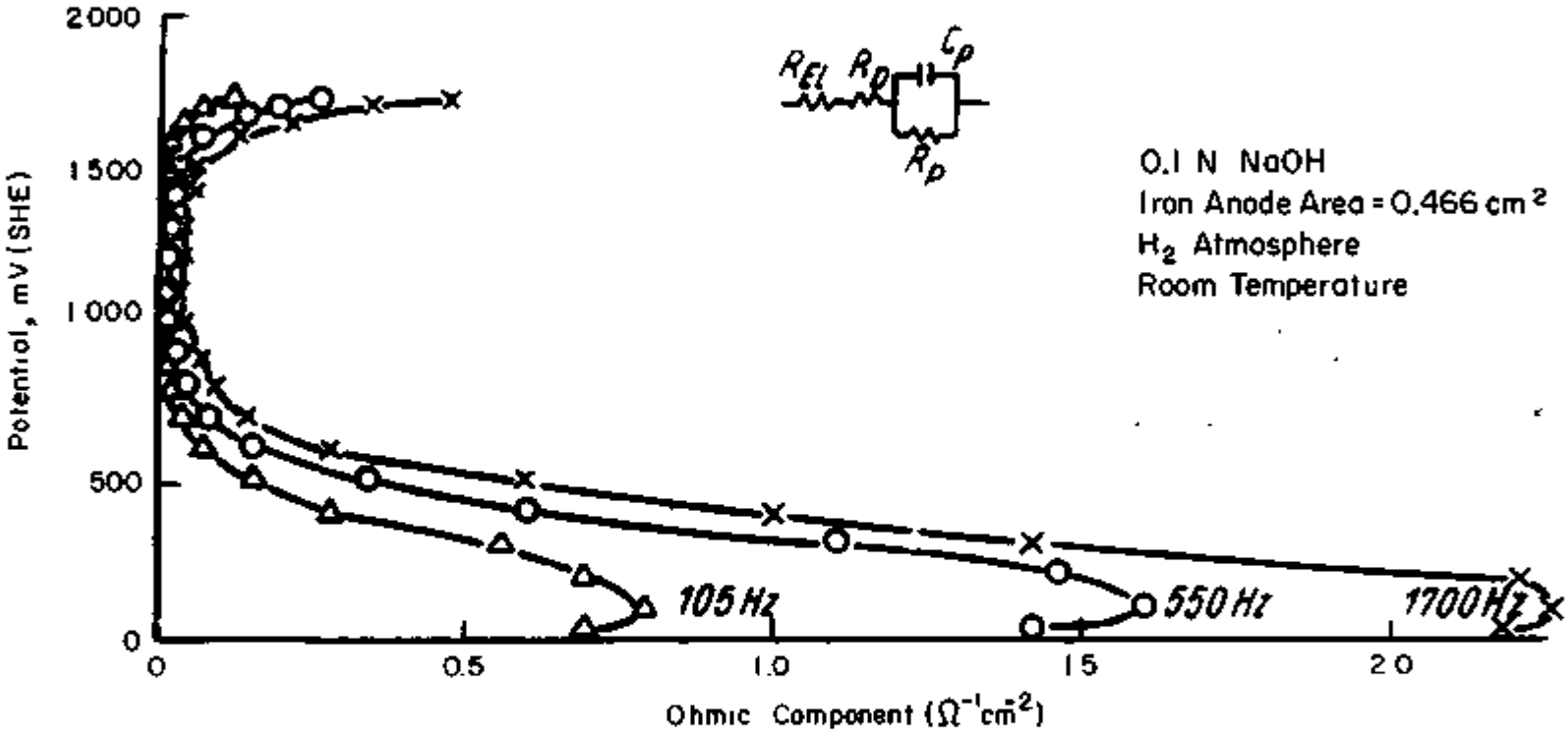

Fig. 27 - Plot of ohmic component ($1/R_p$) against applied electrode potential (anodic).[73]

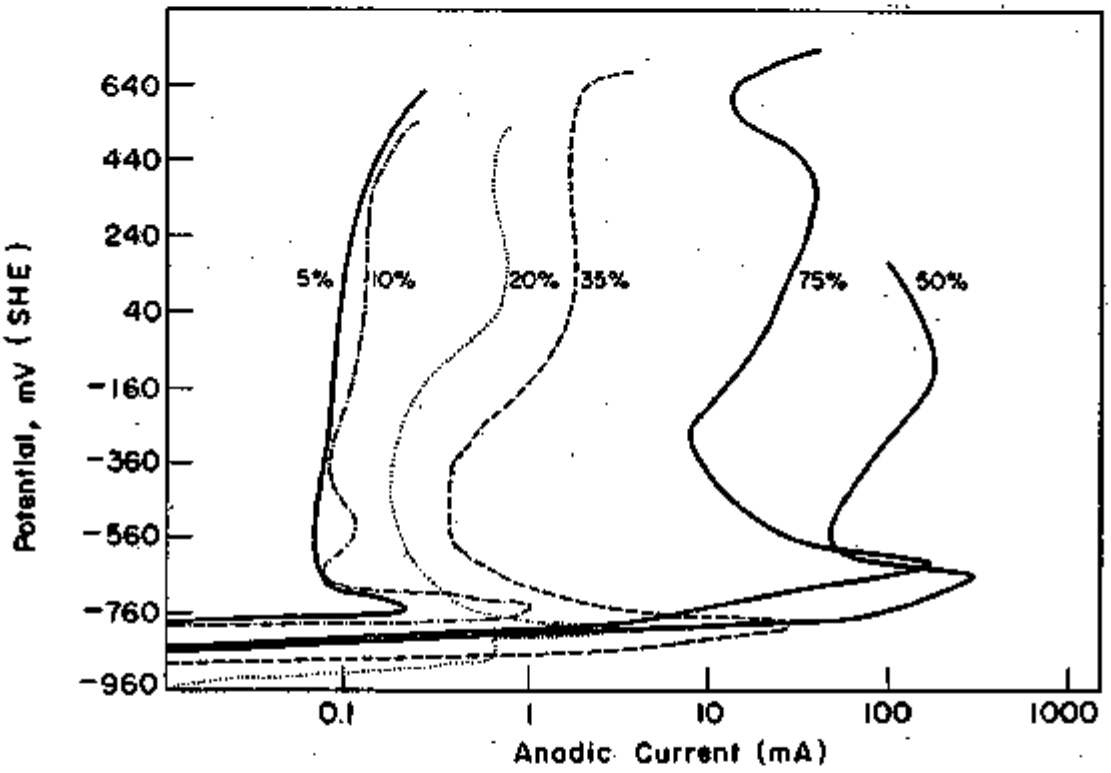

Fig. 28 - Polarization curves for mild steel in boiling NaOH solutions of various strengths.[39]

adsorption; (ii) a chloride-to-hydroxide ratio of 1 is necessary to activate (degrade passivity) a passive iron electrode under the conditions studied and (iii) at room temperature and in 0.1N sodium hydroxide solution, even a sulphate-to-hydroxide ratio of 20 did not degrade passivity.

PURINS and LIEPINA[74] have studied the activation by chloride ions. POPOVA and KABANOV[75] have investigated the effects of activation of iron by chloride and sulphate in a detailed way. They obtained galvanostatic anodic polarization curves at 90°C by either adding chloride to hydroxide or hydroxide to chloride, keeping concentration of one of these ions in solutions constant. Similar experiments were performed with sulphate. In 5-10N sodium hydroxide, at sufficiently high current densities, as 0.05A/cm^2, iron electrodes passivated, oxygen began to evolve, and iron dissolved forming ferroate ions (FeO_4^{2-}) regardless of chloride or sulphate was present or absent. In dilute solutions of sodium hydroxide, chloride did not affect the process of solution of iron. The activating effect of chloride became noticeable at a chloride-to-hydroxide ratio of 1. A similar degree of activation by sulphate occurred at a much lower concentration of hydroxide. The high rate of solution of iron at 90°C was ascribed to more uniform corrosion than at room temperature. Rapid corrosion in the presence of chloride occurred in concentrations less than 0.5N sodium hydroxide. RAJAGOPALAN et al.[76] reported the results of potentiodynamic data, presumably at room temperature, in 0.1 and 0.01N sodium hydroxide solutions with chloride and sulphate added individually. They found a similar critical ratio of unity of chloride to hydroxide for activation to take place. Sulphate ions did not cause any change in the passivation behavior of iron in 0.1N sodium hydroxide up to the highest ratio studied (sulphate-to-hydroxide ratio of 20).

ROZENTSVEIG et al.[77] investigated the effect of sulphur (as sodium sulphide) on anodic behavior of iron electrode in 5N sodium hydroxide solutions at room temperature. The adsorption of sulphur on prior cathodically reduced (at 0.75 mA/cm^2) and anodically polarized (at 0.3 mA/cm^2) iron electrodes was studied in 5N sodium hydroxide between 10^{-5} and 9×10^{-3}N with respect to S^{*2-}. Cathodically reduced and anodically oxidized specimens were exposed to radioactive sulphur solutions for one hour, and then radioactivity was measured. Their results are given in Table IV. Based on their measurements, they reached the following conclusions: (i) adsorption of sulphur as sulphide on iron leads to a sharp increase in its rate of anodic dissolution in alkali; (ii) saturation of the iron surface continues for a long time, but even the small amount of adsorbed sulphur instantly at the start of the process leads to a marked acceleration of the anodic dissolution of iron; and (iii) radioactive tracer study shows that a reduced surface of an iron electrode adsorbs more sulphur and holds it more strongly than anodically oxidized iron.

Table IV - Effect of Sulphur Content in the Solution on the Amount of Adsorption (after ROZENTSVEIG et al.)[77]

S^{2}*, N	Mean Activity Count min/cm^2 of Apparent Surface	Sulphur Adsorbed g-atom of S/cm^2 of Apparent Surface
10^{-5}	222	2.5×10^{-10}
10^{-4}	1485	18×10^{-10}
10^{-3}	10600	13×10^{-9}
9×10^{-3}	55600	7×10^{-8}

S^{2} means radioactive sulphide anion.

c. Studies in potassium hydroxide - Cathodic polarization has been investigated by TSYGANOV and BUYANOVA,[78] BATRAKOV et al.,[79] TURAPOV and MURTAZAEV,[80] SCHWARTZ and SIMON,[81] AFANAS'EV et al.[82,83] and SCHWABE.[84]

TSYGANOV and BUYANOVA[78] studied cathodic processes by applying negative currents in the range of 10^{-4} to 1 A/cm^2 and monitoring the potential for Armco iron in 5N KOH at 30°C. For each applied current density they measured potentials for periods of three minutes. Potential changes of up to 0.5 V were observed indicating considerable variation in the state of the surface over relatively short times.

BATRAKOV et al.[78] measured polarization at low temperatures in the range -20 to +20°C in 5N potassium hydroxide. Figure 29 gives the cathodic polarization curves at 20, 10, 0, -10 and -20°C. It can be seen that with an increase in the temperature the cathodic potentials shift towards noble values; thereby lowering the H_2-reduction kinetics. They calculated the energy of activation from Arrhenius equation and the values were between 7.1 and 9.1 kcal/mole. TURAPOV and MURTAZAEV[80] have investigated the cathodic polarization behavior of metal-ceramic iron electrodes in 7, 10, 12.65 and 17.2N potassium hydroxide at 75 ± 0.1°C. Theoretically, the hydrogen reduction kinetics should decrease (i.e., potential shift to noble values) with increasing alkali concentration. In the cathodic current density range of 20 to 300 mA/cm^2 they observed irregular changes in the cathode potentials with increasing concentration or potassium hydroxide. TURAPOV and MURTAZAEV[80] attempted to account for the irregular changes in potentials on the basis of reduction of water activity as hydroxide concentration is increased and thereby lowering the hydrogen evolution kinetics, as

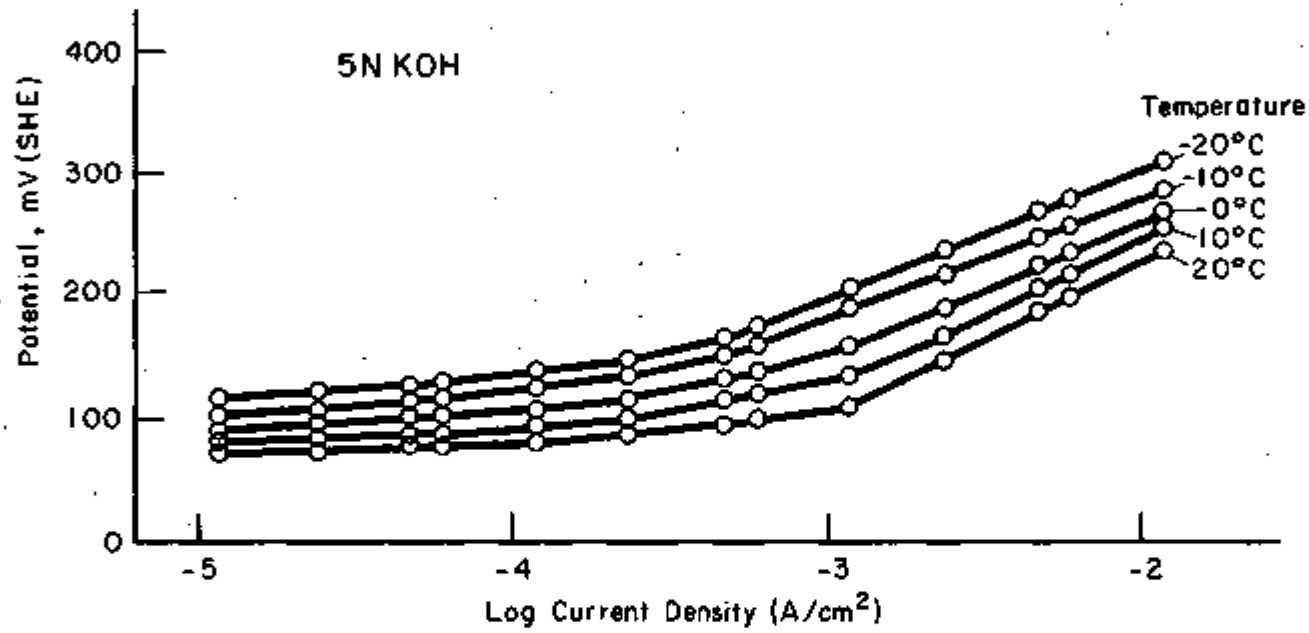

Fig. 29 - Cathodic polarization curves for a smooth iron electrode with coating of electrodeposited iron in 5N KOH at various temperatures.[78]

given in Eq. (10). Their reasoning is correct only as far as progressive decrease in hydrogen reduction kinetics is observed with increase in KOH concentration.

SCHWARTZ and SIMON[81] studied the behavior of carbonyl and ingot iron in 4N potassium hydroxide at 90°C. They determined the galvanostatic cathodic polarization curves. They concluded that the hydrogen liberation reaction followed the Volmer-Hevrovsky mechanism, the partial reactions of which are hindered variously, depending upon the state of the electrodes. These reactions are given below:

$$H_2O + e \rightarrow H_{ad} + OH^- \quad \text{(Volmer reaction)} \qquad (15)$$

$$H_{ad} + H_2O + e \rightarrow H_2 + OH^- \quad \text{(Hevrovsky reaction)} \qquad (16)$$

AFANAS'EV et al.[82,83] investigated the effects of hydrogen peroxide (2-5N) on cathodic reduction of molecular oxygen ($\frac{1}{2}\,O_2 + H_2O_2 + 2e \rightarrow OH^- + HO_2^-$) in 0.1N potassium hydroxide solutions. At low concentrations of hydrogen peroxide, the surface is insufficiently oxidized and behaves as an inert electrode. At too high concentration, the oxide on the electrode is disintegrated by vigorously generated bubbles of oxygen and the electrode becomes active.

SCHWABE,[84] using circulating electrolyte, determined the effects of adding 10^{-4} to 2.5N potassium chloride to 10^{-3} to 2N potassium hydroxide at 25°C. The minimum potassium chloride concentration with activating effect for $i = 1$ mA/cm^2 as function of the potassium hydroxide concentration is given in Table V. At 3 to 4N potassium hydroxide, iron was not activated even in saturated solutions of potassium chloride. The duration for which passivity can be sustained was determined as a function of the velocity of the flow of electrolyte past the electrode and potassium chloride concentration. When the potassium chloride concentration is smaller than potassium hydroxide concentration and the flow velocity is sufficiently high, the electrode can be kept passive for a fairly long time ($t_p \rightarrow \infty$); when the flow is stopped, immediate activation takes place. At high potassium chloride concentrations, however, t_p is decreased by the flow of the electrolyte. In the first few seconds of passivation, they observe the following relation:

$$E_m = E_p - (t-t_p)^3 \cdot K_3 \qquad (17)$$

where E_m is the changing potential with time t, E_p is the passivation potential, t_p is the passivation time, and K_3 is constant. Further, they found that K_3 increases approximately in proportion to c_{Cl^-}/c_{OH^-}.

Table V - Minimum KCl Concentration with Activating Effect for i = 1 mA/cm^2 on Iron as a Function of KOH Concentration at 25°C (after SCHWABE)[84]

KOH (m/l)	10^{-3}	10^{-2}	0.05	0.10	0.15	0.2	0.5	1	2
KCl (m/l)	10^{-4}	10^{-3}	10^{-2}	0.03	0.07	0.1	0.33	0.75	2.5

Based on these observations, they proposed that anodic dissolution will not take place until the halogen ions have displaced chemisorbed oxygen or adsorbed OH^-. This process might occur in accordance with Frumkin's mechanism:

$$(MeOH)_{ad} + X^- \rightarrow Me(OH,X^-)_{ad} + nH_2O \qquad (18)$$

$$Me(OH,X^-)_{ad} + mH_2O \rightarrow MeOH + X^- + \theta \qquad (19)$$

In this case Me = K, X^- = Cl^-, and θ is the coverage.

6. Polarization with Inhibitors

Effects of additives to alkaline solutions on the electrochemical behavior of the iron electrode have been studied by AMMAR and AWAD,[65] and HUMPHRIES and PARKINS.[33] Effects of added substances to potassium hydroxide solutions have been studied by LEVINA,[85] SCHWARTZ and SIMON,[81] and TURAPOV and MURTAZAEV.[86]

The kind of inhibitors studied can act to reduce the activated reduction or oxidation kinetics, can accelerate the amount of film formation, or can stabilize the passive films by reducing the defect mobility. Essential patterns exhibited by the above studies are given below.

1. Changes of potential with time indicate that some amines function by reducing the available area for hydrogen discharge. The relative effectiveness is explained on the basis of adsorption.

2. Transient kinetics exhibited by some of these amines is explained on the basis of attractive and repulsive interactions between adsorbed atomic hydrogen and organic molecules.

3. Some of the inhibitors like tannin, silica, and phosphates, function by raising the overvoltage for the hydrogen evolution reaction.

4. Addition of potassium cyanide apparently cause the ultimate formation of protective magnetite layer via a hexacyano complex.

AMMAR and AWAD[85] measured cathodic potentials in 0.2N sodium hydroxide with the following substances added: ethylamine, n-butylamine, dimethylamine, tri-n-propylamine, benzylamine, pyridine, quinoline, picric acid, p-benzoquinone and m-dinitrobenzene. They measured the changes in potential with time, with and without the above inhibitors, in 0.2N sodium hydroxide at a current density of 2.5 mA/cm^2. Table VI shows that benzylamine, pyridine, ethylamine, n-butylamine and saturated quinoline shifted the potentials toward active direction, while dimethylamine, tri-n-propylamine, p-benzoquinone, m-dinitrobenzene and picric acid shifted toward nobler values. The effects of increasing the concentration of ethylamine, dimethylamine and n-butylamine and picric acid on cathode potential is given in Table VII. For amines, the potentials shift toward active values with increasing concentration; whereas for picric acid, which is an activator, this value decreases. The numerical increase of potential upon adding butylamine, ethylamine, benzylamine, pyridine and saturated quinoline could be explained on the basis of decrease in the available surface area for hydrogen discharge, thus increasing the current density. Butylamine having more negative potential than ethylamine is ascribed due to the stronger adsorption in the case of butylamine. On the other hand, nobler shifts by picric acid, p-benzoquinone, and m-dinitrobenzene are attributed to the depolarization of the hydrogen evolution reaction. They account for the changes of potential on the addition of these substances on the basis of attractive or repulsive interactions between the adsorbed atomic hydrogen and organic molecules.

HUMPHRIES and PARKINS[33] studied the potentiostatic polarization behavior of mild steel in boiling 35% sodium hydroxide solutions containing saturated sodium sulphate, 5% sodium silicate, 16% quebracho, 14% sodium nitrate, 0.2% potassium permanganate, and 0.2% red lead added individually. While these substances produced no inhibitive effect on the corrosion rate they caused a substantial reduction in the anodic peak. On the other hand, quebracho, silicate and sulphate, which have inhibitive effects, did not suppress the active peak. LEVINA's[85] potential-time curves in 5N KOH also support the inhibitive effects of quebracho and silicate. Figure 30 shows schematic cathodic and anodic polarization curves explaining the accelerating effects of nitrate, sulfate, and lead oxide.

The suppression of the active peak by these additions result from an increase in the cathodic polarization current corresponding to depolarization of the cathodic reaction, and the consequent intersection of the anodic polarization curve by the cathodic curve at a more noble potential. The additions that led to this effect are all compounds that might be expected to behave as oxidizing agents in alkaline solution, thereby depolarizing the cathodic reaction and causing the measured polarization curve to be intersected before the active anodic peak.

Table VI - Effect of Inhibitors on Cathode Potentials (after AMMAR and AWAD)[65]

η	Compound	Concentration (M)	Potential (mV), -ve
Increase	Benzylamine	0.1	18
	Pyridine	0.1	30
	Ethylamine	0.1	40
	n-butylamine	0.1	120
	Satd. Quinoline		70
Decrease	Dimethylamine	0.1	7
	Tri-n-propylamine	0.01	40
	p-benzoquinone	0.01	20
	m-dinitrobenzene	0.01	100
	Picric acid	0.01	200

Table VII - Effect of Inhibitor Concentration on Cathode Potentials (after AMMAR and AWAD)[65]

Compound	Concentration mole/l	Change in η, (mV), -ve
Ethylamine	10^{-1}	417
	10^{-2}	382
	10^{-3}	350
Dimethylamine	10^{-1}	375
	2×10^{-2}	355
	10^{-3}	313
n-Butylamine	10^{-1}	500
	10^{-2}	398
	10^{-3}	293
Picric Acid	10^{-2}	180
	10^{-3}	325

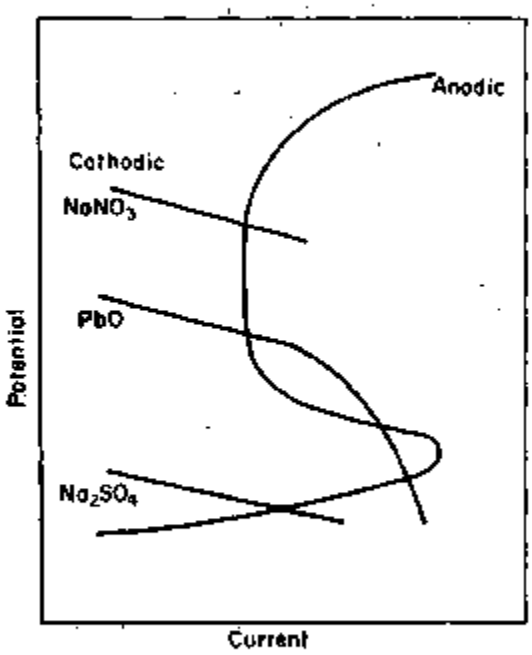

Fig. 30 - Schematic anodic and cathodic polarization curves for mild steel in 35% NaOH containing various additional substances.[33]

SCHWARTZ AND SIMON[81] studied the effects of adding potassium cyanide to 4N potassium hydroxide on the potentiostatic polarization behavior of carbonyl and ingot iron. They suggest the anodic formation of $Fe(CN_6)^{4-}$ by the following reaction. This hexacyano complex dissociates into Fe^{++} and $(CN)^{-}$ and Fe^{++} gets further oxidized to Fe_3O_4.

$$FeO_2^{=} + 6CN^{-} + 2H_2O \rightarrow \left[Fe(CN)_6^{4-}\right] + 4OH^{-} \qquad (20)$$

Using a sintered iron electrode, TURAPOV and MURTAZAEV[88] found that neutral molecules like urea and thiourea are without effect. Also, pyridine and tetrabutylamine produced no improvement. Only anabasine minimized the solution rate of iron and this substance consequently is used as an inhibitor for anodic dissolution of iron in caustic solutions. The addition of potassium iodide displaced the potential toward more positive values, forming a surface compound with iron. Sodium sulfide also produced an inhibitive effect through the formation of protective surface films.

IV. CORROSION OF NICKEL

A. CORROSION UNDER STRESS

Nickel is reported to be a generally satisfactory material for handling hot concentrated caustic solution. The problem of nickel corrosion becomes severe when the environment is anhydrous fused caustic at very high temperatures. Anodic corrosion of nickel in chloride media are limiting cases where nickel corrosion is observed. In 1944 FRASER[87] listed six case histories where cold drawn nickel tubes failed when exposed to caustic soda solutions of high concentrations above ambient temperatures. Aqueous caustic solutions of various concentrations were generally reported to produce transcrystalline cracking. He further carried out tests in which nickel specimens were exposed to molten sodium hydroxide at concentrations of 80% NaOH to anhydrous and showed that specimens failed in a intercrystalline manner. He also reported that internally stressed nickel is susceptible to cracking in fused potassium hydroxide.

McHENRY and PROBST[88] have studied the stress-rupture lives of nickel tubes at 815°C in air and argon with and without hydroxide. Sodium hydroxide has no effect on the strength of nickel in argon. Severe intergranular and surface oxidation of nickel tubes tested in air increased their rupture strength over those tested in argon. This strengthening was partially lost when they contained sodium hydroxide.

B. GENERAL CORROSION

The general corrosion of nickel has been more extensively studied than stress corrosion. The present section will deal with studies on corrosion rates in fused sodium hydroxides, electrochemistry of active and passive nickel, breakdown of passivity when aggressive anions are added to hydroxides and a few comments on corrosion products.

1. Corrosion in Sodium Hydroxide

General corrosion in the fused sodium hydroxide medium has been studied by SIMONS et al.,[89] PEOPLES et al.,[90] CRAIGHEAD et al.,[91] and GREGORY et al.[92] They investigated in the temperature range of 320-815°C. Some of their important observations were: (i) severe plugging of cold zones by nickel deposition in natural and forced convection loops; (ii) rate of attack increased with increasing temperature and is less severe in reducing atmosphere; and (iii) with rotating specimens the rate of attack is ten times greater than under static conditions.

SIMONS et al.[89] have studied the corrosion of nickel in fused sodium hydroxide in the temperature range 480-815°C. They used natural and forced convection loops constructed of pure nickel in which hydrogen

was bubbled through sodium hydroxide; the peak temperatures were 650-815°C, and temperature was cycled from 55 to 110°C. The cold zones were severely plugged by nickel deposition in times ranging from less than 10 to 200 hours. At peak temperatures of 480 and 565°C there was limited nickel transfer. For instance, at 480°C peak and 40° cycle only 0.012 cm of nickel was deposited in the cold zone after 2000 hours.

CRAIGHEAD'S[91] investigations at 536, 675, and 815°C support the observations made by SIMMONS et al.[89] After the corrosion experiments, the solutions were analyzed for nickel. Its concentration was not affected by forming atmosphere (mixture of steam and CO).

PEOPLES et al.[90] have studied the reactions of 20 g of dehydrated sodium hydroxide at 950°C in nickel crucibles for periods ranging from 1 to 165 hours. They proposed possible reaction mechanisms by analyzing the effluents for hydrogen, nickel, water, sodium carbonate and sodium oxide.

With rotating specimens in molten sodium hydroxide between 320-580°C the corrosion under dynamic conditions is ten times greater than under static conditions.[92] In these studies GREGORY et al.[92] also observed plugging of nickel tubes by mass transfer under a thermal gradient. These results are in accord with those of SIMONS et al.[89] and CRAIGHEAD et al.[91] In the temperature range of 320-580°C lithium hydroxide suppressed the corrosion rates.[92]

2. Polarization Behavior

The polarization measurements on nickel electrode have been performed in sodium and potassium hydroxides to study (i) the kinetics of reduction of reducible species such as H_2O and O_2, (ii) passivation phenomena, and (iii) breakdown of passivity when aggressive anions are added to these solutions.

a. Cathodic behavior - Cathodic polarization and hydrogen reduction kinetics in sodium and potassium hydroxide solutions have been studied by WEININGER and BREITER,[93] DELIMARSKII et al.,[94] and KITA and NOMURA.[95] The essential findings in their investigations are: (i) studies with various planes of single crystals did not show significant differences in polarization behavior; (ii) halides reduced the hydrogen overvoltage; and (iii) heats of activation calculated from experimental tafel parameters showed agreements with the theoretical values based on the catalytic hydrogen ion discharge mechanism.

The studies of hydrogen evolution reaction[93] with polycrystalline and single crystal nickel show that different crystallographic orientation have no significant effect on the cathodic tafel slopes. Typical tafel curves which represent the shape of curves under various conditions is given in Fig. 31. The observed differences in tafel slopes on the first polarization sweep and other sweeps can be attributed to the

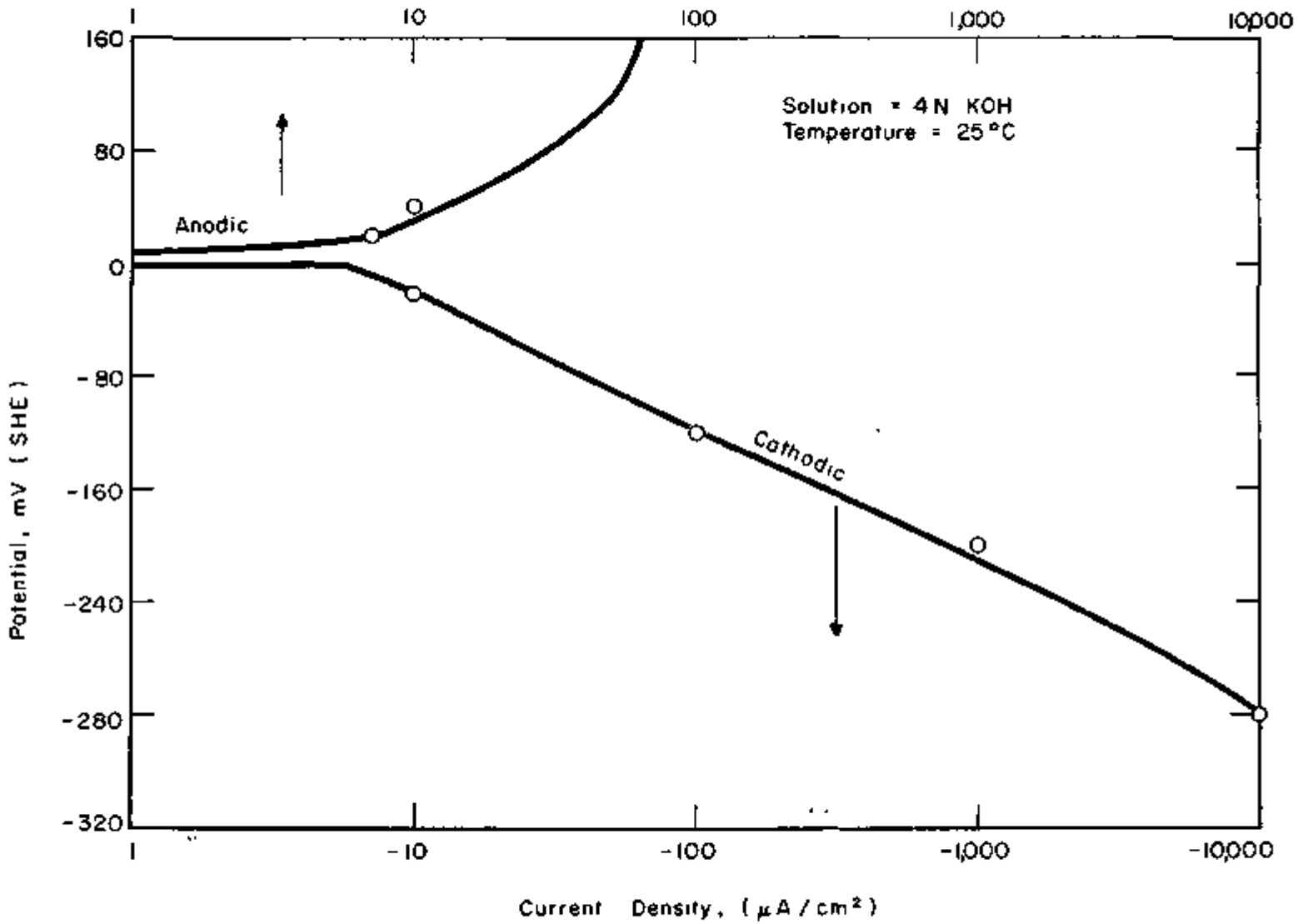

Fig. 31 - Typical shape of anodic and cathodic polarization for nickel electrode in KOH solutions.[93]

presence of oxide films derived during the chemical polishing, and different mechanism existing during the first sweep. Tafel slopes of 152 mV/decade on the first sweep and 89 to 93 mV/decade on subsequent sweeps are observed for {100}, {110} and {111} planes as well as polycrystalline nickel. From these tafel slopes, an exchange current density of 10 $\mu A/cm^2$ is obtained. To provide extra evidence, WEININGER and BREITER,[93] measured the electrode capacitance with voltage by superimposing a small (3 mV peak to peak) a.c. signal on a d.c. voltage.

Figure 32 shows the changes in a.c. capacitance with electrode potential at 100 Hz on first, second and third sweeps. In contrast to the d.c. polarization measurements, there is not much difference in these curves on first, second and third sweeps indicating that the nature of the electrode surface is not significantly altered. Figure 33 is the plot of parallel conductance against potential (ohmic component) calculated from the capacitance measurements. These two figures are essentially the same, but for the additional peak in the $1/R_p$ vs. potential curve which can be attributed to the contribution of an impedance term caused by slow electrochemical formation and removal of adsorbed layers of hydrogen atoms and hydroxyl radicals.

Figure 34 shows the schematic potential-capacitance curve in the potential range -300 to +300 mV. The observed tafel slopes, and the relatively small value of capacity in the cathodic region suggest that the hydrogen discharge involves the weakly bonded hydrogen atoms and the rate determining step is given by Eq. (21).

$$Ni + H_2O + e = Ni\text{-}H + OH^- \qquad (21)$$

The heats of activation $\Delta H^{\ddagger}$ and pre-exponential factor log have been calculated on the basis of catalytic mechanism of hydrogen discharge ($H^+ + e \rightarrow H(a)$ and $2H(a) \rightarrow H_2$) taking into consideration the repulsive interactions between hydrogen adatoms and the critical complex by the proportional approximation.[95] The plot between theoretically calculated $\Delta H^{\ddagger}$ and η is given in Fig. 35. $\Delta H^{\ddagger}$ is almost constant and has the value of 18.5 kcal/mole in the range of overvoltage from 120 to 600 mV in the region where the tafel law applies. Figure 36 gives the cathodic tafel lines for spherical nickel electrodes polarized galvanostatically in 5N sodium hydroxide between 4-45°C. From the tafel slopes, they calculated the heats of activation and pre-exponential term B. The experimental values of $\Delta H^{\ddagger} = 15.7 \pm 2.9$ kcal/mole and $B = 6.7 \pm 2.2$ are in good agreement with the theoretical values.

While WEININGER and BREITER[93] prefer Volmer-Hevrovsky's mechanism involving weak hydrogen-metallic bond, KITA and NOMURA[95] support the HORIVTI's catalytic mechanism involving the activated complexes, and their distributions and interactions with hydrogen adatoms.

b. Anodic passivation - Anodic passivation phenomena for nickel in caustic environments have been investigated by DEZIDER'EVA and FAIZULLIN,[96] DAVIES and BARKER,[97] and STERN and CARLTON.[98] The

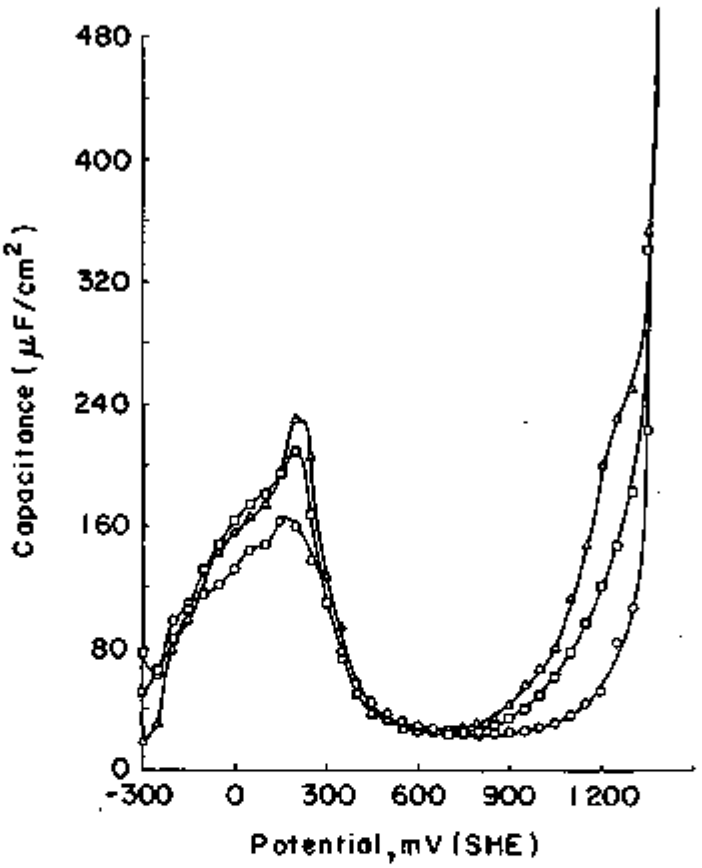

Fig. 32 - Capacity (C_p) as a function of potential for polycrystalline nickel electrode in 4N KOH saturated with argon, measured at 100 Hz: O = first sweep, □ = second sweep, and △ = third sweep.[93]

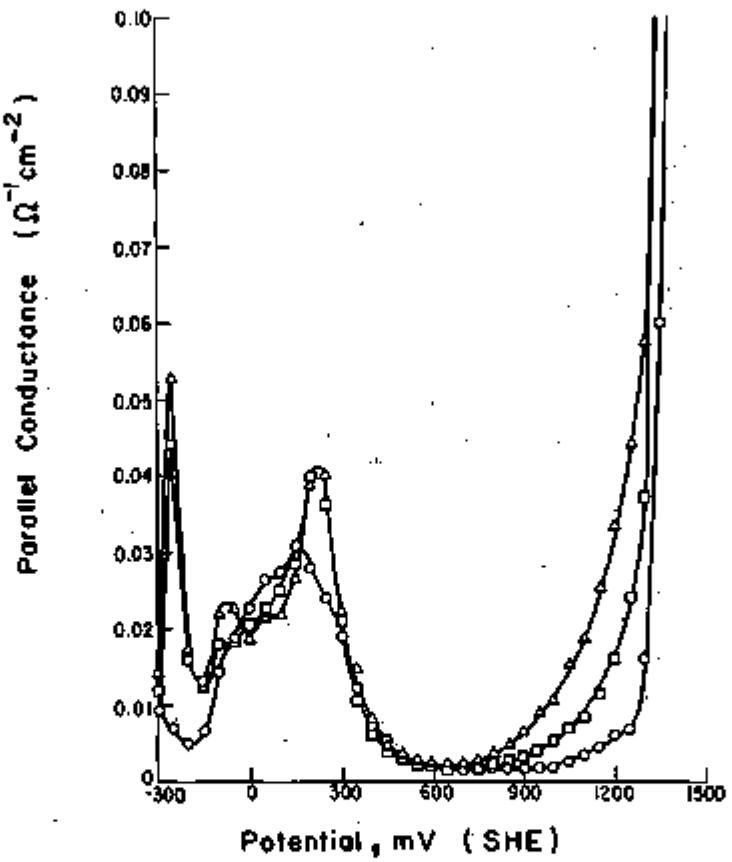

Fig. 33 - Parallel conductance ($1/R_p$) as a function of potential for polycrystalline nickel electrode in 4N KOH solution saturated with argon, measured at 100 Hz: ○ = first sweep, □ = second sweep, and △ = third sweep.[93]

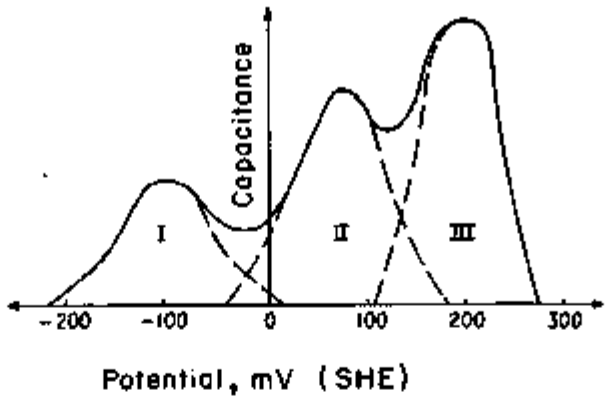

Fig. 34 - Schematic capacitance-potential curve in the low potential region for idealized nickel electrode in KOH.[93]

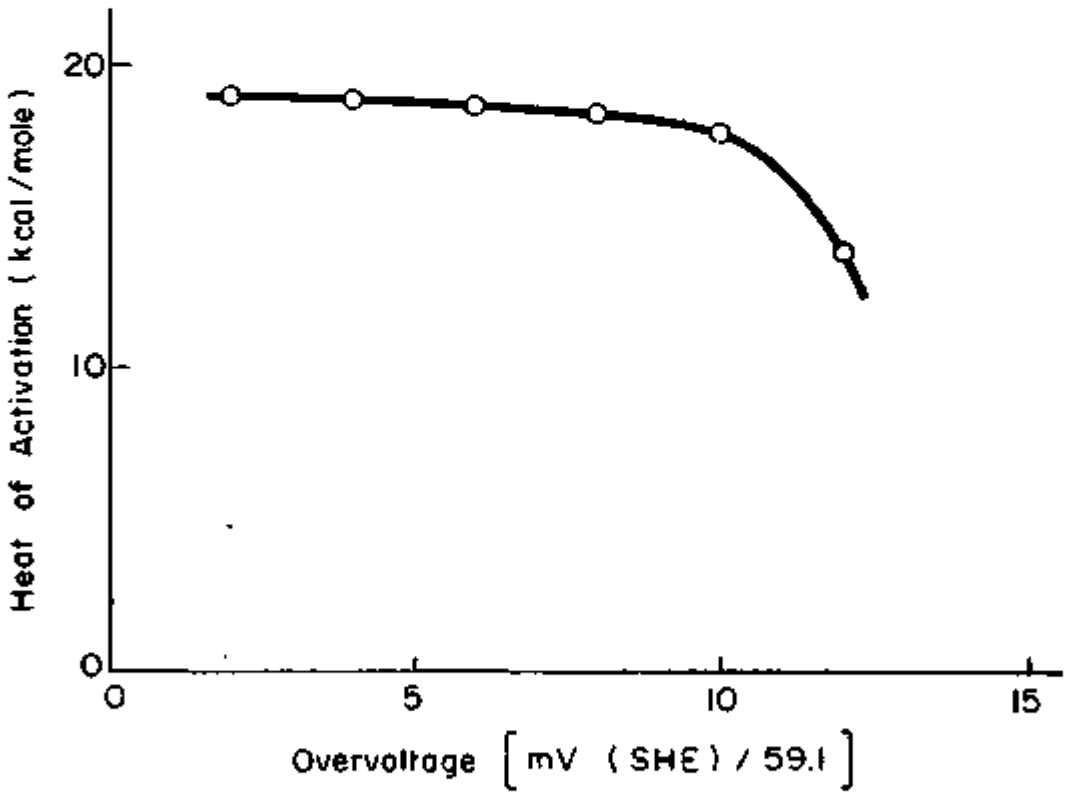

Fig. 35 - Theoretical value of $\Delta H^{\neq}$ as a function of overvoltage of nickel at 25°C.[95]

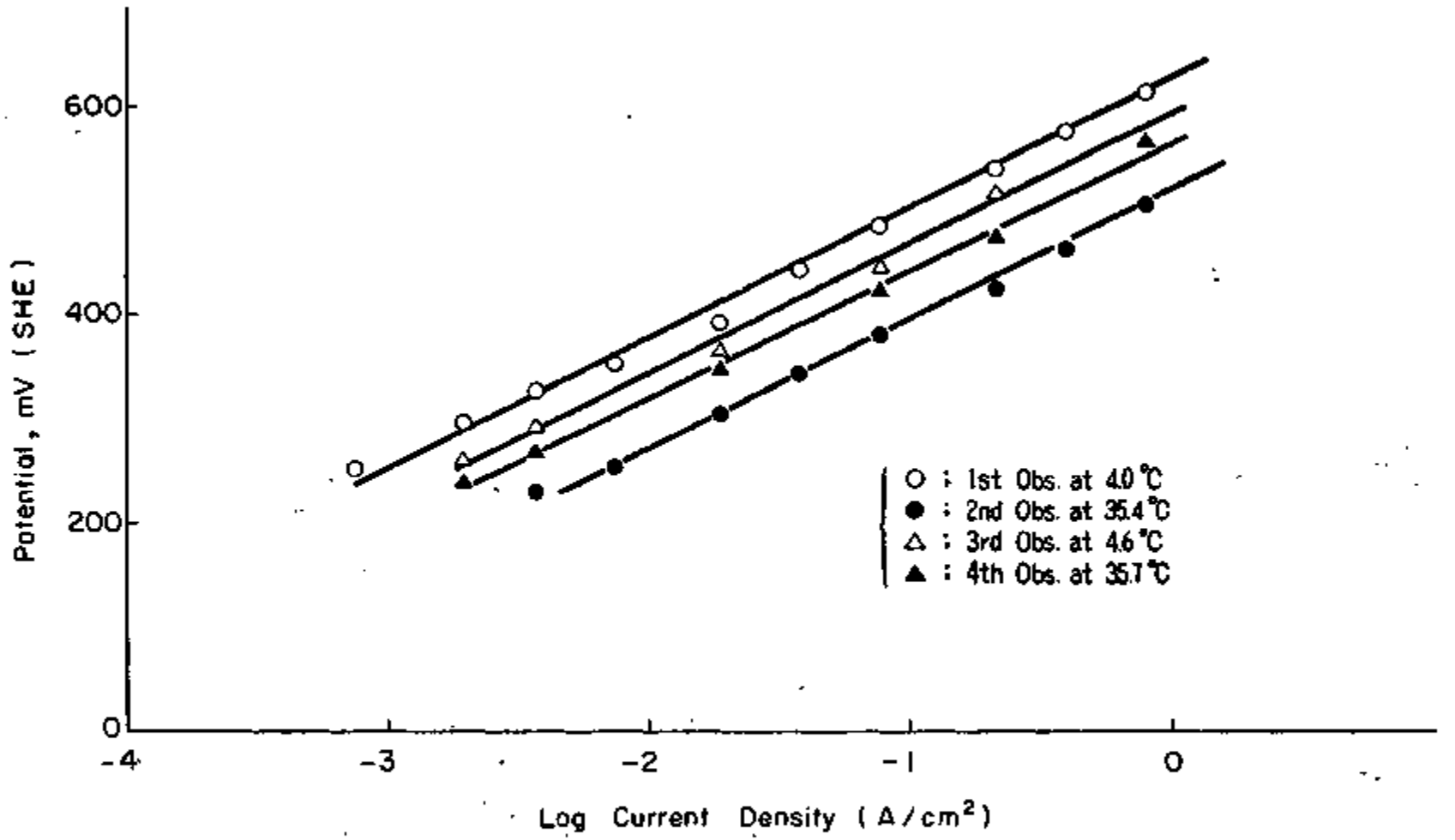

Fig. 36 - Successive observations of $\log_{10} i_+ \sim \eta$ relation on nickel in 5.04N NaOH solution.[95]

primary approach used by these investigators is the method of potential transients with constant anodic or cathodic applied currents. These investigators studied effects of temperature, concentration of solution, and magnitude of applied currents. They agree on finding the existence of an $Ni(OH)_2$ and a Ni_3O_4 or Ni_2O_3 in temperatures near room temperature. They also find that traces of oxygen promote rapid passivation in the temperature range of 500°C in fused NaOH.

DEZIDER'EVA and FAIZULLIN[96] studied the effects of sodium hydroxide concentration (0.01, 0.1, and 1N), temperature (25, 50, and 100°C) and current densities (15, 45, 100 and 200 $\mu A/cm^2$) on the anodic oxidation of nickel. An increase of current density (15-200 $\mu A/sq\ cm^2$) and decrease of concentration (0.01-1N) accelerated the passivation of nickel. The speed of passivation was found to be independent of temperature. This temperature independence suggests that the oxide layer is formed by oxidation of the surface by reprecipitation of the oxides on the surface.[96] Similar effects of temperature are observed at high temperatures (420-500°C) also by STERN and CARLTON.[98] In addition, it is found that in the presence of small amounts of oxygen, oxide formation takes place. The effects of oxygen and temperature are summarized in Fig. 37.

DAVIES and BARKER[97] have studied the changes of potential with time by galvanostatically polarizing the nickel electrode in 0.1N sodium hydroxide at 25°C. Anodic current densities of 2.5, 6.0 and 7.5 $\mu A/cm^2$ were employed. Figure 38 shows the potential-time curves under the above conditions. Two potential arrests are observed. The first arrest takes place between -0.61 V and -0.52 V. These values correspond to those observed in the case of the iron electrode and supports the theory that oxidation of iron and nickel electrodes is generally similar. The oxidation of nickel proceeds according to the following reaction in the POURBAIX[15] diagram for nickel (Fig. 2):

$$Ni + 2H_2O \rightarrow Ni(OH)_2 + 2H^+ + 2e \qquad (22)$$

for which the equilibrium potential is given by the following equation:

$$E = 0.11 - 0.0591\ pH \qquad (23)$$

The redox potentials are coincident with the observed values. By measuring the quantity of electricity the amount of oxygen evolved can be calculated from which it can be seen that during the first arrest, a monomolecular layer of NiO or $Ni(OH)_2$ is formed. The second potential arrest occurred at +0.125 and +0.175 mV_H corresponding to the oxidation of $Ni(OH)_2$ to Ni_3O_4 according to the equation,

$$3Ni(OH)_2 \rightarrow Ni_3O_4 + 2H_2O + 2H^+ + 2e \qquad (24)$$

for which the equilibrium potential is given by

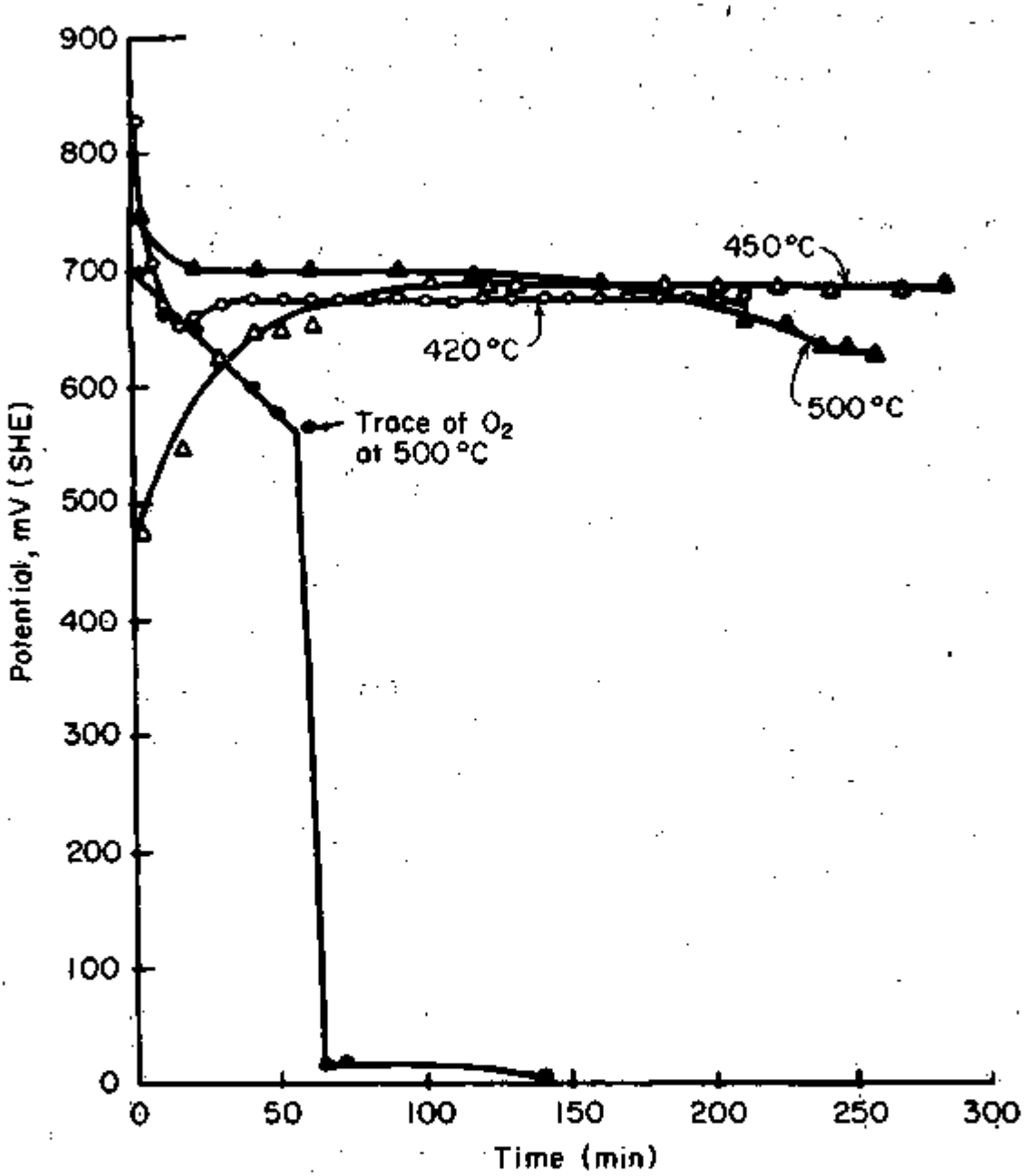

Fig. 37 - Effect of temperature and oxygen contamination on electrode potentials of nickel in fused NaOH.[98]

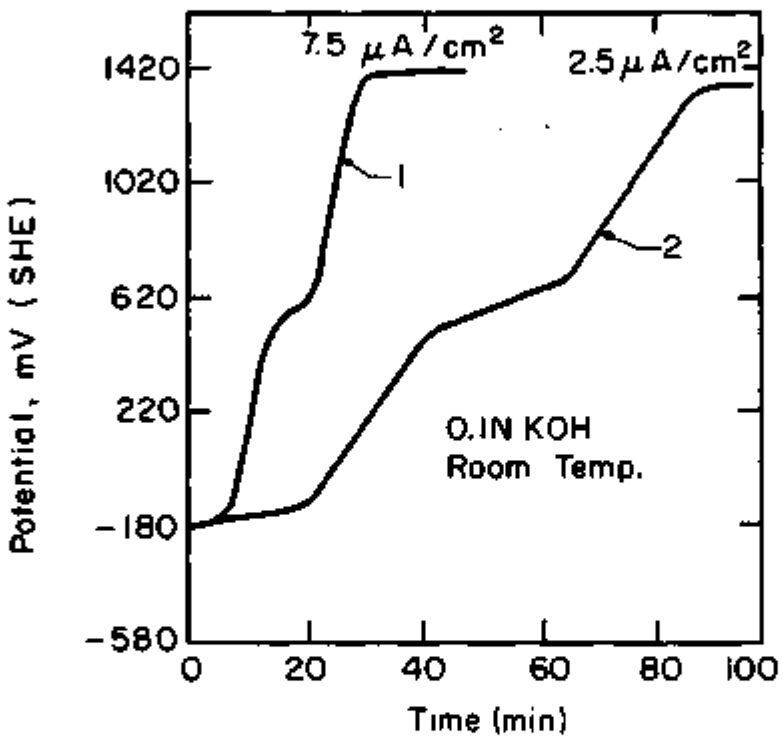

Fig. 38 - Anodic potential-time curves for nickel in KOH solution.[97]

$$E = 0.90 - 0.0591\ pH \qquad (25)$$

Calculated values agree with the above experimentally observed values. The following reaction also is thermodynamically possible:

$$2Ni(OH)_2 \rightarrow Ni_2O_3 + H_2O + 2H^+ + 2e \qquad (26)$$

The redox potentials, +0.26 to +0.34 V calculated from the equilibrium equation for this reaction coincide with the higher limits of the observed second potential arrests. By calculating the amount of oxygen evolved during this arrest, they predict the final formation of nonstoichiometric oxide corresponding to $NiO_{1.8}$. Similar oxides formed on the iron electrode.

c. Activated kinetics for oxygen evolution - Anodic polarization behavior has been studied by ELINA,[99] VOICHKOVA and KRASILSH'CHIKOV,[100] TSINMAN,[101] PIONTELLI,[102] and WEININGER and BREITER.[93]

The interesting features in these investigations are: (i) oxygen evolution proceeds through the decomposition of oxides in sodium and potassium hydroxide solutions and, (ii) studies on single crystals failed to reveal significant changes in polarization behavior with different orientations.

The anodic polarization curves in 0.01-5N sodium hydroxide solutions at 25°C shows two tafel slopes, 35 mV/decade below 2 mA/cm^2 and 100 mV/decade above this current density.[99] Similar observations have been made in potassium hydroxide solutions (0.01-5N KOH and 25, 80 and 95°C.[100] The curve, was comprised of two branches, the first being due to oxide formation and the second due to O_2 evolution. The position along the O_2 evolution line could be fitted according to the equation:

$$\eta = A + 0.7\ RT/F\ \ln i - 1.74\ RT/F\ \ln C \qquad (27)$$

where A is the constant; C is the hydroxyl concentration; η is the potential; R is the gas constant; and F, Faraday, T, temperature in °K, and i are the current densities.

The oxygen overvoltage on nickel electrodes having different surface conditions (oxidized, unoxidized) is independent of alkali activity at low current densities.[101] Table VIII gives the effects of OH concentration of $d\eta/d/\log$ and potential at $i = 10^{-4}$ A/cm^2 under various surface conditions. All the electrodes showed concentration-independent tafel slopes. The potentials determined by the dilution method (by measuring the steady state potential changes at a given current on diluting the solution from 5N to 0.04N) at various concentrations are given in Table IX. These values confirm the concentrations independent behavior under various surface conditions.

Table VIII - Slopes of Polarization Curves for a Nickel Anode in Sodium and Potassium Hydroxide Solutions (after TSINMAN)[101]

(Electrodeposited Nickel; Preliminary Polarization at $i = -1\ A/cm^2$, 24 hr)

	NaOH					
Concentration, M	9.5	7.5	5	2.5	1	0.4
$d\eta/d \log i$, mV	30	32	31	31	31	33
η at $i = 10^{-4} A/cm^2$, mV	238	244	238	226	238	242
	KOH					
Concentration, M	7.4	5	3.7	2.2	1.3	0.6
$d\eta/d \log i$, mV	35	34	33	32	33	46
η at $i = 10^{-4} A/cm^2$, mV	232	233	232	249	250	272

	Massive Nickel - NaOH (prepolarized, $-0.6 A/cm^2$, 20 hr)				
			Unoxidized electrodes		
Concentration, M	9.5	1	9.5	1	0.1
$d\eta/d \log i$, mV	32	33	44	44	43
η at $i = 10^{-4} A/cm^2$, mV	232	239	265	281	347

Table IX - Variation of Potential with NaOH Concentration at $i = 10^{-4} A/cm^2$ (dilution method) (after TSINMAN)[101]

c, M	Potential η (mV) at Time (min)* after Concentration Change
	Unoxidized electrode
5	steady value 275 mV
1	15'-277 mV
0.2	2'-277; 8'-277 mV
0.04	4'-281; 15'-282; 30'-283; 50'-281; 70'-285 mV
0.2	2'-278; 8'-278; 30'-278 mV
1	1'-280; 30'-280 mV
	Unoxidized electrode
0.04	steady value 319 mV
0.2	3'-317; 9'-315 mV
1	3'-311; 5'-311; 35'-300; 150'-304 mV
	Oxidized electrode (0.6 A/cm^2, 20 hr)
5	steady value 241 mV
1	3'-239; 20'-241 mV
0.2	3'-241; 15'-244 mV
0.04	5'-250; 10'-250; 24'-248; 33'-249 mV
0.2	4'-245; 10'-244; 16'-244; 28'-245 mV
1	8'-240; 60'-240 mV

*Note: In the table time is denoted by primes

The anodic and cathodic polarization measurements in the work of WEININGER and BREITER[93] was discussed earlier. They showed that crystallographic orientation does not have any effect on the anodic kinetics in H_2-saturated 0.1N sodium hydroxide solution at 25°C. This idea has been established quite earlier by PIONTELLI et al.,[102] but these authors did not carry out detailed investigations.

The lack of dependence of O_2 overvoltage on alkali concentration surface state and crystal orientation, suggests that O_2-evolution mechanism on oxidized and bare surfaces proceed by the same mechanism.[101]

Two mechanisms based on slow decomposition of Ni_2O_4 and NiO_2 are suggested:[101]

1. By formation and decomposition of Ni_2O_4:

$$OH^- \rightarrow OH + e \quad (28)$$
$$OH + OH^- \rightarrow O^- \; H_2O \quad (29)$$
$$O^- + Ni_2O_3 \rightarrow Ni_2O_4 + e \quad (30)$$
$$Ni_2O_4 \rightarrow O + Ni_2O_3 \quad (31)$$
$$2O \rightarrow O_2 \quad (32)$$

2. By formation and decomposition of NiO_2:

$$OH^- \rightarrow OH + e \quad (33)$$
$$OH + NiOOH \rightarrow NiO_2 + H_2O \quad (34)$$
$$2NiO_2 + H_2O \rightarrow 2NiOOH + O \quad (35)$$
$$2O \rightarrow O_2 \quad (36)$$

d. Structure of passive films on nickel electrodes - By measuring the electrode capacitance the anodic phenomena occurring on nickel electrode in hydroxide media have been further studied by ELINA et al.,[99] WEININGER and BREITER[93] and DELIMARSKII.[94] The significant features from their work are (i) capacitance-potential curves show significant peaks corresponding to the changes in type of electrochemical reaction; and (ii) capacitance measurements suggest that the oxide in melts behave as semiconductors.

The capacitance-potential curves[93] measured in argon saturated 4N potassium hydroxide solution at 25°C is given in Fig. 33. A differential capacitance of 22 $\mu F/cm^2$ is observed in the +600 - +800 mV_H range which is double-layer capacitance. As this value did not increase on successive sweeps, it can be inferred that surface area has not changed. The higher values at higher anodic potentials are Faradic pseudo capacitances due to electrode reactions. At anodic potentials of 1450 mV_H, capacitance rises to 500 to 550 $\mu F/cm^2$. This value corresponds to the formation of higher oxide NiO·OH. However, the lower portion is of importance as different adsorption and $Ni(OH)_2$ precipitation reactions take place. This region between -300 to +300 mV_H is drawn schematically in Fig. 34 showing three humps which are characterized by the following scheme of reactions:

(i) -100 mV_H and above: Electrochemical adsorption of hydroxide -- $Ni + OH^- \rightarrow Ni\text{-}OH + e$ (37)

(ii) The above reaction is accompanied or even may be replaced by oxidation of strongly adsorbed hydrogen atoms -- $Ni\text{-}H + OH^- \rightarrow Ni + H_2O + e$ (38)

(iii) +100 mV_H and above: formation of $Ni(OH)_2$ -- $Ni + 2OH^- \rightarrow Ni(OH)_2 + 2e$ (39)

The passivation of nickel in fused sodium hydroxide in the temperature range of 340 - 480°C has been studied by DELIMARSKII et al.[94] They found that the passivation of nickel is associated with an increase in the differential capacitance. The increase of capacitance with oxide formation is rather unusual. It is probable that the oxide behaves as a semi-conductor in the alkaline melt. Figure 39 shows the plot of dispersion capacitance and ohmic resistance as a function of alternating frequency. The ohmic component falls with time and becomes constant when the electrode is completely passive. Since certain electrometallurgical processes in alkalis involve intermetallics they were interested in studying the effects of adding 1 and 2 moles of Na_3Bi to the hydroxide melt. Their results are given in Fig. 40. The capacitance is reduced and the resistance is increased due to the reduction of oxide film by this intermetallic compound.

The x-ray structure analyses of anodically grown films in 6×10^{-3}N to 3N potassium hydroxide solutions in the temperature range of 5-80°C at several hours to ten days showed the existence of $Ni_3O_2(OH)_4$, $\beta Ni(OH)_2$ and α or β-NiO·OH.[103]

In the low concentration alkali solution at higher temperatures, the nickel oxylhydroxides produced were of lower valency of nickel and vice versa. The formation of another nickel oxyhydroxide (of unknown structure) also is observed.

e. Breakdown of passivity - As in the case of iron electrode here also breakdown of passivity occurs by agressive anions like chloride. The course of passivity breakdown can be studied either by galvanostatic or potentiostatic polarization measurements or by studying the changes in potential with time. Such effects by chlorides were investigated by LUKOVTSEV and LEVINA,[104] POSTLETHWAITE,[105] SCHWABE and RADEGLIA[106] and effects of other halide anions by TSYGANOV and ZAKRZHEVTSKAYA.[107] The essential points in their studies are (i) a chloride-to-hydroxide ratio of greater than 1 is essential to activate a passive nickel electrode; (ii) this ratio becomes even larger when concentrated solutions of hydroxides are used and in this case even saturated chloride solutions did not have any effect; (iii) temperature changes produced erratic effects and, (iv) activation proceeds through adsorption of halides over the metal surface and equilibrium interchange of the oxide ions of the lattice.

At constant current of 10^{-5} A/cm^2 the following changes in potential η were produced with the addition of varying amounts of sodium hydroxide to 0.2N potassium chloride solutions:

x,N of NaOH	Change in Potential, $\Delta\eta$ (mV, +)
1.0-0.01	88-92
0.01-0.001	22
0.001-0.0001	6-8

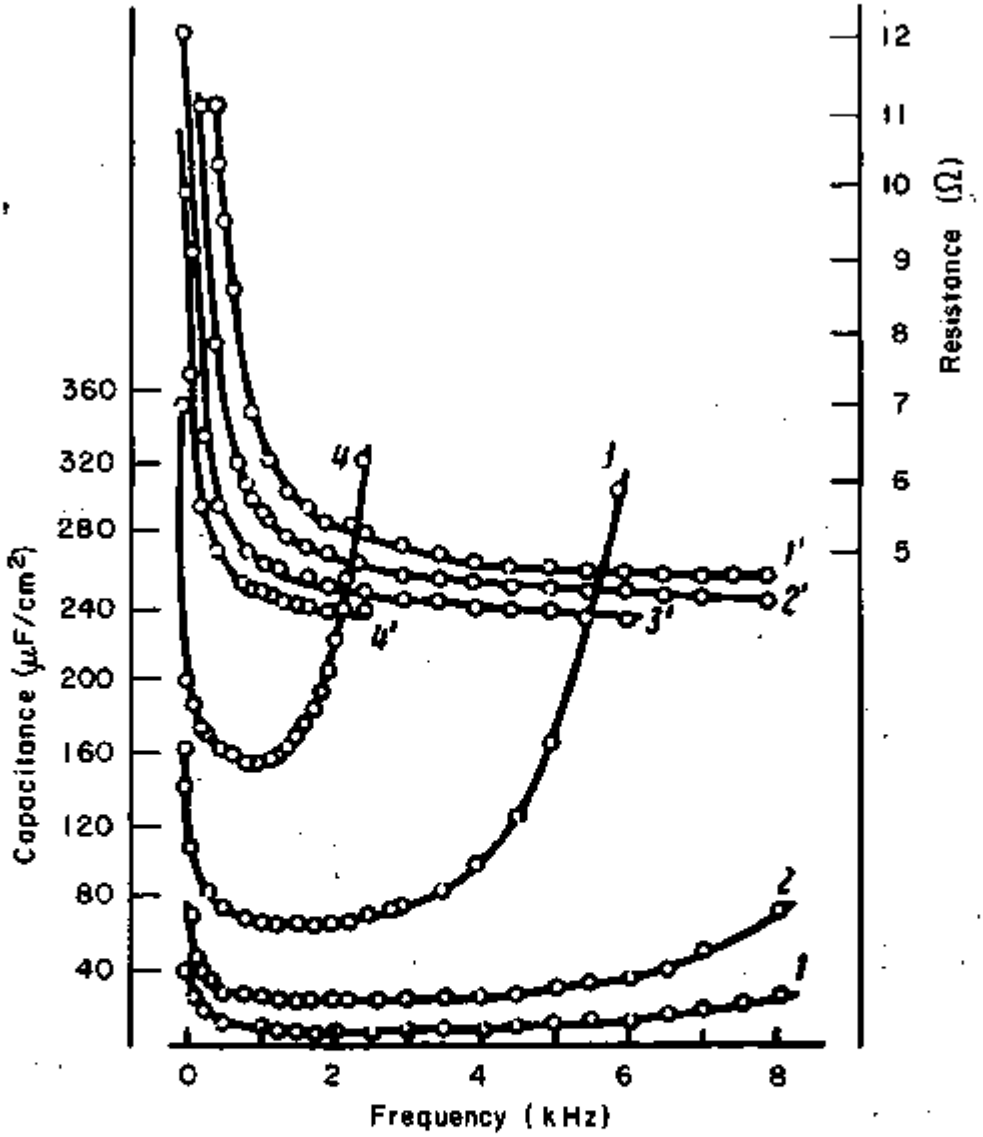

Fig. 39 - Dispersion of capacitance (curves 1-4) and ohmic resistance (curves 1'-4') of a nickel electrode in molten NaOH.[94]

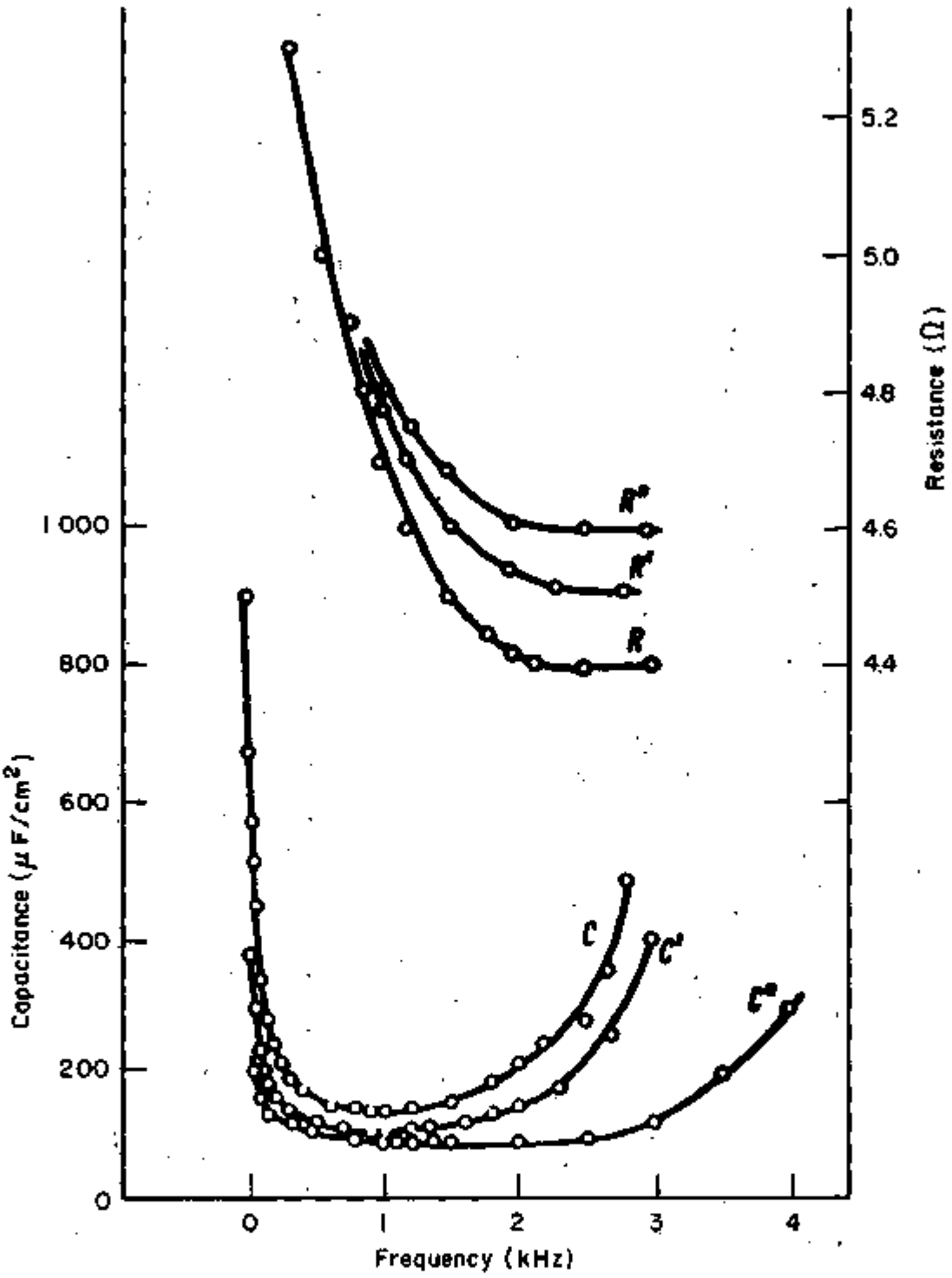

Fig. 40 - Influence of the intermetallic compound Na_3Bi on capacitance and resistance of a nickel electrode; mole % in sodium hydroxide: C', R'-1; C'', R''-2.[92]

Polarization measurements with these mixtures suggest that $(d\eta/di) \propto (1/x)$ at low concentrations of hydroxide and $(d\eta/di) \propto (1/x^2)$ at higher concentrations (between x, the concentration of NaOH, equals 0.1N and 0.1N).[104] They tried to account for these observations by processes of desorption.

The effects of chloride additions to sodium hydroxide (10^{-3} to 5N in the temperature range 25-275°C on the breakdown of passivity of nickel was studied by POSTLETHWAITE.[105] Figure 41 shows the effect of chloride addition on potentiostatic polarization behavior at (a) low chloride concentrations and (b) concentrations above critical values. At low concentrations hydrogen evolution takes place below $E_o(H/H^+)$ and O_2 above $E_o(H_2O/O_2)$. Between these potentials, an anodic current of 0.1 $\mu A/cm^2$, corresponding to the passive dissolution, was observed. Above critical chloride concentration, nickel dissolved and part of it precipitated as $Ni(OH)_2$. Figure 42 shows the plot relating breakdown and repassivation potential against pH at 25° and 0.01, 0.1 and 1N and saturated sodium chloride added. These potentials were determined by the potentiokinetic method. Higher lines represent the breakdown potential, while lower lines represent the repassivation potential. The values of breakdown potentials were in the range 0-1000 mV_H, depending on the concentration. Breakdown of passivation of either grade nickel did not occur in 5N sodium hydroxide with saturated sodium chloride.

The critical chloride-to-hydroxide ratio required for breakdown increases with hydroxyl concentration. The induction time for breakdown is dependent on the potential, the chloride-to-hydroxyl-ratio, and hydroxyl concentration. Breakdown times in the range 0.1 to 2000 minutes were obtained. As in the case of iron electrode, a critical ratio of 1 was required in 0.01, 0.1 and 1N sodium hydroxide. Figure 43 shows effect of temperature on breakdown and repassivation potentials of pure nickel in various alkaline chloride solutions. The trends shown in the figure are confusing. The effect of temperature is to stimulate the attack up to 175°C, but above this the trend is reversed; the critical potentials move to the higher values, and both the induction time and critical chloride concentration were raised. Passivation breakdown is accompanied by the precipitation of nickelous hydroxide over the whole temperature range, but the mode of attack changes from characteristic pitting at 25°C to more general attack at elevated temperatures where metal is removed over an expanding area. The galvanostatic experiments at different temperatures gave similar results to those observed by potentiostatic methods.

The voltage-time behavior of nickel at 1 mA/cm^2 after adding 0.05-0.6N potassium chloride to the mixture of 0.07N potassium hydroxide and 1.3N ammonia has been investigated by SCHWABE and RADEGLIA.[106] Figure 44 shows the potential-time curves under the above conditions. The changes of potential with time could be fitted into the following equation:

$$E_t = E_p - A\left[\frac{C_{HAL}}{C_{OH}}\right]\left[1-e^{-kt}\right] \qquad (40)$$

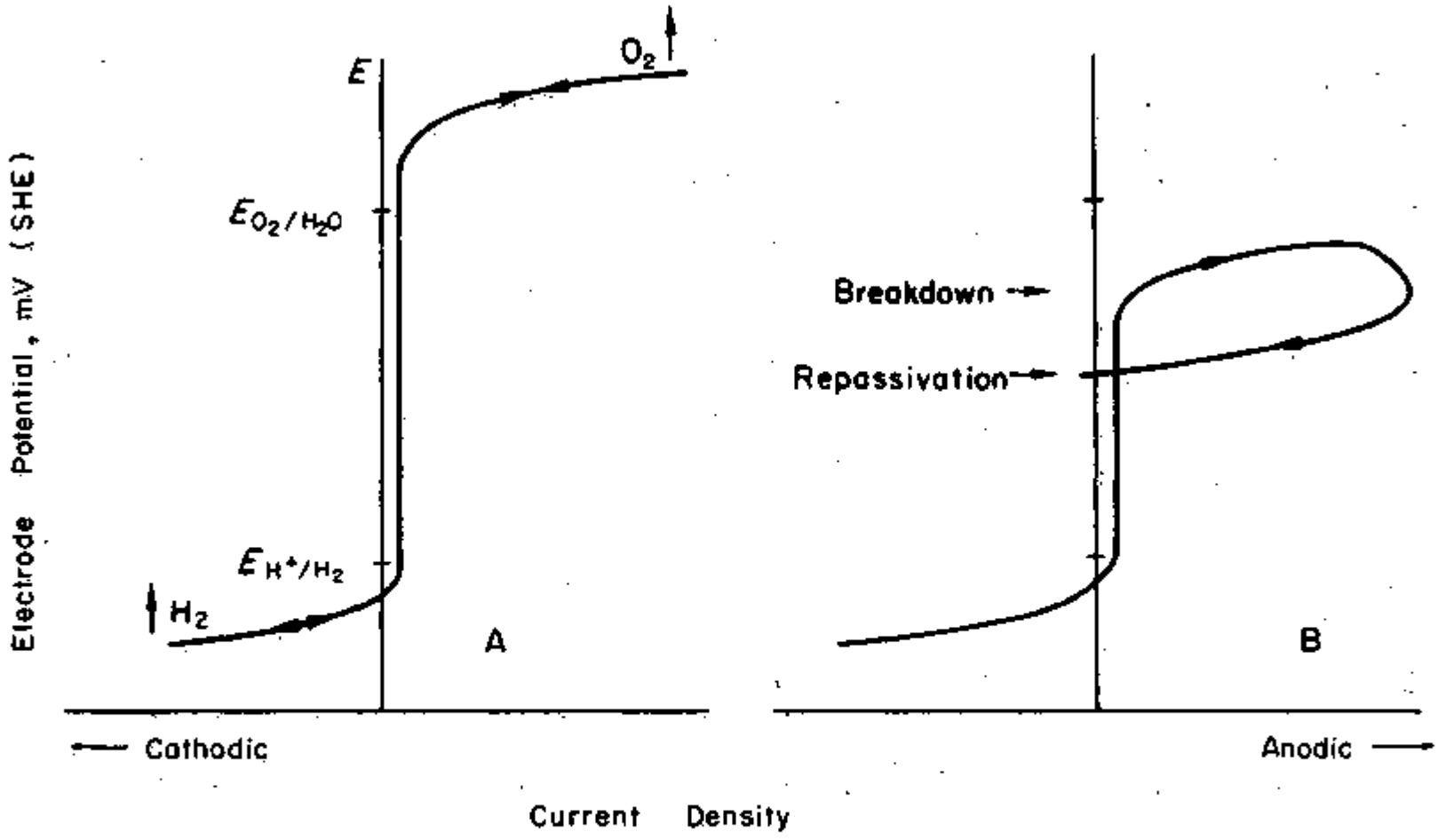

Fig. 41 - Effect of chloride additions on the potentiostatic behavior of nickel in alkaline solutions: (a) low chloride concentrations, (b) chloride concentration greater than the critical value.[105]

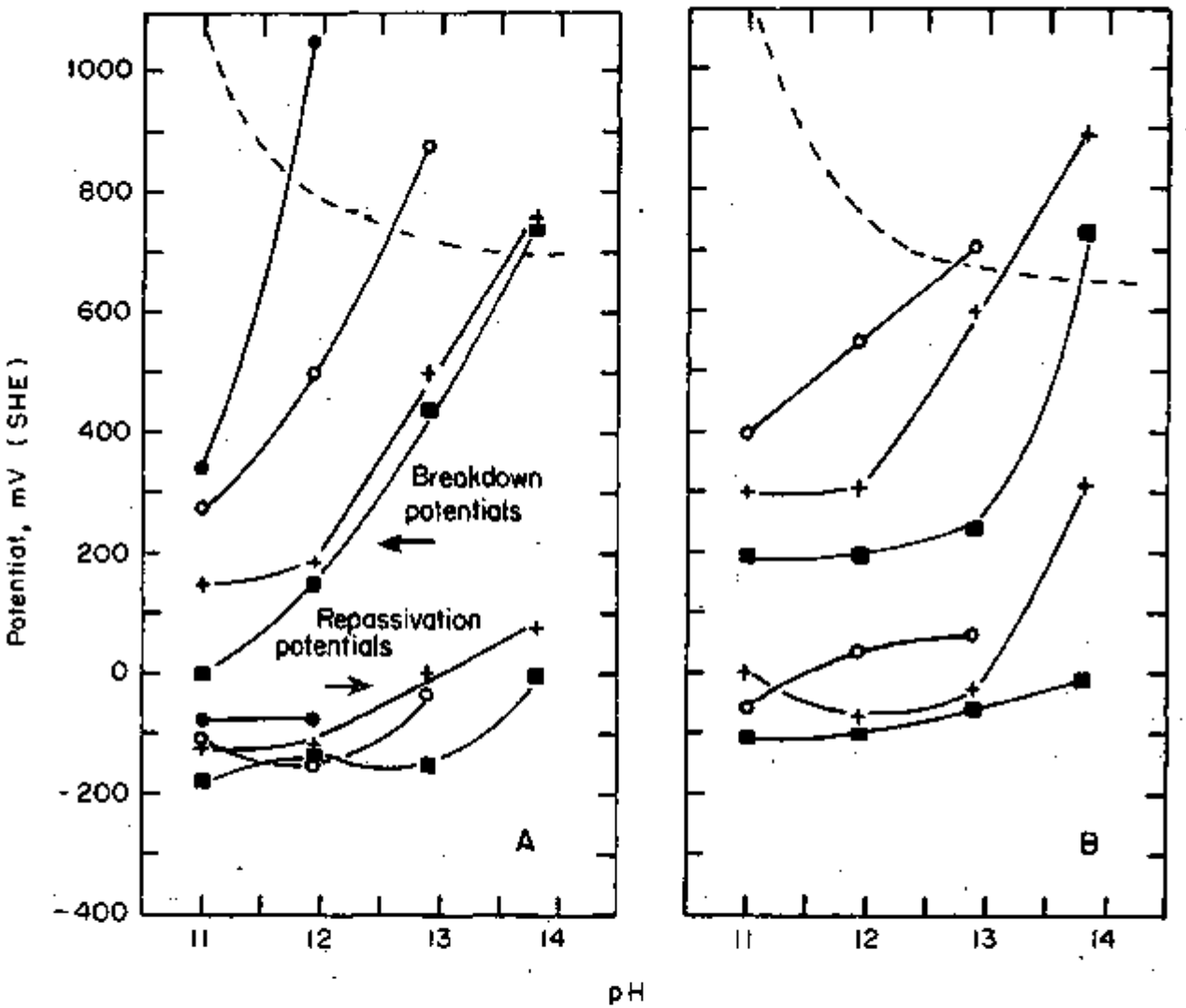

Fig. 42 - Breakdown and repassivation potentials: (a) commercial nickel and (b) pure nickel in alkaline chloride solutions at 25°C. ● = 0.01M NaCl, ○ = 0.1M NaCl, + = 1M NaCl, ■ = saturated NaCl; ---O_2 evolution potential for 100μA/cm^2.[105]

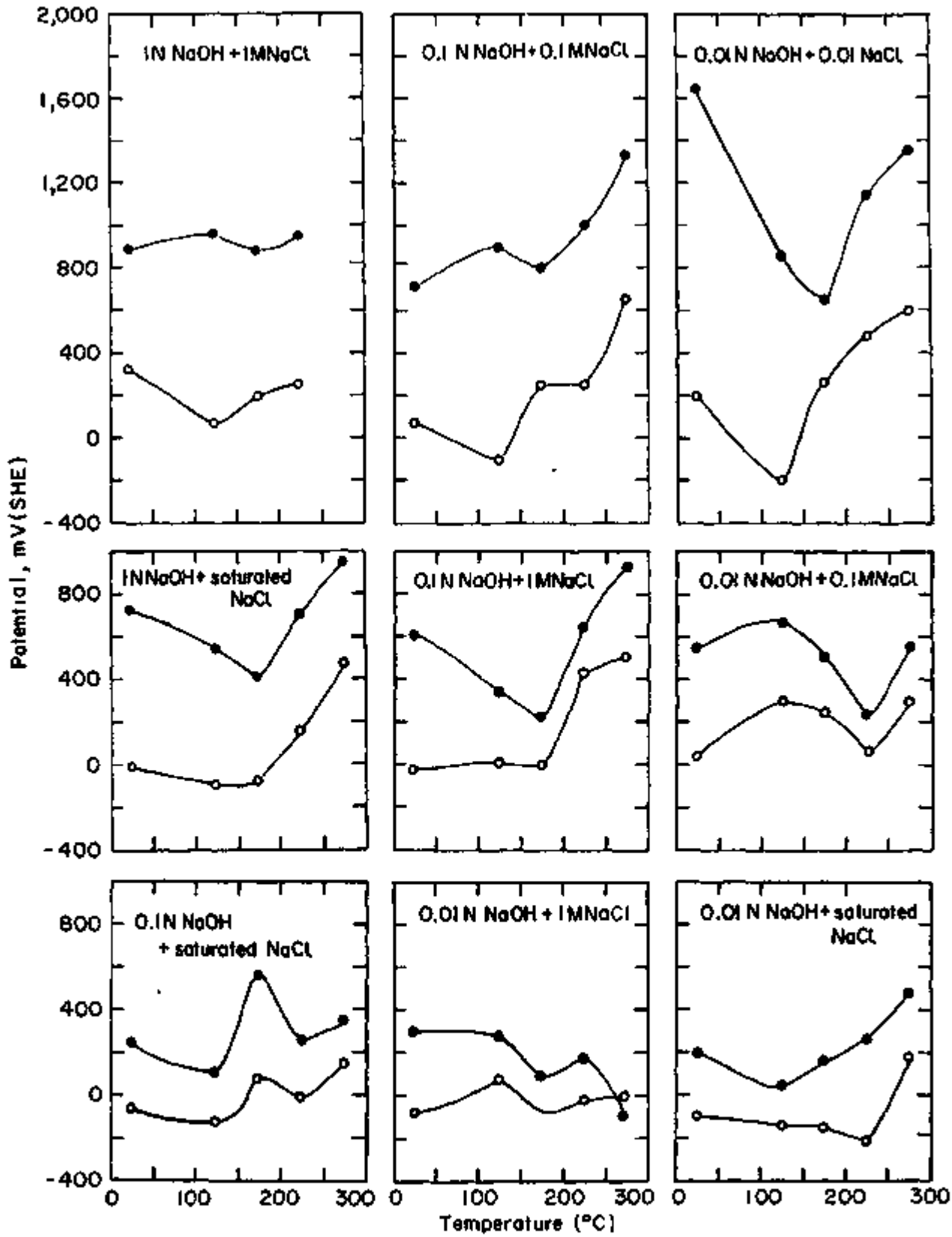

Fig. 43 - Effect of temperature on breakdown and repassivation potentials of pure nickel in alkaline chloride solutions: ○ = breakdown potentials, = repassivation potentials.[105]

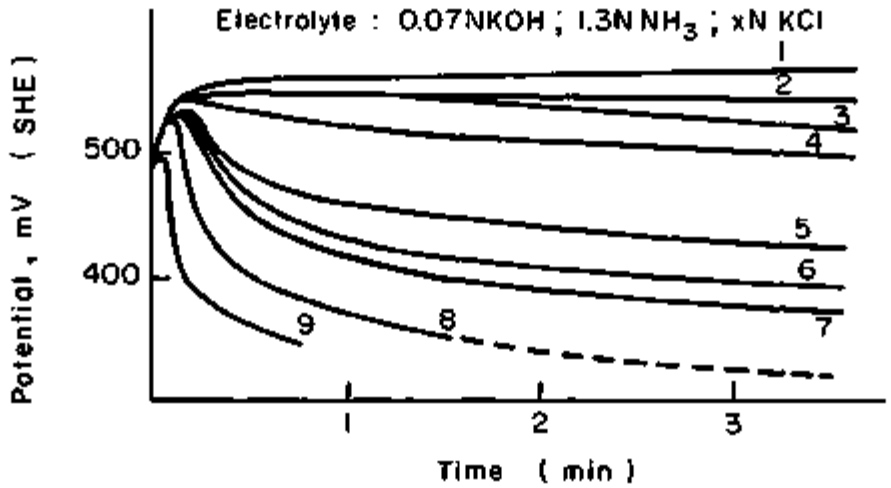

Fig. 44 - Effect of chloride concentration on electrode potential of a nickel electrode polarized at a current density of 1 mA/cm^2. M concentration of NaCl: Curve No. (1) = 0, (2) = 0.05, (3) = 0.08, (4) = 0.1, (5) = 0.2, (6) = 0.25, (7) = 0.3, (8) = 0.4, (9) = 0.6.[108]

where E_t is potential time at t, E_p is passivation potential at t = 0, C_{HAL} is halide concentration and C_{OH} is hydroxyl concentration; k and A are constants.

Similar activating effects on passivity of nickel were observed by the additions of other halides; namely, bromide, fluoride, and iodide.[107]

The above findings suggest that the breakdown of passivity is due to equilibrium exchange between halide and chemisorbed oxygen over nickel.

V. CORROSION OF CHROMIUM

Neither stress corrosion nor general corrosion experiences of pure chromium are reported in alkaline media. The existing information concerns only electrochemical studies.

A. ELECTROCHEMISTRY OF CHROMIUM ELECTRODE IN HYDROXIDE SOLUTIONS

The electrochemistry of the chromium electrode in alkaline media has been studied with respect to cathodic and anodic behavior and the properties of the oxides.

The cathodic behavior has been studied by AMMAR et al.[108] and FAIZULLIN and LEVINA.[109]

In the pH range 2.02-11.8 between current densities 7.5×10^{-5} to 7.5×10^{-4} A/cm^2 cathodic tafel slopes of 0.15-0.17 V/decade were observed.[108] While studying the anodic behavior, overall polarization curves for chromium in 1N and 10N potassium hydroxide are reported by FAIZULLIN and LEVINA.[109] Only the cathodic branch has been identified in these curves, besides which there is no indication of the values corresponding to this branch, nor the analysis of obtained cathodic portion of these curves.

The anodic behavior has been reported by AMMAR et al.,[108] KISS,[110] AGLADZE and IONATAMISTIVILI[111] and FAIZULLIN and LEVINA.[109] The essential features in these observations are:

(i) Chromium in sodium hydroxide solution goes into solution as hexavalent chromium;

(ii) The rates of anodic process by the stationary and non-stationary method was proportional to a first and second order, respectively, with respect to $(OH)^-$;

(iii) Polarization curves exhibit three distinct regions corresponding to anodic oxidation and cathodic reduction processes; and

(iv) Thermo-emf examination of semi-conduction properties of nickel corresponds to p-type of oxide.

The anodic polarization of chromium electrodes in 10-70% sodium hydroxide solution at 35°C and different current densities up to 30 A/dm^2 caused chromium to dissolve rapidly as Cr^{6+}.[111] The anodic tafel slopes in the pH range of 2.02-11.8 and current densities from 7.5 x 10^{-5} to 1.5 x 10^{-3} A/cm^2 had a value of 130-170 mV/decade.[108]

By the stationary and nonstationary methods, in the pH range of -0.4 to 14, the rates of anodic process is proportional to the first and second power of $(OH)^-$, respectively. The above work, done by KISS,[110] is in an obscure reference. By the nonstationary method it is meant to change the concentration of hydroxide at a constant potential and measure the steady state current densities. The slope of log [concentration of OH^-] vs. log [steady state current density] determines the reaction order. On the other hand, in the stationary method the steady state currents can be measured in different solutions at constant potentials. The measurement of reaction orders provide a direct insight into the transport processes of species which is the key factor in determining the electrochemical corrosion processes. This may be the method adopted by KISS.[110]

The anodic polarization behavior of chromium electrode in potassium hydroxide solution has been studied in greater detail by FAIZULLIN and LEVINA.[109] Cathodically activated, electrolytically pure chromium was anodically polarized. The structure of the passive film and the amount of chromium in solution were analyzed. They observed that the self-passivation and the open-circuit potentials in deaerated and oxygenated systems were quite different from that of $Cr/Cr(OH)_3$ and Cr/Cr_2O_3 systems. They assume the formation of nonstoichiometric oxides of adsorption type on the electrode surface. An examination of the semi-conducting properties of the oxide films by the thermal-emf method shows that oxides formed in KOH solutions have p-type of conductivity.

The polarization curves in 1N and 10N KOH were composed of three regions. From -1.05 to the corrosion potential, the reduction processes dominate and currents are negative. From the corrosion potential to +0.1 V (1N KOH) or 0.06 V (10N KOH) there is a region of anodic passivation. Above this region the current density increases owing to the formation of higher soluble oxides. The $K_2CrO_4^=$ concentration in solution 20 minutes below 1 volt is less than 0.38 g/l.

The composition of the passive film corresponds to Cr_2O_3. The primary anodic process is controlled by the reactions $OH^- = OH + e$ and

$H_2O = OH + H^+ + e$. The OH reacts with the chromium metal to form adsorbed oxides of the Cr(OH) or CrOOH types. The adsorption of OH radicals favors the formation of nonstoichiometric oxides with cationic vacancies, thus producing p-type conductivity of the oxide films. At potentials above 0.2 V, the passivation film is still preserved, which might be a result of a continuous formation of soluble oxides by the anodic oxidation of the oxide layer. The oxide stoichiometries are comparable to the oxides of iron and nickel.

VI. CORROSION OF BINARY ALLOYS OF IRON, NICKEL, AND CHROMIUM IN CAUSTIC ENVIRONMENTS

A. IRON-NICKEL

General corrosion behavior has been studied by SHARMIN et al.[112] and the anodic polarization behavior by DEZIDER'EVA and SAGEEVA.[113]

The corrosion rates of rotating disk steel specimens containing 2-3% nickel in 3% sodium hydroxide solutions at 140°C are found to be considerably less (by a factor of 2-3) than ordinary steels. This behavior is accounted for by surface enrichment of nickel when the iron dissolves away.[112]

The effects of nickel in nickel-iron alloys on the anodic polarization behavior in 1N NaOH solution at 25°C has been investigated by SAGEEVA.[113] As the nickel content in the alloy is reduced from 75% to 32% they find the passivity is reduced. The passive film on the 75% nickel alloy is a solid solution of iron oxides in nickel hydroxide ($Ni(OH)_2$). The rings on the electron diffraction patterns of alloys containing 49 and 32% nickel are probably due to the superposition of various phases.

B. IRON-CHROMIUM

The corrosion behavior has been studied by SAKIYAMA and FUJIMOTO.[114] Anodic polarization behavior of this system has been studied by AGLADZE and IONATAMISTIVILI[111] and DENHOIM.[115] They found that, (i) higher chromium alloys are more resistant to corrosion than lower ones; and (ii) passivity in these alloys arises out of the formation of $(FeCr)_3O_4$.

SAKIYAMA and FUJIMOTO[114] reported that the chromium-iron alloys in 47% sodium hydroxide solutions containing 0-5% $NaClO_3$ at 90°C are not corrodible. They also found that the higher chromium compositions were more resistant than the lower ones.

During the anodic polarization measurements on ferrochromes in 10-70 g/l sodium hydroxide at 35°C it is reported that the film formation and nature of the passive film was dependent on the concentration of sodium hydroxide solution -- a brittle film being observed at low concentrations. The behavior of alloys containing 4, 8, 12, 16 and 20% chromium in pH 8 buffers comprised of various anions like nitrates, sulphates, chlorides at 30°C has been studied in detail. The complete active-passive range was covered and differential capacities measured; charging curves based on coulomb consumption were also plotted. Passivity in these alloys arises from the formation of $(FeCr)_3O_4$. The exact chromium content at the passive limit varies with the anion in the solution, but it is between 12-16% chromium. In alloys containing chromium above the mentioned limit, the dissolution from the alloy surface provides trivalent cations to stabilize the surface film in which Fe_3O_4 films is unstable with respect to Fe^{++}. The passivity occurs when 25% of the trivalent states are occupied by Cr^{+++}.

VII. CORROSION OF IRON-NICKEL-CHROMIUM ALLOYS

This alloy system includes the stainless steels, Incoloys and Inconels. The compositions, corresponding to the various specifications, are given in Table X. The phase limits of these alloys are shown by the phase diagram in Fig. 45. The special category of the stainless steels is an austenitic type in which the alloys contain 6-22% nickel and 16-26% chromium. The austenitic stainless steels are hardened by cold-working and are usually face-centered-cubic. Incoloys contain 30-50% nickel and Inconels contains more than 50% nickel.

A. STRESS CORROSION CRACKING

When compared to chloride environments, caustic environments have been less studied. WILLIAMS,[116] as early as 1946, reported the failure of some austenitic steel turbine blades when exposed to caustic environments. Also, HOAR and HINES[117] cited a case of cracking in 50% sodium hydroxide at 390°C. Williams[118] has reviewed the caustic cracking situation, including his preliminary results, in 1957. This review is followed by two brief communications by SNOWDEN,[119] and WANKLYN and JONES.[120] In a recent review LATANISION and STAEHLE[8] brought out significant features about SCC of iron-nickel-chromium alloys in caustic solutions.

In the present section, the stress corrosion cracking will be considered with respect to the effect of variables like sodium hydroxide concentration, temperature, superheat and dew-point, stress level, alloying elements and heat treatments on on the failure behavior.

Table X - Chemical Composition Limits and Ranges for Stainless Steels (after LATANISION and STAEHLE)[8]

Designation or Type Number	C	Mn, Max	Si Max	P Max	S Max	Cr	Ni	Other Elements
			I. Martensitic Chromium Steels					
403	0.15 Max	1.00	0.50	0.040	0.030	11.50-13.00		
410	0.15 Max	1.00	1.00	0.040	0.030	11.50-13.50		
414	0.15 Max	1.00	1.00	0.040	0.030	11.50-13.50	1.25-2.50	
416	0.15 Max	1.25	1.00	0.06	0.15 Min	12.00-14.00		Mo:0.60 Max
416 Se	0.15 Max	1.25	1.00	0.06	0.06	12.00-14.00		Se:0.15 Min
420	Over 0.15	1.00	1.00	0.040	0.030	12.00-14.00		
431	0.20 Max	1.00	1.00	0.040	0.030	15.00-17.00	1.25-2.50	
440A	0.60-0.75	1.00	1.00	0.040	0.030	16.00-18.00		Mo:0.75 Max
440B	0.75-0.95	1.00	1.00	0.040	0.030	16.00-18.00		Mo:0.75 Max
440C	0.95-1.20	1.00	1.00	0.040	0.030	16.00-18.00		Mo:0.75 Max
501	Over 0.10	1.00	1.00	0.040	0.030	4.00-6.00		Mo:0.40-0.65
502	0.10 Max	1.00	1.00	0.040	0.030	4.00-6.00		Mo:0.40-0.65
			II. Ferritic Chromium Steels					
405	0.08 Max	1.00	1.00	0.040	0.030	11.50-14.50		Al:0.10-0.30
430	0.12 Max	1.00	1.00	0.040	0.030	14.00-18.00		
430F	0.12 Max	1.25	1.00	0.06	0.15 Min	14.00-18.00		Mo:0.60 Max
430F Se	0.12 Max	1.25	1.00	0.06	0.06	14.00-18.00		Se:0.15 Min
446	0.20 Max	1.50	1.00	0.040	0.030	23.00-27.00		N:0.25 Max
			III. Austenitic Chromium-Nickel Steels					
201	0.15 Max	5.50-7.50	1.00	0.060	0.030	16.00-18.00	3.50-5.50	N:0.25 Max
202	0.15 Max	7.50-10.00	1.00	0.060	0.030	17.00-19.00	4.00-6.00	N:0.25 Max
301	0.15 Max	2.00	1.00	0.045	0.030	16.00-18.00	6.00-8.00	
302	0.15 Max	2.00	1.00	0.045	0.030	17.00-19.00	8.00-10.00	
302B	0.15 Max	2.00	2.00-3.00	0.045	0.030	17.00-19.00	8.00-10.00	
303	0.15 Max	2.00	1.00	0.20	0.15 Min	17.00-19.00	8.00-10.00	Mo:0.60 Max
303 Se	0.15 Max	2.00	1.00	0.20	0.06	17.00-19.00	8.00-10.00	Se:0.15 Min
304	0.08 Max	2.00	1.00	0.045	0.030	18.00-20.00	8.00-12.00	
304L	0.03 Max	2.00	1.00	0.045	0.030	18.00-20.00	8.00-12.00	
305	0.12 Max	2.00	1.00	0.045	0.030	17.00-19.00	10.00-13.00	
308	0.08 Max	2.00	1.00	0.045	0.030	19.00-21.00	10.00-12.00	

Table X (continued)

Designation or Type Number	C	Mn Max	Si Max	P Max	S Max	Cr	Ni	Other Elements
			Austenitic Chromium-Nickel Steels (cont'd)					
309	0.20 Max	2.00	1.00	0.045	0.030	22.00-24.00	12.00-15.00	
309S	0.08 Max	2.00	1.00	0.045	0.030	22.00-24.00	12.00-15.00	
310	0.25 Max	2.00	1.50	0.045	0.030	24.00-26.00	19.00-22.00	
310S	0.08 Max	2.00	1.50	0.045	0.030	24.00-26.00	19.00-22.00	
314	0.25 Max	2.00	1.50-3.00	0.045	0.030	23.00-26.00	19.00-22.00	
316	0.08 Max	2.00	1.00	0.045	0.030	16.00-18.00	10.00-14.00	Mo:2.00-3.00
316L	0.03 Max	2.00	1.00	0.045	0.030	16.00-18.00	10.00-14.00	Mo:2.00-3.00
317	0.08 Max	2.00	1.00	0.045	0.030	18.00-20.00	11.00-15.00	Mo:3.00-4.00
321	0.08 Max	2.00	1.00	0.045	0.030	17.00-19.00	9.00-12.00	Ti:5 x C, Min
347	0.08 Max	2.00	1.00	0.045	0.030	17.00-19.00	9.00-13.00	Cb-Ta:10 x C, Min
348	0.08 Max	2.00	1.00	0.045	0.030	17.00-19.00	9.00-13.00	Cb-Ta:10 x C, Min Ta:0.10 Max, Co:0.20 Max
			IV. Precipitation Hardening Stainless Steels					
PH 15-7 Mo	0.07 Max	0.70	0.40			15.00	7.00	1.15Al, 2.25M
PH 17-4	0.04 Max	0.40	0.50			16.50	4.25	0.25Cb, 3.6Cu
PH 17-7	0.07 Max	0.70	0.40			17.00	7.00	1.15Al
AM-350	0.10 Max	0.75	0.35			16.50	4.25	2.75Mo, 0.10N
AM-355	0.13 Max	0.85	0.35			15.50	4.25	2.75Mo, 0.12N
			V. Others					
Inconel 600	0.04 Max	0.20	0.20		0.007	15.8	76.0	7.20Fe
Inconel 625	0.05 Max	0.15	0.30		0.007	22.0	61.0	3Fe, 4Cb, 9Mo
Inconel 718	0.04 Max	0.20	0.20		0.007	19.0	52.5	18.0Fe, 0.60Al, 0.80Ti, 5.2Cb, 3Mo
Inconel X750	0.04 Max	0.70	0.30		0.007	15.0	73.0	6.75Fe, 0.80Al, 2.50Ti, 0.85Cb
Incoloy 800	0.04 Max	0.75	0.35		0.007	20.5	32.0	46.0Fe, 0.30Cu
Incoloy 804	0.06 Max	0.90				29.0	43.7	24.50Fe, 0.40Cu
Incoloy 825	0.03 Max	0.65	0.35		0.007	21.5	41.8	30Fe, 1.80Cu, 0.15Al, 0.90Ti, 3.0Mo
Nimonic 75	0.10 Max	0.45	0.45		0.007	20.5	77.6	0.50Fe, 0.20Al, 0.35Ti

Table X (continued)

Designation or Type Number	C	Mn Max	Si Max	P Max	S Max	Cr	Ni	Other Elements
				Others (cont'd)				
Tenelon	0.08 Max	14.70	0.52	0.025	0.006	18.0		0.13Mo, 0.11Cu, 0.40N
Incoloy 16-1	0.03 Max					16.75	1.09	1.51Mo, 0.90Cu
Carpenter 20	0.07 Max	0.7				20.0	29.0	2.00Mo, 3.00Cu
*Carpenter 7 Mo	0.20 Max	1.0				23-28	2.5-5	1-2Mo
CD4MCu	0.04	1.0				25-27	4.7-6.0	1.75-2.25 Mo, 2.75-3.25Cu

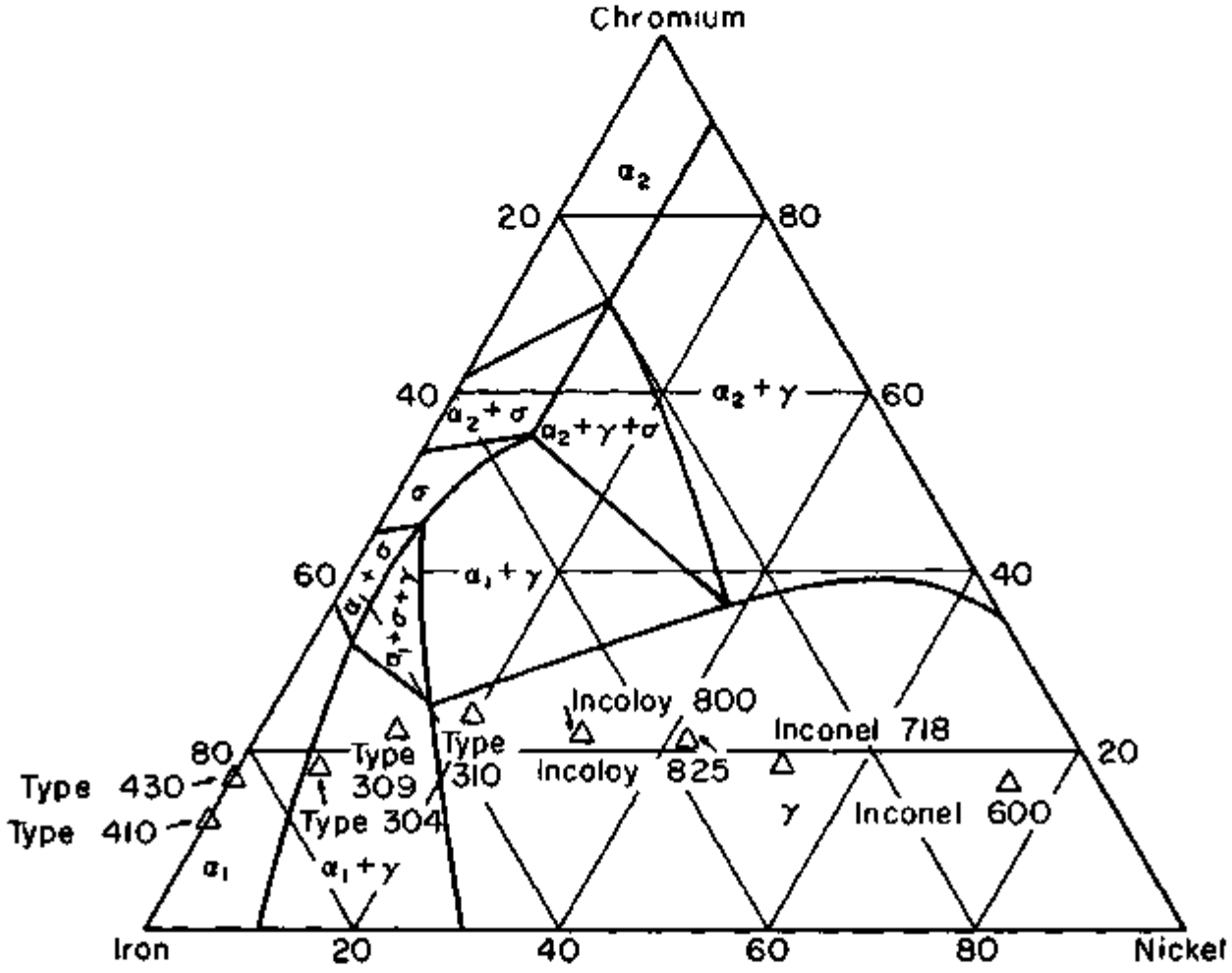

Fig. 45 - Isotherm of Fe-Ni-Cr alloy system at 400°C.
[Pugh and Nisbet, Trans. AIME, 188, 268 (1950)]

1. Effect of Hydroxide Concentration

The effect of hydroxide concentration has been studied by the following authors with respect to specific environments: sodium hydroxide -- SWANDBY,[121] SNOWDEN,[122] CORIOU and GRALL,[123] SIDOROV and RYABCHENKOV,[124] PICKETT et al.,[125] and HOWELLS;[126] potassium hydroxide -- SNOWDEN,[122] and CORIOU et al.,[127,128] lithium hydroxide -- BORMANN and GALONIAN[129] and PEMENT.[130] The essential conclusions of these investigations are: (i) rate of cracking decreases with decreasing sodium hydroxide; (ii) concentration below which cracking would not occur is dependent on stress, temperature and heat treatment; and (iii) sodium hydroxide is more aggressive than potassium hydroxide and lithium hydroxide.

Figure 46 summarizes the data on resistance of 304 and 316 stainless steels to various concentrations of sodium hydroxide and boiling point curve as a function of sodium hydroxide concentration. It can be seen from this figure that at low concentrations, the temperatures have to be raised above boiling point for cracking to take place, at medium concentrations it will occur even below boiling point, and at high concentrations up to 80%, cracking takes place at boiling point.

The general trend with hydroxide concentration is that the resistance of the specimen to cracking increases with decreasing hydroxide concentration (Type 347 - Table XI, Type 321 - Fig. 47).[122,124] The concentration below which cracking would not occur is supposed to be 0.1% for both potassium and lithium hydroxides with the 347-type stainless steels.[122,129,130] The fact that this value is dependent on stress level and temperature is clearly demonstrated in SIDOROV and RYABCHENKOV,[124] and PICKET et al.[125] work, where it can be seen that at a stress level of 42, 660 psi the critical concentration below which cracking would not occur is less than 3% at 200 and less than 1% at 300°C, respectively (Fig. 47).

The influence of sodium hydroxide concentration on SCC of Type 347 stainless steel has been investigated in liquid sodium as well as aqueous environments by HOWELLS,[126] in the temperature range 362-454°C. The solution was freed of oxygen contamination. HOWELLS' results are presented in Table XII. At 454°C cracking occurred at all concentrations when sodium hydroxide was in molten sodium. All cracking in this study was transgranular.

The relative aggressiveness of hydroxides can be arranged in the following order: Na > K > Li, (Tables XIII and XIV).[123,127,128] Sodium hydroxide appears to be twice as aggressive as potassium hydroxide.

In the case of lithium hydroxide solutions, PEMENT[130] has established a useful parameter; namely, the cracking index. It is given

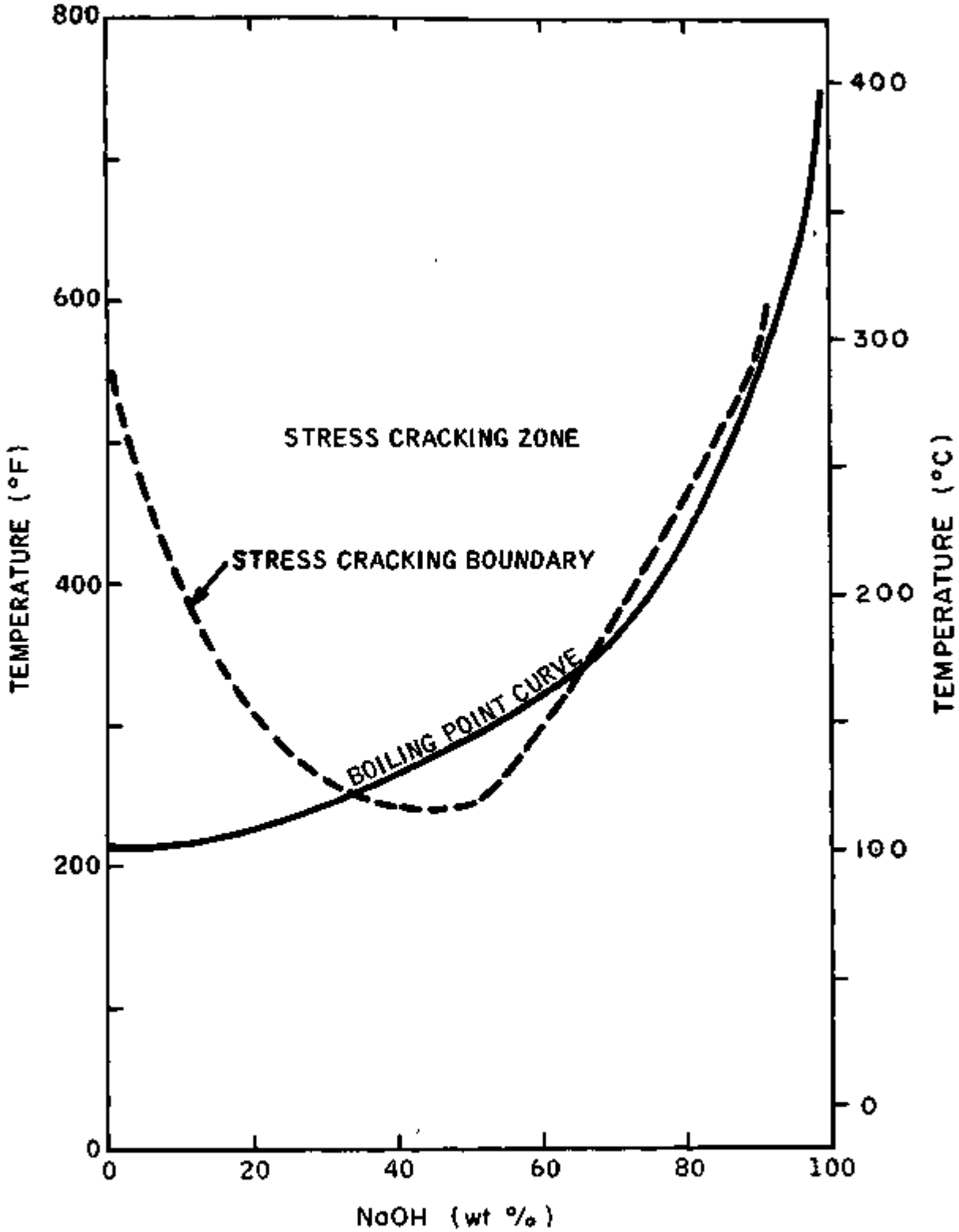

Fig. 46 - Temperature and concentration of sodium hydroxide necessary to produce stress corrosion cracking in types 304 and 316 stainless steels.[121]

Table XI - Effects of Concentration, Stress, and Temperature on Specimen Lives in KOH and NaOH Solutions (after SNOWDEN)[122]

Effect of Concentration at 300°C and 22,400 psi			Effect of Stress at 300°C			Effect of Temp. with 22,400 psi Stress		
Wt.%	Life with KOH, hr	Life with NaOH, hr	Applied Stress, psi	Life with 20% KOH, hr	Life with 20% NaOH, hr	Temp., °C	Life with 20% KOH, hr	Life with 20% KOH, hr
50	7.8	2.1	44,800	2.0	...	300	3.8, 19.8	1.1, 1.8
20	3.8, 19.8	1.1, 1.8	22,400	3.8, 19.8	1.1, 1.8	250	12.2, 55.7	3.6, 1.6
5	51.2, 17.0	0.4, 15.1	16,800	... ...	137	200	40.8, 82.6	177.8
1	17.9, 150 UB*		11,200	16.9, 30.3	112, 118	175	43.7, 195.8	
0.1	551 UB*		4,480	28.5, 88.5	400 UB*	150	500 UB*	

*Unbroken

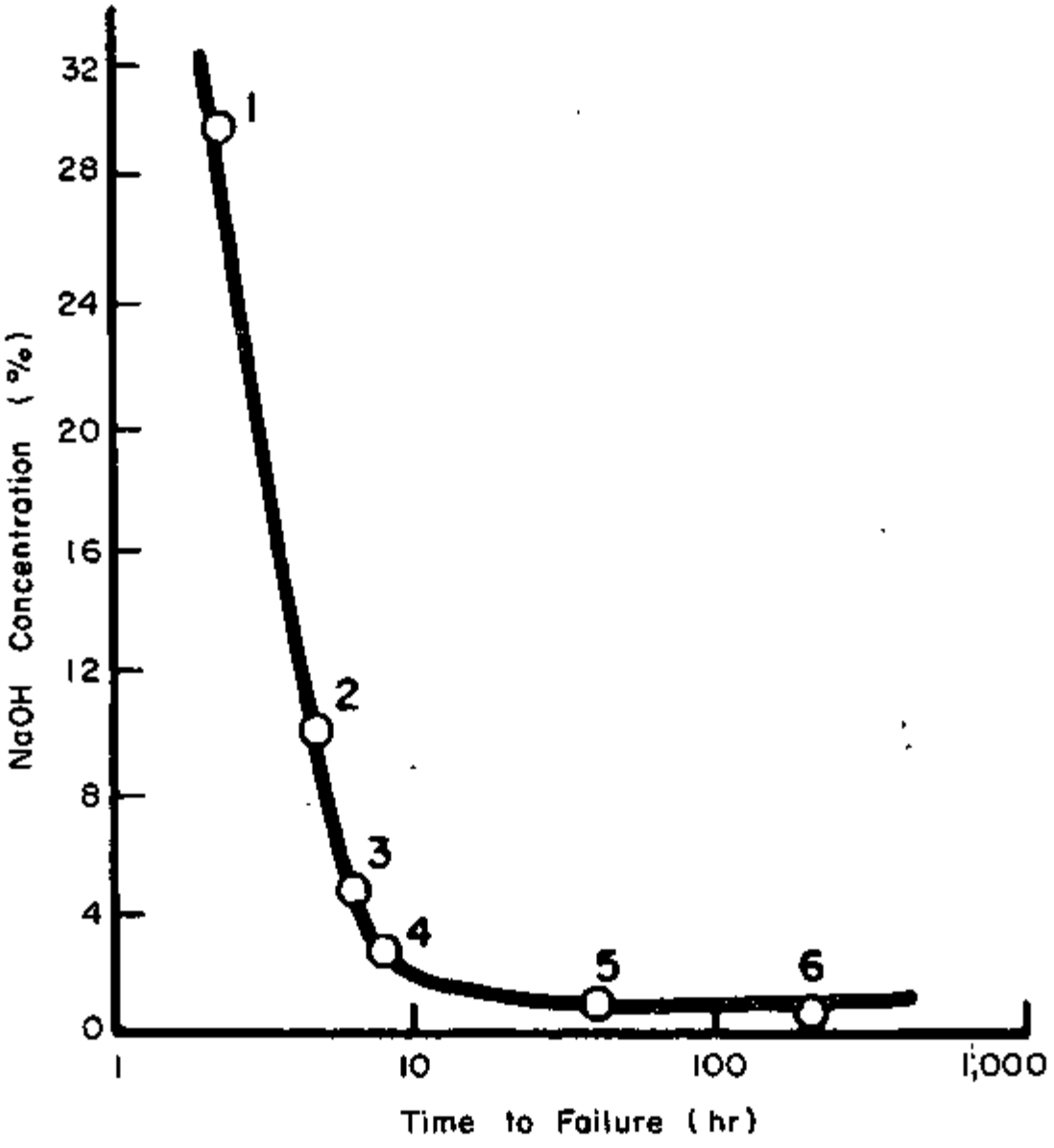

Fig. 47 - Dependence of time-to-failure of essentially type 321 stainless steel on concentration of NaOH solution (tests at 42,000 psi, 330°C).[124]

Table XII - Incidence of Cracking in Type 347 Stainless Steel U-Bends Exposed to Sodium Hydroxide Solutions (after HOWELLS)[126]

Temp. °C	Mixture	Days	Cracking
454	16% NaOH in Na	30	yes
454	30% NaOH in Na	20	yes
454	60% NaOH in Na	30	yes
454	100% NaOH	14	yes
454	96% NaOH in H_2O	30	no
399	100% NaOH	30	no
399	95% NaOH in H_2O	30	no
362	100% NaOH	30	no
362	80% NaOH in H_2O	1	yes

Table XIII - Chemical Compositions of Various Stainless Steels Studied (after CORIOU)[128]

Designation	C	Cr	Ni	Mo	Si	Mn	Other Elements
17/13 Mo Cu	0.018	17.6	13.0	2.5	0.4	0.8	Cu 1.66
17/13 Mo. .	0.024	17.6	13.4	2.8	0.6	1.6	
18/14 Si. .	0.027	17.7	14.4	0.7	3.9	0.7	
17/10 . . .	0.017	17.5	10.5		0.3	1.0	
17/15 . . .	0.025	17.2	14.9		0.5	1.0	
17/25 . . .	0.016	17.1	24.5		0.5	1.0	
17/35 . . .	0.025	17.3	34.7		0.5	1.1	
17/45 . . .	0.014	17.3	44.3		0.5	1.1	
17/65 . . .	0.008	17.5	64.5		0.5	1.1	
17/77 . . .	0.026	17.8	77.5		0.5	1.1	
15/78 . . . (Inconel 600)	0.040	14.0	78.4		0.2	0.1	Ti 0.2

Table XIV - Comparative Behavior of 0.06C, 17.4Cr, 12.0Ni, 2.2Mo 0.4Ti, 1.8Mn and 0.4Si Percent Stainless Steel in Hydroxides of K, Na and Li (after CORIOU)[128]

O_2 = 0.1 mg/l

Concentration	Time to Failure		
	Potassium Hydroxide	Sodium Hydroxide	Lithium Hydroxide
0.25N	8-10 hr	4-6 hr	Not cracked - 6 months
0.25N	8-10 hr	2-4 hr	"
0.025N	3-4 months	Not cracked-4 months	"
0.0025N	3-4 months	Not cracked-4 months	"

by the formula $100/n \sum_{i=1}^{n} \frac{1}{t_i}$ where n is the number of samples tested and t is the failure time of i^{th} sample. Cracking index is the indication of probability of failure. The cracking index increases with increasing concentration. PEMENT reports cracking index values of 0.070 to 0.728, 0.13 to 0.556 and 0.1 to 9.7 in the temperature and concentration ranges of 260°C, 1.00-4.86M; 287.5, 1.00-4.95; and 315.5°C, 4×10^{-7} to 4.9M, respectively.

2. Effect of Stress

The effect of stress has been studied by SNOWDEN,[122] PICKETT et al.,[125] HOWELLS[126] and AZHOGIN.[131]

The effect of stress on failure times of 347 niobium stabilized steels in 20% sodium and potassium hydroxides at 300°C was studied. With increase from 4480 to 44,800 psi, failure times decrease from 88.5 to 2.0 hours. A similar trend is reported by PICKETT et al.,[125] with 304 austenitic stainless steel in 1% sodium and potassium hydroxide at 343°C. It is reported that depth of cracks was roughly proportional to applied stress.[126]

The data on the effect of tensile stress on failure time could be fitted into the equation $(\sigma-\sigma_{cr})\ \tau = k$, where σ is the tensile stress, σ_{cr} is critical stress, τ is time for cracking, and k is a constant,[131] With potassium hydroxide solution containing sodium nitrite, this equation becomes $(\sigma-72.6)\ \tau = 158.4$.

3. Effect of Temperature

The temperature determines the region of caustic concentrations in which cracking would occur and the rate of crack propagation. In accordance with the expectations, SNOWDEN[122] found that an increase in the temperature between 150-300°C decreases the specimen life from 500 hours (unbroken) to 1.1 hours in 20% potassium and sodium hydroxide solutions (Table XI).

4. Effect of Steam and Superheat

SNOWDEN[122] investigated the effect of dew point and superheat environments on the cracking of contaminated specimens in the temperature range of 275-350°C. The contamination was achieved by immersion in 30% solution and exposing to steam. There was a shift in the mode of cracking, and it was predominantly transgranular as shown in Fig. 48. Potassium hydroxide contaminated specimens cracked intergranularly below the melting point of potassium hydroxide (380°C) and transgranularly above this temperature.

5. Effect of Alloying Elements

The effect of alloying elements has been studied by SNOWDEN,[132] KAGAN and MIKHAILOVA,[133] TRUMAN and PERRY,[134] AKOLZIN et al.,[135] COPSON and ECONOMY,[136] and CORIOU et al.[127,128] The highlights of their investigations are: (i) increased nickel offers greater SCC resistance to the alloy; (ii) the beneficial effect of nickel is quite dependent upon chromium level in the alloy as shown by TRUMAN and PERRY,[134] and (iii) the addition of molybdenum reduced the resistance to cracking.

Results of tests with a number of austenitic, ferritic and martensitic steels in 20 and 5% sodium and potassium hydroxide solutions are summarized in Table XV which gives failure times with 20% sodium hydroxide at 300°C. The results of austenitic stainless steels with 20% sodium hydroxide were quite erratic. Increased nickel content giving a more stable austenite confers greater resistance to SCC. The 12Cr-12Ni and 25Cr-20Ni have very good resistance under all the test conditions. The beneficial effect of nickel is hampered when the chromium level is as high as 20 or 25%. At 10 and 15% chromium, increasing nickel did lead to some delay in failure. Very high nickel alloys are beneficial. Inconel is resistant to cracking (Table XVI and Fig. 49).[134] Using 15 and 30% deformed specimens at 380 and 550°C in 1% NaOH, similar beneficial effects of nickel have been established. It was found that in all cases, except 17-20Cr and 8-11Ni, inter- or transgranular cracking was observed in 2000 hours (Tables XVII and XVIII).[133] In another investigation by CORIOU et al.,[128] it is shown that up to 15% nickel the alloys cracked readily. For nickel contents above 25%, stress appeared to cause intergranular corrosion. From their investigations, they suggested that alloys with 17% chromium and 30 to 45% nickel withstood corrosion even at 600°C.

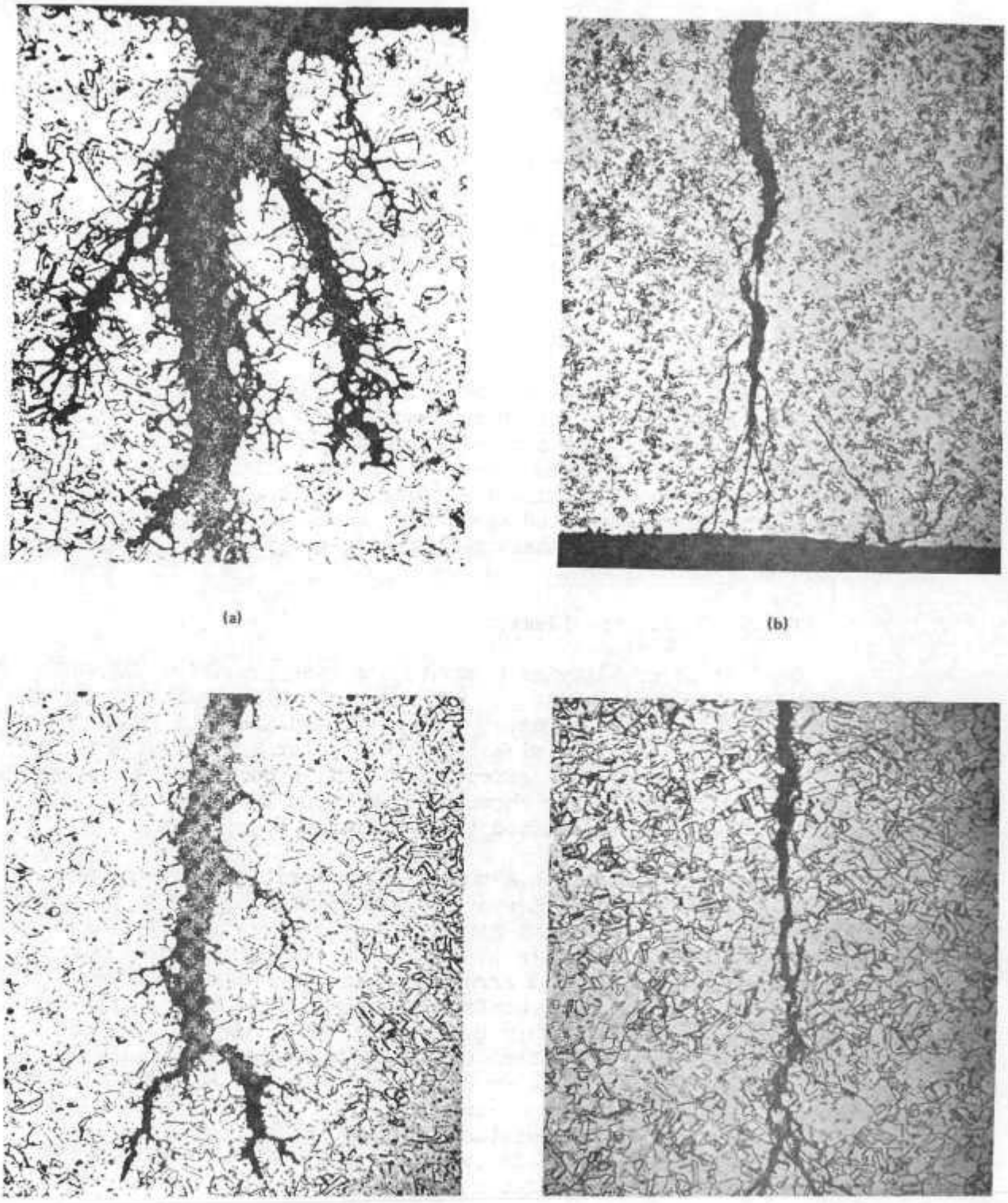

Fig. 48 - Typical stress corrosion cracks in 18-9Nb stainless steel exposed to hydroxide solutions under various conditions: (a) intergranular cracking with 50% NaOH at 300°C (300x); (b) transgranular cracking with sodium hydroxide in steam (100x); (c) intergranular cracking with KOH below its melting point in steam (200x); (d) transgranular cracking with KOH heated above its melting point in steam (200x).[122]

Table XV - Behavior of Various Fe-Cr-Ni Alloys in Caustic Alkali Environments (after SNOWDEN)[132]

Cr	Ni	Other Additions	Life Obtained on Specimens at 22,400 psi and 300°C in Solution of: 20% NaOH	Life Obtained on NaOH Contaminated Specimens Tested at 29,620 psi steam at: 330°C and 1,500 lb/in^2 (superheated)
18.24	10.78		3·7 h	117 h (Na_2SiO_3 added) 42 h to NaOH
17.80	8.70		8·1 h	632 h
18.56	9.00	0.61Ti	17·8,284·7, 302 h, 515 h NF	
18.48	9.20	0.52Ti	4.05 h	341 h NF
17.72	9.55	0.35Mo, 0.78Ti, 0.224S	42.7 h	
17.76	8.34	2.83Mo	8.9 h	189 h NF, 307 h
17.84	9.50	1.22Nb		18 h, 90 h NF, 110 h
17.72	8.75	0.80Nb	1·6, 1·8, 15·3 h	15 h, 276 h NF
17.16	8.40	0.66Nb	3.7, 27 h	
15.90	11.84	1.23Mo, 1.10Nb		15 h
12.32	12.60	0.29Mo, 0.18Cu	1.2,20.2 h	343 h
23.93	21.70		14.6, 150.8 h	679 h NF
20.76	0.15		2.5, 6.5 h	
20.50	0.16	2.08Mo, 1.17Nb	1.0, 58.6 h	485 h NF, 1012 h NF
21.64	0.15	2.05Mo, 1.19Nb	55.0 h	
13.88	5.51	1.75Mo, 0.38Nb, 1.63Cu	6.2, 10.7, 37.9 h**	909 h NF+

**Aged 2 h 560°C

+Aged 1 h 550°C

Table XVI - Compositions of Materials Tested (wt %)
(after TRUMAN and PERRY)[134]

C	Si	Mn	Cr	Ni	Mo	Cu
0·03	0·33	0·49	10·04	15·10		
0·03	0·37	0·50	15·16	15·05		
0·05	0·46	0·47	15·48	14·90	2·50	
0·05	0·41	0·51	15·52	14·95	4·94	
0·05	0·47	0·46	15·36	14·90	5·12	2·05
0·05	0·59	0·49	15·28	15·40	5·00	4·10
0·02	0·10	0·51	20·24	14·90		
0·03	0·41	0·50	24·24	15·05		
0·02	0·32	0·44	10·00	25·60		
0·02	0·33	0·49	15·24	25·40		
0·05	0·40	0·51	15·52	24·65	2·50	
0·05	0·51	0·46	15·04	25·00	4·88	
0·05	0·55	0·49	15·28	25·60	4·94	2·00
0·04	0·57	0·48	15·40	24·80	5·00	4·00
0·02	0·43	0·49	20·40	25·30		
0·02	0·45	0·48	25·36	25·60		
0·03	0·59	0·43	10·26	34·75		
0·02	0·42	0·52	15·04	35·20		
0·04	0·50	0·47	15·08	35·80	2·50	
0·04	0·55	0·46	15·60	33·80	4·88	
0·05	0·63	0·47	15·16	34·70	4·94	2·00
0·04	0·44	0·47	15·06	36·15	5·00	4·00
0·02	0·39	0·52	19·96	35·80		
0·02	0·46	0·49	24·96	35·15		
0·02	0·39	0·47	10·28	45·20		
0·02	0·28	0·49	15·08	45·70		
0·04	0·56	0·47	15·44	45·20	2.40	
0·03	0·46	0·47	15·08	45·50	4·88	
0·05	0·66	0·48	15·28	46·70	4·95	2·05
0·05	0·60	0·46	15·16	45·40	5·06	4·00
0·02	0·42	0·44	20·16	45·90		
0·02	0·43	0·45	25·16	45·40		

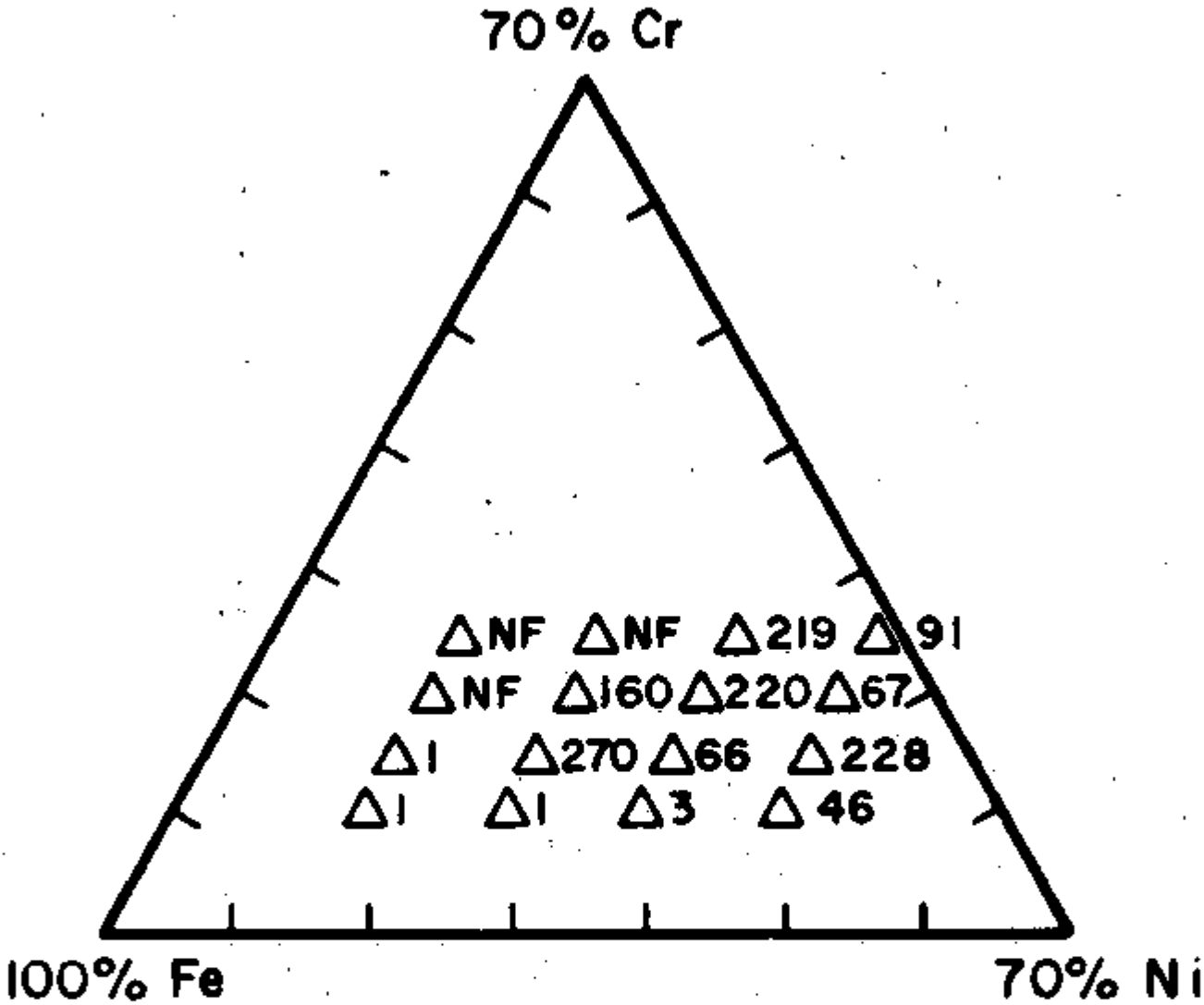

Fig. 49 - Time-to-failure in hours for alloys as shown above in 50% NaOH at 300°C/2000 psi O_2 and 20,000 psi: F-failed, perforated by cracking; C-cracked but not perforated; U-not cracked; U(P)-not cracked but some elongated pits.[134]

Table XVII - Chemical Composition of the Steels Investigated by KAGAN and MIKHAILOVA[133]

Type of Steel	Concentration of Elements, %											
	C	Si	Mn	S	P	Cr	Ni	W	Mo	Nb	Ti	Co
ÉYa1T	0.12	0.8	2.0	0.030	0.035	17.0-20.0	8.0-11.0				(C-0.03)5 to 0.8	
LA1	0.16	0.55	0.7	0.020	0.025	14-16	14-16	0.8-1.2	1.8-2.2		0.15-0.35	2.8-3.2
ÉI405	0.12	0.80	1.0	0.025	0.030	16.0-17.0	12.5-14.5		2.0-2.5	0.95-1.25		
ÉI257	0.10	0.40	0.32			14.60	14.02	2.27	0.45			
ÉI257	0.10	0.50	0.38	0.010	0.021	15.48	15.25	2.32	0.50			
ÉI257T	0.10	0.46	0.45	0.016	0.020	13.19	13.8	2.15	0.52		0.45	
ÉI694 experimental	0.10	0.21	1.34	0.020	0.012	15.0	15.0			0.50		
ÉI694 industrial	0.09	0.52	1.40	0.021	0.017	13.9	17.0			1.05		
ÉI695 experimental	0.10	0.14	1.41	0.026	0.020	14.61	18.46	2.17		0.75		

Table XVIII - Time Preceding Appearance of Corrosion Cracks on Samples in Sodium Hydroxide (after KAGAN and MIKHAILOVA)[133]

Medium	Testing Period, hr	Type of Steel										
		ÉI257		ÉI257Ti		ÉI694 Experimental	ÉI694 Industrial	ÉI695	LA1	ÉI405	ÉYa1Ti	ÉI257
		Deformation, %										
		15	30	15	30	15	15	15	5	15	30	30
	500	None	None	--	--	None	--	None	None	None	None	--
	575	--	--	--	--	--	None	--	--	--	--	--
	875	--	--	--	--	--	None	--	--	--	--	--
NaOH	1500	None	--	Cracks	--	--	--	--	--	--	--	Cracks
	2000	Cracks	--	--	--	Cracks	--	--	Cracks	--	--	--
	3350	--	--	--	--	--	--	--	--	--	None	--
380°C	4000	--	--	--	--	--	--	--	--	--	None	--
	4200	--	--	--	--	--	--	--	--	--	None	--
	200	None	None	--	--	None	None	Cracks	None	None	None	
	1500	--	--	Cracks	None	--	--	--	--	--	--	
NaOH	1700	Cracks		--	--	Cracks		None	Cracks	--	None	
	3000	--	--	--	Cracks	--	--	--	--	--	None	
	3200	--	--	--	--	--	--	--	--	--	None	
	3400	--	--	--	--	--	--	--	--	--	None	

AKOLZIN et al.,[135] have compared the corrosion behavior of stainless steels which contained lower nickel when compared to 1Kh18N9T (C0.1, Cr 19.8, Ni 10.2, Ti 0.6) and also contained Mn and N. Their compositions are given in Table XIX. They studied these alloys in 4% sodium hydroxide at 310°C at 120 atmospheres. The behavior of I, II and III were comparable with 1Kh18N9T while that of IV, V and VI was quite inferior. A consistent explanation is impossible because of the numerous alloying elements in their alloys. Still the superior behavior can be attributed to the low chromium in the system which coincides with explanations offered by TRUMAN and PERRY.[134]

Table XIX - Compositions of Steels Tested by AZHOGIN[131]

Sample No.	Designation	Composition, %
I	OKh 18N 5G 10A	C 0.08, Si 0.35, Mn 10.7, S 0.012, P 0.001, Cr 18.0, Ni 4.5, N 0.2
II	1Kh 14N 3G 14T	C 0.12, Si 0.48, Mn 14.5, S 0.008, P 0.01 Cr 16.5, Ni 3.2, N 0.03, Ti 0.42
III	OKh 14N 3G 11BA	C 0.07, Si 0.62, Mn 10.72, S 0.006, P 0.003, Cr 14.0, Ni 3.0, N 0.26, Nb 1.26
IV	1Kh 18N 5G 10BA	C 0.08, Si 0.43, Mn 10.8, S 0.01, P 0.001, Cr 17.65, Ni 4.5, N 0.21, Nb 0.97
V	OKh 18N 5G 10BA	C 0.07, Si 0.38, Mn 10.5, S 0.015, p 0.001, Cr 17.65, Ni 4.6, N 0.36, Nb 0.92
VI	OKh 20N 5G 12BA	C 0.07, Si 0.42, Mn 13.15, S 0.027, P 0.013, Cr 20.1, Ni 5.23, N 0.49, Nb 0.94

Effect of carbon content on the mode of cracking changes with increasing carbon content from transgranular to intergranular type, and the latter mode persists despite the ice-brine quenching of the specimens annealed at 1050°C.

The effects of 2.5% molybdenum, silicon and nickel on the stress corrosion behavior in 2.5N sodium hydroxide at 360°C were studied by CORIOU et al.[128] It was found that molybdenum led to more cracks while silicon made little difference.

6. Effects of Heat Treatment

This aspect has been studied by STROCCHI et al.,[137] BOND et al.,[138] and COPSON and ECONOMY.[136]

The effect of various heat treatments on the stress corrosion behavior of 316 stainless steels in 16.5-23% sodium hydroxide at 10 atmospheres and 180-190°C for 10-15 hours were studied. The cold-worked and loop-shaped specimens exhibited several microcracks whether or not the specimen was welded. The straight annealed and water-quenched specimens showed no embrittlement, but did show microcracks if the specimen contained a weld. Annealed and water-quenched loop specimens showed cracks in the regions of high stress.[140]

Constant load tests were performed with boiling sodium hydroxide (25% at 111°C) on 430 and 434 type stainless steels, under various heat treatments, by BOND et al.[138] From Table XX it can be inferred that heat treatments did not have any effect in producing cracking, but produced uniform intergranular corrosion. The failure times for these alloys were 336 and 428 hours.

Table XX - Results of Exposing 0.020" Diameter Specimens of Ferritic Steels to Boiling 25% Sodium Hydroxide at a Stress of 53,000 psi (after BOND et al.)[138]

Alloy	Heat Treatment	Exposure Time, hr	Remarks
430, Heat B	annealed	336 NF[a]	uniform corrosion
430, Heat B	1 hr, 900 F		
430, Heat B	15 min, 1800 F	428 NF	intergranular attack
430, Heat A	15 min, 1800 F		
434, Heat A	annealed	336 NF	uniform corrosion
434, Heat A	1 hr, 900 F	355 NF	uniform corrosion
434, Heat A	15 min, 1800 F	336 NF	intergranular attack
434, Heat B	15 min, 1800 F	336 NF	intergranular attack
Mild Steel	1500 F		

[a]No failure

COPSON and ECONOMY[136] have studied the stress corrosion behavior of a whole series of austenitic stainless steels, Inconels, and Incoloys in lithium hydroxide solutions (pH 10) at a temperature of 316°C. Their results are summarized in Table XXI. From Table XXI it can be observed that failures occurred in case of Inconel 600 (6-M and S heats), 304, 304L and 347 stainless steels and Incoloy 800 (2-A and S) and Inconel 625 (2-M, A and S) irrespective of the heat treatment.

Table XXI - Fracture Data for Various Stainless Steels Exposed to Lithium Hydroxide (pH 10) (after COPSON and ECONOMY)[136]

Test Duration, 18 weeks[a]
Temp., 800°F (310°C); Gas Phase above Solution, Air

Alloy Designation	Heat[b]	Maximum Depth in Mils of Cracks in Crevice Area of Each Double U-Bend Specimen	
Inconel 600	2-M	0	80(14)
	-CR	-	-
	-A	0	0
	-S	0	0
	-P	110(2)	110(2)
	-T	-	-
Inconel 600	4-M	-	-
Inconel 600	5-M	0	0
	-A	0	0
	-S	0	0
Inconel 600	6-M	55(14)	80(12)
	-S	115(2)	115(2)
Inconel 600	7-M	0	80(4)
Inconel 600	8-M	0	0
Stainless Steel 304	2-A	40(8)	50(8)
	-S	50(2)	80(2)
Stainless Steel 304L	A	30(8)	40(8)
	S	40(2)	80(10)
Stainless Steel 347	A	20(4)	30(8)
	S	20(8)	20(14)
Incoloy 800	1-A	-	-
	-S	-	-
Incoloy 800	2-A	10	16
	-S	100(4)	115(4)
Inconel 625	2-M	3	38
	-A	30(12)	30(12)
	-S	7	8

[a]Numbers in parentheses indicate weeks in test if less than full test duration.
[b]M = mill annealed; CR = M + cold rolled 40%; A = 1 hr 2050°F, water quench (except 1950°F for stainless steels Incoloy alloys);
S = A + 2 hr 1250°F, AC; P = S + 24 hr in 15% HNO_3 + 5% HF, RT; T = CR + 40 min 1650°F, AC.

B. PREVENTION OF STRESS CORROSION CRACKING

Anodic inhibitors and maintenance of inert atmosphere are the two methods which have been tried to prevent caustic SCC of Fe-Ni-Cr alloys. Investigations in this area have been carried out by SNOWDEN,[122,139] GULYA'EV et al.,[140] HOWELLS,[126] SIDOROV and RYABCHENKOV,[124] and KAGAN and MIKHAILOVA.[138] The findings of these studies are

(i) phosphates and sulphates offer partial prevention of cracking;

(ii) in some conditions a ratio of phosphate-to-hydroxide of 1:4 is required to prevent cracking;

(iii) inert atmospheres helped in preventing stress corrosion cracking of 1Kh18N9T stainless steels; and

(iv) 3% sodium chloride addition has an inhibitive effect.

From Tables XXII and XXIII, it can be seen that phosphates, nitrates, etc., had effect only in the steam phase. In an aqueous media these salts did not have any effect; in a steam phase, the specimens which did not fail showed either intergranular or transgranular cracks.[122,139] In another investigation, even a high $SO_4^{=}/OH^{-}$ ratio of 5 is found to suppress but not eliminate, cracking completely (see Table XXIV). HOWELLS[126] showed that a phosphate-to-hydroxide ratio of 1:4 to be adequate to prevent cracking, as shown in Fig. 50.

A 3% sodium chloride addition to hydroxide solution at 330°C was also found to have inhibitive effects (Fig. 51).[124]

C. GENERAL CORROSION

UHLIG and MATTHEWS[141] studied corrosion rates and potential changes with time, SMITH and HOFFMANN[142] the corrosion products, and CAVALLARO and BIGHI[143,144] studied the effects of dissolved gases on the inhibiting behavior.

Figure 52 shows the weight loss and number of pits plotted against grams of sodium hydroxide (1-80 g/l) added to 4% sodium chloride at 90°C. It can be seen from this figure that number of pits and weight loss decreases rapidly even when 0.5 g/l sodium hydroxide was added. Afterwards, weight loss becomes almost independent of the concentration. A minimum concentration of sodium hydroxide required to produce corrosion is 8%.[141]

Examination of the microstructure of corrosion product layers formed in fused sodium hydroxide at 815°C on 304 and 347 stainless steels, revealed that corrosion product layer consisted of a metallic network threading through a metallic matrix.[142]

Table XXII - Tests in Steam with 347 Type Stainless Steel in Mixtures of Phosphate, Sulphate, Nitrate and Bisulphate with Sodium Hydroxide (after SNOWDEN)[139]

Steam Pressure = 1500 psi, Temp., = 330°C, Stress = 29,210 psi

Ratio of NaOH Inhibitor in 30% NaOH Solution to Coat Specimen	Duration of Test (hr)	Observations
NaOH/Na_3HPO_4 2/1	5	Many small cracks besides fracture
NaOH/Na_2HPO_4 1/2	460 NF[a]	A number of very small cracks
NaOH/NaH_2PO_4 1/1	117 NF	No cracking
NaOH/$NaNO_2$	966 NF	Several large cracks, general intercrystalline attack
NaOH/$NaNO_3$	313	Many small cracks besides fracture
NaOH/Na_2SO_4	1112	Intercrystalline fracture, general intercrystalline attack
NaOH/$NaHSO_4$	1958 NF	No cracking
Typical result with plain NaOH	110	Severe transcrystalline cracking

[a]NF = No failure

Table XXIII - Tests with 347 Type Stainless Steels in Hydroxide Solutions, to which Phosphate, Sulphate and Nitrates are Added Individually (after SNOWDEN)[139]

Temp., 300°C, N_2 at 1000 psi + air at 200 psi, stress = 22,400 psi

% NaOH and Inhibitor	Duration of Test (hr)	Observations
20% NaOH-5% NaH_2PO_4	67	Many transcrystalline cracks, a few intercrystalline cracks
17% NaOH-7% Na_3PO_4	217, 679 NF[a]	No cracking, general corrosion in failed specimen
10% NaOH-4% Na_3PO_4	363	Transcrystalline fracture, no other cracking
5% NaOH-5% Na_3PO_4	3.0	Transcrystalline fracture, no other cracking
20% NaOH-8% Na_3PO_4	2.0, 2.6	Transcrystalline fracture, a few transcrystalling cracks
5% NaOH-5% $NaNO_3$	24.7	Failure due to general corrosion, no cracking
5% NaOH-5% Na_2SO_4	32, 48	Transcrystalline cracking
5% NaOH-5% $NaHSO_4$	138	Mixed inter- and transcrystalline fracture, no other cracking
5% NaOH-5% Na_2CrO_4	9	Intercrystalline fracture, no other cracking
Typical results with plain NaOH solutions, 20%	1.8	Severe intercrystalline cracking
Typical results with plain NaOH solutions, 5%	15.1	Severe intercrystalline cracking

[a]No Failure

Table XXIV - Effect of Sodium Sulphate on the Corrosion Behavior of Various Stainless Steels at 380 and 550°C (after KAGAN and MIKHAILOVA)[133]

Medium	Testing Period, hr	Type of Steel										
		É1257		É1257Ti		É1695	Lal	É1405	É1694, Batch		ÉYalTi	É1257
									Experimental	Industrial		
		Deformation, %										
		15	30	15	30	15	5	15	15	15	30	30
Temp. 380°C	200	None	None	--	--	None	None	None	None	None	None	
NaOH	400	--	--	--	--	--	--	--	--	None	--	
1%	1500	--	--	Cracks		--	--	--	--		--	
+ Na_2SO_4	1700	Cracks		--	--	Cracks		None	Cracks	--	None	
5%	3000	--	--	--	--	--	--	None	--	--	None	
	3200	--	--	--	--	--	--	None	--	--	None	
	3400	--	--	--	--	--	--	None	--	--	None	
Temp. 550°C	500	None	None	--	--	None	--	None	None	None		None
NaOH	1500	--	--	None	None	--	None	--	--	--	--	--
1%	2000	None	None	--	--	None	--	None	None	None	None	Cracks
+ Na_2SO_4	2850	--	--	Cracks		--	--	--	--	--	--	--
5%	3350	Cracks		--	--	Cracks	--	Cracks		None	None	--
	4850	--	--	--	--	--	--	--	--	None	None	--

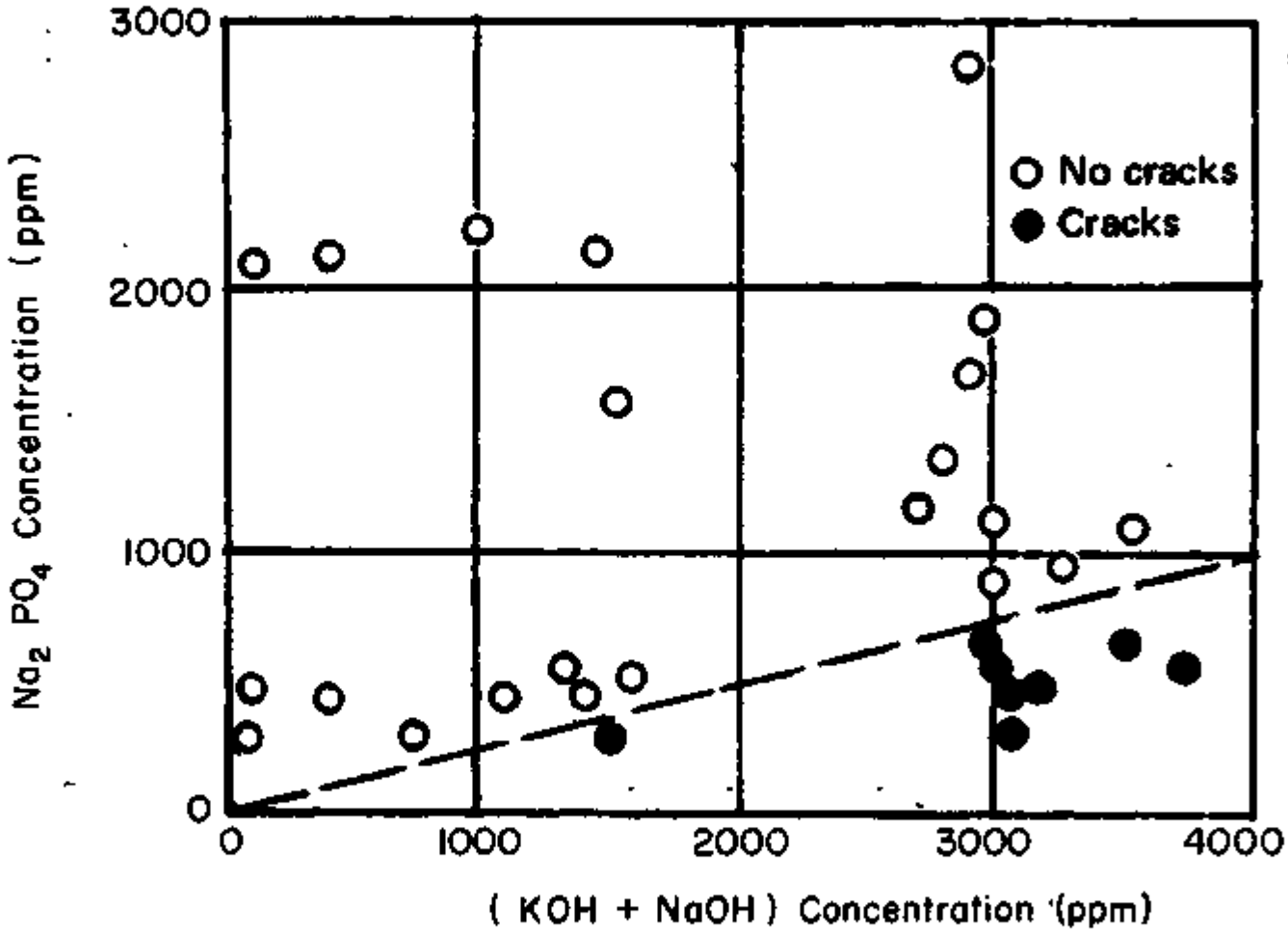

Fig. 50 - Influence of $PO_4^{=}/OH^{-}$ ratio on cracking of U-bend specimen of type 347 stainless steel. Concentration ratios greater than 1:4 seem to inhibit stress corrosion cracking.[126]

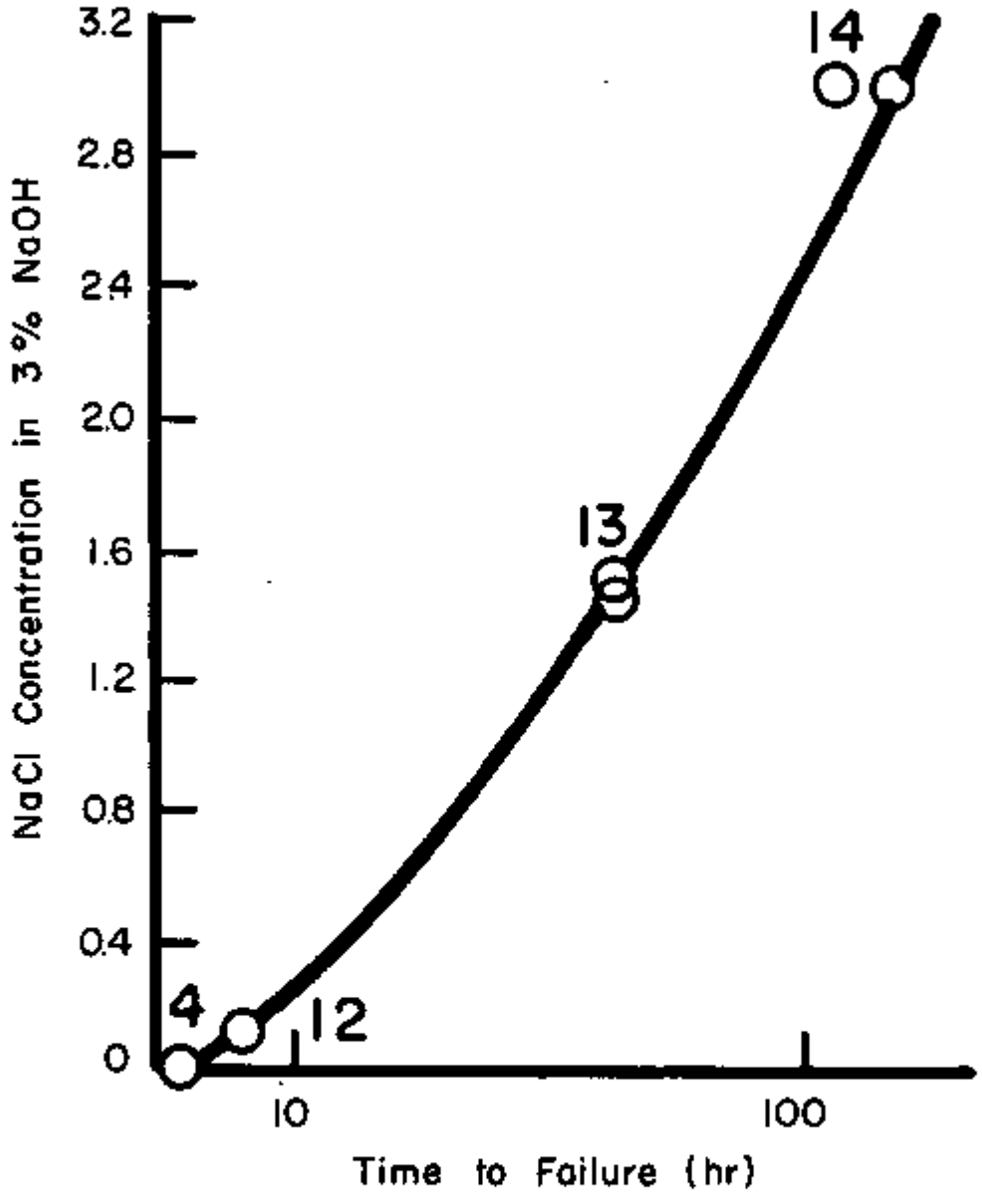

Fig. 51 - Dependence on time-to-failure of essentially type 321 stainless steel on concentration of NaCl in 3% NaOH.[124]

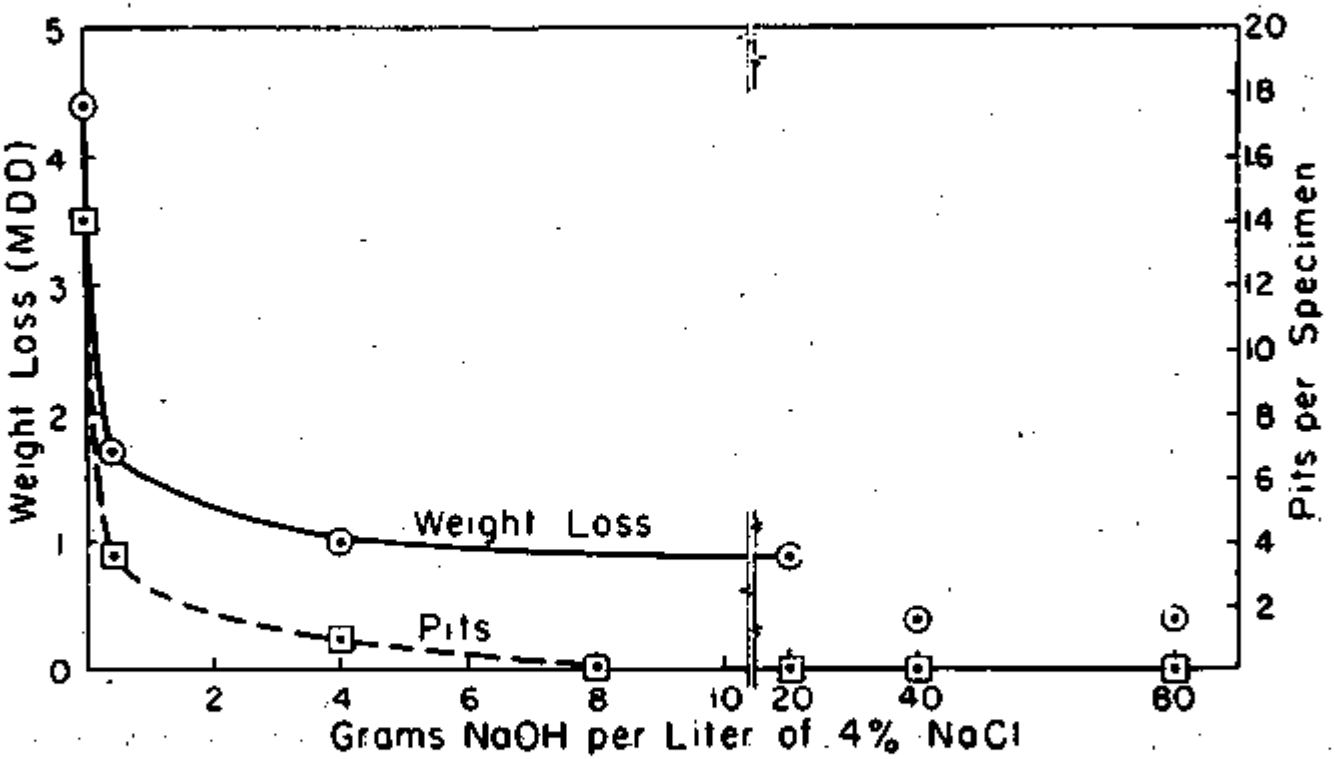

Fig. 52 - Effect of NaOH in 4% NaCl on weight loss and pitting of 18-8 (24 hr test, 90°C).[141]

RENSHAW and FERREE[145] and UHLIG and MATTHEWS[141] studied the passivation phenomena. CAVALLARO and BIGHI[143,144] studied the effects of dissolved gases on the inhibiting behavior of sodium hydroxide.

The open circuit potentials of 430 and 304 steels in 5% sodium hydroxide at room temperature were measured with time.[145] Figure 53 gives the potential-time curves for the above steels. In this solution 304 stainless steels showed active potentials which gradually shifted toward the passive values; 430 steels showed an identical behavior. The time for passivation was one hour in both cases. Figure 54 shows the dependence of electrode potential with concentration of sodium hydroxide in 4% sodium chloride.[141] In this range, traces of sodium hydroxide to 12%, cause potentials to drift toward passive values at the rate of 50 mV_H/decade of NaOH and becomes almost constant. In fact, a shift toward active values after 80 g/l of sodium hydroxide should have been observed if experiments were conducted at 90°C as given in Fig. 52. The effect of bubbling oxygen, nitrogen, and air into the hydroxide solution on pitting behavior has been studied by CAVALLARO and BIGHI.[143,144] Out of the three additions tried, it was found that N_2 additions had inhibiting effects.

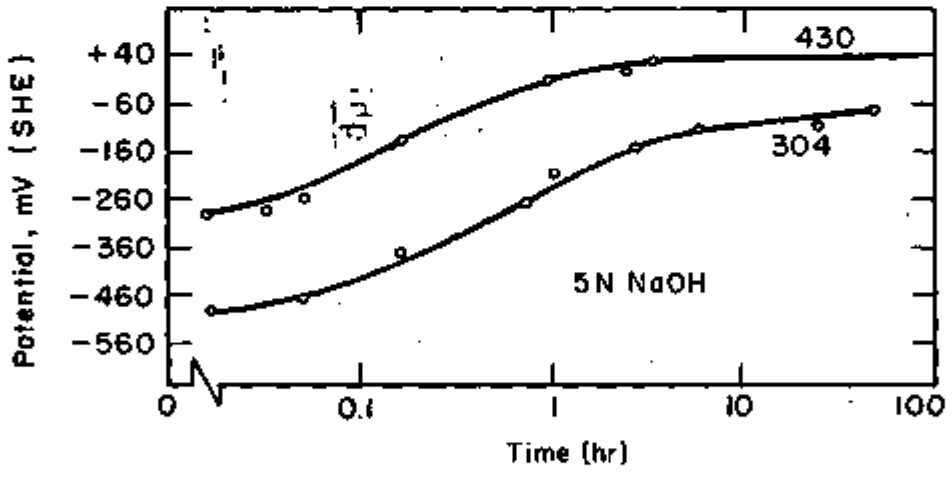

Fig. 53 - Comparison of passivating characteristics of types 304 and 430 stainless steels in 5N NaOH.[145]

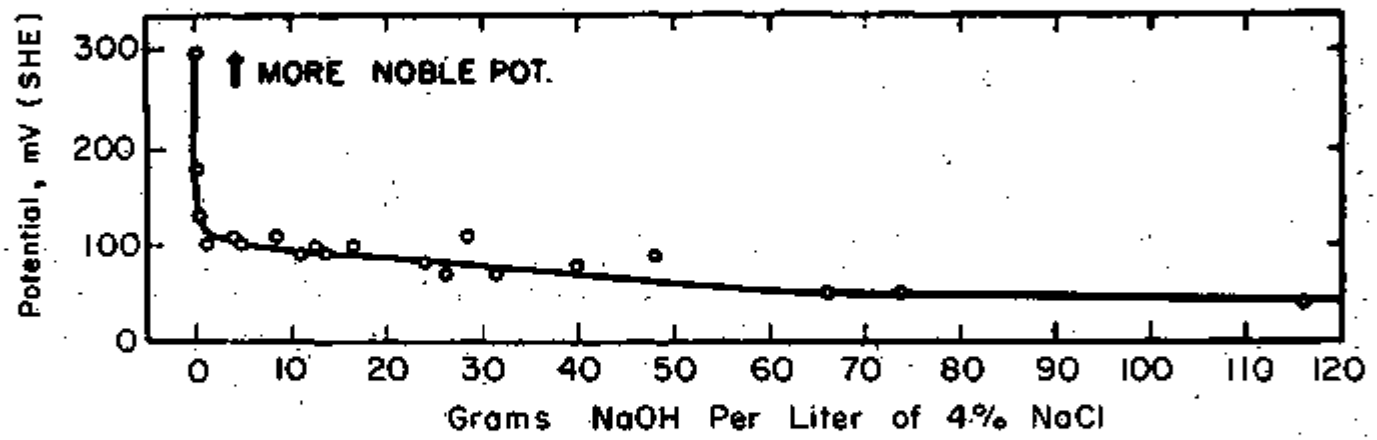

Fig. 54 - Effect of NaOH additions on potentials of 18-8 in 4% NaCl at 25°C.[141]

REFERENCES

1. F. G. Straub, Illinois Experimental Station Bulletin, No. 216, 8 and 12 (1930).

2. H. L. Logan, J. Res., National Bureau of Standards, 66c, 347 (1962).

3. W. C. Schroeder and A. S. Berk, U. S. Bureau of Mines Bulletin 443, U. S. Government Printing Office (1941).

4. L. L. Shreir: "Corrosion," volume 1, published by George Newnes Limited, London (1963).

5. H. L. Logan: "The Stress Corrosion of Metals," John Wiley & Sons, Inc., New York (1966).

6. H. Kaesche: "Die Korrosion Der Metalle, Physikalischchemische, Prinzipien und Aktuelle Problems," published by Springer-Verlag, Berlin (1966).

7. "Stress Corrosion Testing," ASTM, STP 425, Am. Soc. Testing Materials (1967).

8. R. M. Latanision and R. W. Staehle, Conference on Fundamental Aspects of Stress Corrosion Cracking, Columbus, Ohio, September 11-15, (1967). Proceedings published by NACE, 214 (1969).

9. R. N. Parkins, Metallurgical Reviews, 9, No. 35, 201 (1964).

10. R. N. Parkins, Conference on Fundamental Aspects of Stress Corrosion Cracking, Columbus, Ohio, September 11-15, (1967). Proceedings published by NACE, 261 (1969).

11. E. N. Pugh, Met. Soc. Conf. 35, 351 (1965); published (1966).

12. J. C. Scully, Corrosion Science, 7, 197 (1967).

13. H. W. Schmidt et al., Corrosion, 7, 295 (1951).

14. J. J. Harwood, ibid., 6, 290 (1950).

15. M. Pourbaix: "Atlas of Electrochemical Equilibria Solutions," translated by J. A. Franklin, by Pergamon Press (1966).

16. A. A. Berk, Chem. and Ind., 360 (1953).

17. R. N. Parkins, ibid., 180 (1953).

18. F. A. Champion, ibid., 967 (1957).

19. W. C. Schroeder and A. A. Berk, Amer. Inst. of Min. and Met. Eng., 120, 387 (1936).

20. C. D. Weir, Proc. Inst. of Mech. Engineers, 163, W. E. P., No. 55, 18 (1950).

21. G. L. Shvarts, I. G. Volikova and Yu. S. Kuznetsova, Sbornik Statei Vsesoyuz. Nauch. - Issledovatel. i Konstrukt, Inst. Khim. Mashinostroen, 25, 87 (1958); Chem. Abs., 54, 19416h (1960).

22. N. L. Evans, Foundry Trade J., 62, 102 (1940).

23. P. Hamer and E. W. Colbeck, Chem. and Ind., 163 (1944).

24. R. Rath, ibid., 600 (1953).

25. F. F. Azhogin, Zhur. Priklad. Khim., 39, No. 11, 2515 (1966); Chem. Abs., 66, 68195 (1967).

26. K. Bohnenkamp, Conference on Fundamental Aspects of Stress Corrosion Cracking, Columbus, Ohio, September 11-15, (1967). Proceedings published by NACE, 374 (1969).

27. S. W. Parr and F. G. Straub, Univ. of Illinois Bulletin, 177 (1928).

28. W. C. Schroeder, A. A. Berk and R. A. O'Brien, Metals and Alloys, 8, 320 (1937).

29. U. R. Evans: "An Introduction to Metallic Corrosion," published by Edwin Arnold, 117 (1963).

30. J. Venczel and G. Wranglen, Corrosion Science, 4, 137 (1964).

31. H. Grafen, Corrosion Science, 7, 177 (1967).

32. H. Grafen and D. Kuron, Arch. fur das Eisenhuttenwesen, 36, 4, 285 (1965).

33. M. J. Humphries and R. N. Parkins, Corrosion Science, 7, 747 (1967).

34. M. J. Humphries and R. N. Parkins, Conference on Fundamental Aspects of Stress Corrosion Cracking, Columbus, Ohio, September 11-15, (1967). Proceedings published by NACE, 384, (1969).

35. F. P. A. Robinson and L. G. Nel, 2nd. International Conference on Metallic Corrosion (1963); Proceedings, 172 (1966).

36. I. G. Podgornyi, Izvest. Vysshikh Uchebn. Zavedenii, Chernaya Met., 6, No. 3, 148 (1963); Chem. Abs., 59, 4848d (1963).

37. E. P. Partridge, C. E. Kaufmann and R. E. Hall; Trans. Amer. Soc. Mech. Eng., 64, 417 (1942).

38. W. Radekar and H. Grafen, Stahl and Eisen, 76, 1616 (1956).

39. C. D. Weir, Trans. Amer. Soc. Mech. Eng., 70, 253 (1948).

40. C. D. Weir and P. Hamer; Chem. and Ind., 71, 1040 (1952).

41. G. G. Pocheptsova and S. V. Timchenko, Khim. Neft. Machinostr., 10, 22 (1966), Chem. Abs., 66, 5166 (1967).

42. V. A. Maslov and V. T. German, Svaroch. Proizv., No. 8, 36 (1962); Chem. Abs., 57, 13488g (1962).

43. W. Sakwa and J. Marcinkowska, Ochrona Przed Koroza, 8, No. 5, 106 (1965); Chem. Abs. 64, 4702 (1966).

44. T. Mukaibo and S. Masukawa, Denki Kagaku, 33, No. 8, 576 (1965); Chem. Abs. 64, 372g (1966).

45. K. Masamichi and N. Saburo, Sumimoto Kinzoku, 19, No. 4, 494 (1967); Chem. Abs., 69, No. 12, 45526 (1968).

46. R. S. Thornhill, Centre Belge Etude et Document. Eaux, Bull. Trimestr., 213 (1961); Chem. Abs., 57, 569f (1962).

47. O. Asai and N. Kawashima, Denki Kagaku, 33, No. 6, 444 (1965).

48. E. C. Potter and G. M. W. Mann, 1st Intern. Cong. on Metallic Corrosion, London (1961); Proceedings, 417 (1962).

49. J. E. Castle and G. M. W. Mann; Corrosion Science, 6, No. 6, 253 (1966).

50. W. A. Fraser and M. C. Bloom, Corrosion, 18, 163t (1962).

51. M. C. Bloom, G. N. Newport and W. A. Fraser, J. Electrochem. Soc., 111, No. 12, 1343 (1964).

52. J. Kato and Y. Arai, Kogyo Kagaku Zasshi, 63, 1576 (1960); Chem. Abs., 57, 510 i (1962).

53. C. L. Foley, J. Kruger and C. J. Bechtoldt; J. Electrochem. Soc., 114, No. 10, 994 (1967).

54. L. Liepina, A. Vaivads and Z. Osis, Zhur. Fiz. Khim., 29, 35d (1955); Chem. Abs. 50, 16302f (1956).

55. R. Shalon and M. Raphael, Bull. Res. Council, Israel, 7c, 65 (1959); Chem. Abs. 54, 39091 (1960).

56. W. K. Kratzer, U. S. Atomic Energy Comm., HW - 79316 (1963).

57. M. C. Bloom, W. A. Fraser and M. Krulfeld, Corrosion, 18, 401t (1962).

58. M. C. Bloom, M. Krulfeld and W. A. Fraser; ibid; 19, No. 9, 327t (1963).

59. O. Asai and N. Kawashima, Denki Kagaku, 34, No. 9, 761 (1966).

60. O. Asai, ibid., 35, No. 9, 638 (1967).

61. O. Asai and N. Kawashima, ibid., 34, No. 3, 201 (1966).

62. O. Asai and N. Kawashima, ibid., 35, No. 10, 702 (1967).

63. O. Asai, ibid., 35, No. 12, 857 (1967).

64. M. Kowaka, M. Kitamura and T. Nakajima, Sumimoto Kinzoku, 18, No. 4, 468 (1966); Chem. Abs., 69, No. 16, 61029n (1968).

65. I. A. Ammar and S. A. Awad, J. Phys. Chem., 60, 871 (1956).

66. T. Hurlen, Electrochim. Acta, 8, No. 8, 609 (1963).

67. I. A. Bagotskaya, Doklady Akad. Nauk. S. S. S. R., 107, 843 (1956); Chem. Abs., 51, 892i (1957).

68. S. Schuldiner and C. M. Shepherd, J. Electrochem. Soc., 115, 916 (1968).

69. J. Tousek, Collect. Czech. Chem. Commun., 28, 1273, 2843 (1963).

70. K. E. Heusler, K. G. Weil and K. F. Bonhoeffer, Z. Phys. Chem., 15, 149 (1958).

71. I. P. Hancock and J. E. O. Mayne, J. Appl. Chem., 9, 345 (1959).

72. M. N. Ronzhin and A. I. Golubev, Korroziya Metal. i. Splavov, Sb. No. 2, 166 (1965); Chem. Abs., 64, 18954f (1966).

73. C. A. Knorr, K. Francke and M. Breiter, Z. Electrochem., 63, 226 (1959).

74. B. Purins and L. Liepina, Latvijas PSR Zinatnu Akad. Vestis, 6, 109 (1958); Chem. Abs., 53, 12138h (1959).

75. T. I. Popova and B. N. Kabanov, Russ. J. Phys. Chem., 35, No. 6, 4634 (1961).

76. K. S. Rajagopalan et al., Corrosion Science, 5, No. 1, 59 (1965); 8, No. 8, 557 (1968).

77. S. A. Rozentsveig, N. Yu. Uflyand and Z. V. Shcherbakova, Russ. J. Phys. Chem., 36, No. 3, 288 (1962).

78. N. E. Buyanova and G. A. Tsyganov, Kokiady Akad. Nauk. Uzbek S. S. R. No. 1, 23 (1955); Chem. Abs., 52, 1815b (1958).

79. V. V. Batrakov, A. P. Pyankova and Z. A. Iofa; Russ. J. Phys. Chem., 38, No. 5, 733 (1964).

80. M. K. Turapov and M. K. Murtazaev, Doklady Akad. Nauk Uzbek S. S. R., No. 2, 31 (1959); Chem. Abs., 54, 5291h (1960).

81. W. Schwartz and W. Simon, Ber. Bunsenges. Physik. Chem., 67, 108 (1963); Chem. Abs., 58, 12167h (1963).

82. A. S. Afanas'ev, V. I. Sotnikova and V. I. Sviridenko, Tr. Dnepropetr. Met. Instt., 44, 141 (1961); Chem. Abs., 60, 2548c (1963).

83. A. S. Afanas'ev, et al., Ukrain Khim. Zhur., 27, 624 (1961); Chem. Abs. 56, 8442f (1962).

84. K. Schwabe, J. Electrochem. Soc. 110, No. 6, 663 (1963).

85. S. D. Levina, J. Appl. Chem. U. S. S. R., 29, 1457 (1956).

86. M. K. Turapov and A. M. Murtazaev, Izvest. Akad. Nauk. Uzbek. S. S. R., Ser. Khim. Nauk., No. 2, 61 (1957); Chem. Abs., 53, 9852c (1957).

87. O. B. J. Fraser, Symposium on Stress Corrosion Cracking of Metals, ASTM, AIME, 458 (1944).

88. Howard T. McHenry and H. B. Probst, Natl. Advisory Comm. Aeronaut. Tech. Note, No. 3987, 23pp. (1958).

89. E. M. Simons, N. E. Millar, J. H. Stang and C. V. Weaver, U. S. A. E. C., BMI - 1118, 44pp. (1956).

90. R. S. People, P. D. Millar and H. D. Hannan, U. S. A. E. C., BMI - 1041, 11pp. (1955).

91. C. M. Craighead, L. A. Smith, E. C. Phillips and R. I. Jaffee, U. S. A. E. C., AECD, 3704, 55pp. (1952).

92. J. N. Gregory, M. Hodge and J. V. G. Iredale, Atomic Energy Res. Estab., C/M 273, 11pp. (1956); C/M 272, 9pp. (1956).

93. J. L. Weininger and M. W. Breiter, J. Electrochem. Soc., 111, No. 6 707 (1964).

94. Yu. K. Delimarskii, O. G. Zarubitskii and I. G. Pawlenka; J. Appl. Chem., U. S. S. R., 38, No. 12, 2755 (1965).

95. H. Kita and O. Nomura, J. Res. Instt. Catalysts, Hokkaido Univ., 12, No. 3 107 (1965).

96. S. P. Dezider'eva and F. F. Faizullin, Uchenye Zapiski Kazan, Gosudarst; Univ. im. V. I. Ulyanova-Lenina, Obschche Univ. Sbornik, 17, No. 2, 166 (1957); Chem. Abs. 54, 6362 (1960).

97. D. E. Davies and W. Barker, Corrosion, 20, No. 2, 47t (1964).

98. K. H. Stern and J. K. Carlton, J. Phys. Chem., 58, 965 (1954).

99. L. M. Elina, et al., Zhur. Fiz. Khim., 28, 785 (1954); Chem. Abs. 48, 12588c (1954).

100. L. M. Volchkova and A. I. Krasilsh'chikov, Zhur. Fiz. Khim., 23, 441 (1949); Chem. Abs., 43, 6523d (1949).

101. A. I. Tsinman, Russ. J. Phys. Chem., 37, No. 6, 714 (1963).

102. R. Piontelli, et al., Atti Accad. Nazl. Lincei, Rend. Classe Sci. Fis., Mat. Nat., 34, Nos. 5, 480 (1963); Chem. Abs., 60, 5073g (1964).

103. T. Seiyama, M. Abo and W. Sakai, J. Chem. Soc., Japan, Ind. Chem. Sect., 57, 343 (1954).

104. P. Lukovtsev and S. Levina, J. Phys. Chem. U. S. S. R., 21, 599 (1947).

105. J. Postlethwaite, Electrochim. Acta, 12, 333 (1967).

106. K. Schwabe and R. Radeglia, Werkstoffe U. Korrosion, 13, 281 (1962).

107. A. V. Zakrzhevtskaya and G. A. Tsyganov, Izvest. Akad. Nauk. Uzbek. S. S. R., Ser. Khim. Nauk., No. 2, 13, 27 (1957); Chem. Abs., 53, 9853dg (1959).

108. I. M. Issa, I. A. Ammar and H. Khalifa, J. Phys. Chem. 59, 492 (1955).

109. F. F. Faizullin and V. K. Levina, Zashch. Metal., 2, No. 6, 623 (1966); Chem. Abs., 66, 61234 (1967).

110. Laszlo Kiss, Magy. Kem. Folyoirat., 70, No. 2, 77 (1962); Chem. Abs., 52, 13466b (1958).

111. R. I. Agladze, and T. V. Ionatamistivili, Trudy. Instt. Metal. i Gorn. Deta, Akad. Nauk. Gruzin. S. S. R., 7, 157 (1956); Chem. Abs., 52, 13466b (1958).

112. A. A. Sharmin et al., J. Appl. Chem., U. S. S. R., 36, No. 7, 1470 (1963).

113. I. P. Dezider'eva and R. M. Sageeva, Anodnaya Zashchita Metal., Kazansk. Aviats, Inst., Dokl. 1 - Oi. Mezhvuz., Konf. 483 (1964); Chem. Abs., 62, 3663c (1965).

114. K. Sakiyama and M. Fujimoto, Nippon Kinzoku Gakkaishi, 30, No. 7 617 (1966); Chem. Abs., 68, 24070c (1968).

115. N. T. Denholm, 1st Australian Conf. Electrochem., Sydney, Hobart, Australia (1963); Proceedings, 164 (1965).

116. W. L. Williams, Report C - 32 - C, U. S. N. Eng. Exptl. Station, (1946).

117. T. P. Hoar and J. G. Hines , J. Iron & Steel Inst., 182, 124 (1956).

118. W. L. Williams, Corrosion, 13, 539t (1957).

119. P. P. Snowden, Chem. and Ind., 1692 (1958).

120. J. N. Wanklyn and D. Jones, ibid., 888 (1958).

121. R. K. Swandby, Chem. Eng., 69, 186 (1962).

122. P. P. Snowden, J. Iron & Steel Inst., 194, 181 (1960).

123. H. Coriou and L. Grall, Rapport CEA-R 2600, Centre d'Etudes Nucleaires de Saclay.

124. V. P. Sidorov and A. V. Ryabchenkov, Tsentr. Nauchn. Issled. Inst. Teknol. i. Mashinostr, 92, 42 (1959); Chem. Abs., 56, 15246e (1962) Cf. Metall. i. Okralakta Metallov., 25 (1958).

125. A. E. Pickett, W. L. Pearl and M. C. Rowland, Nuclear Applications, 1, 453 (1965).

126. E. Howells, Corr. Technol., 7, 368 (1960).

127. H. Coriou, L. Grall, M. Pelras and H. Willermoz, Collog. Met., Comm. Energie At., 8, 135 (1965); Chem. Abs., 63, 17631f (1965).

128. H. Coriou, L. Grall and M. Pelras, Energ. Nucl., 9, No. 5, 303 (1967).

129. H. L. Bormann and G. E. Galonian, U. S. A. E. C., KAPL-2047 (1959).

130. F. W. Pement, Bettis Technical Review, 16, 112 (1959).

131. F. F. Azhogin, Mezhkristal. Korroziya i Korroziya Metal v. Napryazhen. Sostoyanii, Vsesoyuz. Sovet. Nauch.-Tekh. obshchestv, 231 (1960); Chem. Abs., 55, 16371f (1961).

132. P. P. Snowden, J. Iron and Steel Inst., 197, 136 (1961).

133. D. Ya. Kagan and T. M. Mikhailova, "Intercrystalline Corrosion and Corrosion of Metals under Stress," ed., A. I. Levin, published by Consultants Bureau, N. Y., 179 (1962).

134. J. E. Truman and R. Perry, British Corr. J., 1, 60 (1966).

135. P. A. Akolzin et al., Teploenergetika, 10, No. 8, 54 (1963); Chem. Abs., 60, 3805d (1964).

136. H. R. Copson and G. Economy, Corrosion, 24, No. 3, 55 (1968).

137. P. M. Strocchi, D. Sinigagli and B. Vincentini, Electrochem. Metal., 1, No. 479 (1966); Chem. Abs., 66, 78723v (1967).

138. A. P. Bond, J. D. Marshall and H. J. Dundas, Stress Corrosion Testing, ASTM, STP 425, 116 (1967).

139. P. P. Snowden, Nuclear Eng., 6, 409 (1961).

140. V. N. Gulya'ev el al., Teploenergetika, 8, No. 9, 50 (1961); Chem. Abs., 56, 2230a (1962).

141. J. M. Mathews and H. H. Uhlig, Corrosion, 7, 419 (1951).

142. G. P. Smith and E. E. Haffmann, USAEC, ORNL, 2156, 8pp. (1957).

143. L. Cavallaro and C. Bighi, Metallurgia ital., 44, 361 (1952).

144. C. Bighi, ibid., 46, Supplement to No. 5, 42 (1953).

145. W. G. Renshaw and J. A. Ferree; Corrosion, 7, 353 (1951).